Jon Enes

Mitigation of the aviation sector

LCA of alternative fuels, and future scenarios

Master's thesis in Energy and Environmental Engineering
Supervisor: Helene Muri
Co-supervisor: Anders Hammer Strømman, Jan Klenner
June 2021

Master's thesis

NTNU
Norwegian University of Science and Technology
Faculty of Engineering
Department of Energy and Process Engineering

NTNU
Norwegian University of
Science and Technology

Jon Enes

Mitigation of the aviation sector

LCA of alternative fuels, and future scenarios

Master's thesis in Energy and Environmental Engineering
Supervisor: Helene Muri
Co-supervisor: Anders Hammer Strømman, Jan Klenner
June 2021

Norwegian University of Science and Technology
Faculty of Engineering
Department of Energy and Process Engineering

NTNU
Norwegian University of
Science and Technology

Thesis description

Aviation is contributing to about 5% of global anthropogenic warming, according to estimates. Activity from this sector has increased sharply over recent decades for both freight and passenger transport. With the accompanied rise in emissions, the forcing on the climate has nearly doubled in the last 20 year alone. Emissions from aviation are projected to continue to increase over the coming decades, from the 4.3 billion airline passengers in 2018 to 10 billion in 2040. However, limiting global warming to 2ºC, if not 1.5ºC as per the Paris Agreement, would require drastic emission reductions across all sectors. Providing direction for the transformation of the global aviation sector warrants a solid understanding of the fleet and its composition, alternative fuel options, and the environmental impacts caused by the industry, its system and airplanes, as well as the emerging low carbon technologies.

The main task of this thesis is to perform a full life cycle analysis (LCA) of conventional jet fuel, kerosene, versus alternative fuel options, e.g. synthetic fuel or biofuel. The 'well-to-wake' emission factors may then be incorporated in the fleet stock cohort model developed during the project work. To enable the identification of transformation pathways for the aviation sector, we rely on our understanding of the underlying aircraft fleet dynamics, which is driven by different demand scenarios. A subset of more generic aircraft types can be derived from data (e.g. BADA) and provide higher level detail for the fleet scenario model.

The following tasks are to be considered:

- Collect data on fuel production processes and aircraft type characteristics
- Develop a LCI of jet fuels
- Integrated assessment applying the LCA, with a comparative analysis of the results.
- Create generic aircraft types
- Update future scenarios from fleet model.

Supervisor: Helene Muri

Co-supervisors: Anders Hammer Strømman, Jan Klenner.

The student will have licenced access to the following software and data for the duration of the work:

The LCA software ARDA including the Ecoinvent database for the duration of the thesis work.

The BADA database on aircraft profiles for the duration of the thesis work.

Abstract

The aviation sector is currently responsible for 2.5% of global CO_2 emissions and 5% of net anthropogenic warming, and the sector's emissions are expected to further increase with the increasing air travel demand. Effective mitigation measures are required to ensure large-scale emissions reductions while simultaneously covering the increase in air travel demand. This thesis conducts a LCA of fossil jet fuel and two types of synthetic power-to-liquid (PtL) jet fuels to compare their environmental performance and climate change contributions. In addition, a set of nine generic aircraft representations has been derived from the BADA database. The generic aircraft representations and the LCA results are used to update the aircraft stock cohort model developed in the project pre-phase of the thesis. The updated model proves a higher resolution in the simulation results and quantifies the emission reduction potential of PtL jet fuels on a fleet-wide scale. The LCA results showed a GWP of 94.0 g CO_2-eq/MJ for fossil jet fuel, compared to a GWP of 19.9 and 22.2 g CO_2-eq/MJ for the PtL jet fuels. Implementation of the LCA results in the aircraft stock cohort model showed that using 100% PtL jet fuel in 2050 would reduce the fleet-wide CO_2 emissions by 1524-1591 Mt CO_2/year. High electricity consumption in PtL jet fuel production makes the 30% blend predicted by IEA more feasible, resulting in a reduction of 457-477 Mt CO_2/year in 2050. Including the generic aircraft representations uncovered the importance of the versatile A5A aircraft representation in the future fleet. Despite only representing nine aircraft types in the fleet, the A5A aircraft representation covers 31% of the air travel demand, 43% of the fleet, and is responsible for 24% of the emissions in 2050. The largest aircraft representations, A6-A8, hold a crucial role in the future by representing 21% of the fleet, covering 48% of the demand and being responsible for 57% of the CO_2 emissions in 2050. The simulation results of the updated aircraft stock cohort model show that the use of PtL jet fuels can be a step towards reducing emissions from the aircraft fleet. However, a comprehensive transformation of the entire sector is needed to lower future emissions from aviation substantially.

Samandrag

Luftfartssektoren står per i dag for 2,5 % av verdas årlege CO_2 utslepp og 5 % av det årlege bidraget til global oppvarming. Det er forventa at utslepp frå sektoren fortset å auke i takt med aukande flytrafikk. Effektive utsleppsreduserande tiltak må til dersom store utsleppskutt skal gjennomførast samtidig som flytrafikken skal fortsette å auke. Denne avhandlinga gjennomfører ein livsyklusanalyse av fossilt flydrivstoff, samt to typar syntetiske kraft-til-væske (PtL) flydrivstoff, for å samanlikne deira miljømessige eigenskapar og klimaendringspotensiale. I tillegg har eit sett med flyrepresentasjonar blitt utvikla ved bruk av BADA databasen. Både flyrepresentasjonane og resultata frå livssyklusanalysen har blitt inkludert i bestandskullmodellen utvikla i prosjektoppgåva for å oppdatere modellen. Den oppdaterte modellen gjev difor simuleringsresultat med ei høgare oppløysing og kvantifiserer utsleppsreduksjonspotensialet til PtL flydrivstoffa i stor skala. Resultata frå livssyklusanalysen viser eit potensial for global oppvarming (GWP) på 94 g CO_2-ekv/MJ for fossilt flydrivstoff. For dei syntetiske PtL flydrivstoffa vart dei tilsvarande resultata på 19.9 og 22.2 g CO_2-ekv/MJ. Implementeringa av resultata frå livssyklusanalysen i bestandskullmodellen avdekka at dersom 100% av alt drivstoffbruk frå verdas flyflåte var PtL flydrivstoff i 2050, så ville dette ført til utsleppsreduksjonar på 1524-1591 Mt CO_2/år. Høgt elektrisitetsforbruk i produksjonen av PtL flydrivstoff gjer at ein andel på 30%, i tråd med IEA sine anslag, er meir realistisk for 2050. Dette vil føre til utsleppsreduksjonar på 457-477 Mt CO_2/år i 2050. Ved å inkludere flyrepresentasjonane i bestandskullmodellen vart den sentrale rolla til flyrepresentasjon A5A tydeleggjort som ei viktig og allsidig brikke i den framtidige flyflåten. Til tross for at flyrepresentasjon A5A berre representerer ni flytypar i den globale flåten, så dekker den 31% av flytrafikken, 45% av alle flya i flåten og er ansvarleg for 24% av CO_2 utsleppa i 2050. Dei tre største flyrepresentasjonane, A6-A8, speler òg ei sentral rolle ved å representere 21% av flyflåten, dekke 48% av flytrafikken og vera ansvarleg for 57% av CO_2 utsleppa frå flyflåten i 2050. Resultata frå modellen viser at bruk av PtL flydrivstoff kan vera eit steg i riktig retning for å redusere utsleppa frå global flyfart. Til tross for dette er det tydeleg at ein heilskapeleg transformasjon av heile sektoren må til for å oppnå utsleppsreduksjonar i stor skala frå global luftfart.

Preface

This thesis is written in the spring of 2021 at the Department of Energy and Process Engineering and concludes my master's degree in Energy and Environmental Engineering at the Norwegian University of Science and Technology (NTNU).

To my supervisor Helene Muri, I would like to express my gratitude for the excellent guidance this past year. I want to thank my co-supervisors, Professor Anders Hammer Strømman, for sharing his unique insights and Jan Klenner for helpful discussions throughout the semester. I would also like to thank Lorenzo Usai for all the good answers to my LCA-related questions.

Contents

List of Figures

List of Tables

Abbreviations

A4A	Airlines for America
ASCII	American Standard Code For Information Interchange
ASTM	American Society for Testing and Materials
ATAG	Air Transport Action Group
BADA	Base of Aircraft Data
BMWi	Federal Ministry for Economic Affairs and Energy in Germany
CORSIA	Carbon Offsetting and Reduction Scheme for International Aviation
DAC	Direct Air Capture
EC	European Commision
EPRS	European Parliamentary Research Service
FT	Fischer-Tropsch
FTK	Freight Tonne Kilometer
GDP	Gross Domestic Product
GHG	Greenhouse Gas
GtL	Gas-to-Liquid
HEFA	Hydroprocessed Esters and Fatty Acids
HT	High-temperature
IATA	International Air Transport Association
ICAO	International Civil Aviation Organization
ICCT	International Council on Clean Transportation
IEA	International Energy Agency

IPCC	Intergovernmental Panel on Climate Change
ISO	International Organization for Standardization
LBST	Ludwig-Bölkow-Systemtechnik Gmbh
LCA	Life Cycle Assessment
LCI	Life Cycle Inventory
LCIA	Life Cycle Impact Assessment
NTNU	Norwegian University of Science and Technology
PtL	Power-to-Liquid
RCP	Representative Concentration Pathways
RPK	Revenue Passenger Kilometer
SOEC	Solid Oxide Electrolysis Cell
SSP	Shared Socioeconomic Pathways

1 Introduction

1.1 Background and motivation

Climate change and its effects on human and natural systems is the most significant issue of our time. Since pre-industrial times, anthropogenic greenhouse gas (GHG) emissions have led to a global temperature rise of 1°C (IPCC, 2018a). The effects of human-induced warming are already causing a higher intensity and frequency of extreme weather events, as well as observable impacts on land and ocean ecosystems and the services they provide. Some examples of climate-related risks of human and natural systems are biodiversity loss, species extinction, sea-level rise, food insecurity, damage to human health, extreme weather events, and loss of ecosystems. The climate-related risks and the severity of the impacts increase with global temperature rise and will depend on the rate and duration of warming, as well as the peak temperature (IPCC, 2018b).

Continued warming will cause long-lasting changes in the climate system and cause severe and irreversible impacts on humans, wildlife, and ecosystems. If no action is taken to reduce global GHG emissions, the global mean temperature is expected to increase to 3.7-4.8 °C by 2100, compared to pre-industrial times. This temperature increase would lead to vastly extensive impacts on humans and wildlife worldwide. The global temperature largely depends on cumulative CO_2 emissions, stressing the need for immediate action to be taken (IPCC, 2014b). In 2015, over 190 parties entered into the Paris agreement, intending to limit global warming to well below 2°C and to pursue efforts of limiting warming to 1.5°C. Limiting global warming to below 2°C, if not 1.5°C, requires extensive GHG emission reduction from all economic sectors.

The RCP scenarios are a useful way of describing the relationship between global GHG emissions and human-induced warming. They are frequently used in research and climate modeling and supply a range of global radiative forcing values in 2100 (Van Vuuren et al., 2011). Radiative forcing is a result of GHG emissions and their concentration in the atmosphere, air pollution, and land use (IPCC, 2014a). The scenarios are numbered by their representative radiative forcing levels in 2100 and are associated with different levels of global warming. Similarly, SSP scenarios describe different pathways of socioeconomic

development towards 2100. They assume no impacts of climate change and are a combination of technological development and a narrative storyline (O'Neill et al., 2014). Together, the two scenario types can be combined into SSP-RCP scenarios to describe socioeconomic development related to different levels of global warming. Scenarios SSP1-19 and SSP1-26 represent the emissions pathways where global warming is limited to 1.5°C and below 2°C, respectively. SSP2-45 represent an intermediate scenario, while SSP5-85 represent a high emissions scenario (IPCC, 2014a).

The aviation sector represents a fast-growing economy in an increasingly globalized world. Over the last six decades, the overall growth of the sector has been immense. From 1960 to 2018, the number of revenue passenger kilometers (RPK) performed has risen from 109-8269 billion. In 2018, the associated CO_2 emissions of this activity were responsible for approximately 2.5% of the global CO_2 emissions (D. S. Lee et al., 2020). Including effects of non-CO_2 emissions from aviation, the induced warming from the sector is responsible for 5% of human-induced global warming (D. S. Lee et al., 2009). Although facing a large decline in air travel due to the COVID-19 pandemic, the aviation sector is predicted to recover post-pandemic and continue to grow in the future (Czerny, Fu, Lei, & Oum, 2021). The already substantial GHG emissions from the aviation sector are expected to continue to rise, in line with the increase in air travel demand. Projections from the International Civil Aviation Organization (ICAO) estimate that air travel will more than double the levels of 2018, reaching more than 20 000 RPK in 2045 (ICAO, 2018). These numbers underline the importance of implementing effective emission reduction measures in the aviation sector.

Two long-term aspirational goals aim to reduce emissions from the aviation sector. They consist of achieving carbon-neutral growth in the aviation sector from 2020 and improving fuel efficiency by 2% per year through 2050. (ICAO, 2019b). There are four main measures to mitigate emissions from the aircraft fleet: Enhancing aircraft technology, improved operations, alternative jet fuels, and carbon offsetting. Operational improvements can be implemented right away, while technical enhancements are subject to the fleet turnover rate and are therefore more gradually introduced. International aviation is not a part of the global climate regime. Therefore, ICAO created a Carbon Offsetting, and Reduction Scheme for International Aviation called CORSIA, which is a market-based measure targeting emissions from aviation (ATAG, 2019). Through CORSIA, the aviation sector can offset any growth in emissions beyond 2020 levels while pursuing the emission reduction measures mentioned above.

Alternative jet fuels are the measure with the largest potential of reducing the level of CO_2 emitted by the aircraft fleet and is an essential part of pursuing the aspirational goal of carbon-neutral growth from 2020 (ICAO, 2019c). In addition to having the most

significant potential, alternative jet fuel's drop-in capability makes it possible to reduce emissions without any technical moderation of the aircraft. The International Energy Agency (IEA) estimates that 75% of the total fuel consumption of the aircraft fleet in 2050 must be alternative jet fuels for the aviation sector to comply with the global net-zero targets of 2050. A firm understanding of the life cycle emissions of alternative jet fuels, the development of the aircraft fleet, and the underlying fleet dynamics is essential to provide direction for the needed transformation of the aviation sector.

1.2 State of the art

The following subsections give an overview of previous studies conducted on the subject matter. First, literature investigating alternative jet fuels under the LCA framework is highlighted, followed by previous studies investigating the sector's aircraft fleet development and GHG emissions. Finally, the research gap is established.

1.2.1 Life cycle assessment of jet fuels

Currently, fossil jet fuel makes up more than 99% of total fuel consumption by the aircraft fleet (EPRS, 2020). Well-to-wake life cycle GHG emissions from fossil kerosene are well established. While the combustion emissions are fixed, the well-to-tank emissions largely depend on the crude oil composition used in the production process (EC, 2015). Fossil jet fuel represents the benchmark of which alternative jet fuels must outperform to reduce emissions. Alternative jet fuels can be divided into two main categories: bio-jet fuels and synthetic jet fuels.

Bio jet fuel is a large field to cover due to many possible production pathways, feedstocks used, and the combinations between the two. Therefore, countless life cycle assessments have been conducted on this subject. Bio-jet fuel conversion pathways can be split into four categories: Alcohol-to-Jet, Oil-to-Jet, Gas-to-Jet, and Sugar-to-Jet (W.-C. Wang & Tao, 2016). Alternative jet fuel used in commercial aviation must be ASTM approved. The Hydroprocessed Esters and Fatty Acids (HEFA) and the Fischer-Tropch (FT) pathways are the two approved pathways with the highest technical readiness level (de Jong et al., 2017). Both HEFA and FT jet fuel can be used in commercial aircraft, up to a 50% blend with fossil jet fuel.

The life cycle assessments of bio-jet fuel are split on one key aspect. Some studies include emissions caused by direct land-use change, like (Bailis & Baka, 2010), (Stratton, Wong, Hileman, et al., 2010), (Stratton, Wong, & Hileman, 2011) and (Han, Elgowainy, Cai, & Wang, 2013), while others exclude emissions from land-use change all together, like (Fortier, Roberts, Stagg-Williams, & Sturm, 2014), (Elgowainy et al., 2012), (De Jong

et al., 2017), (Cox, Renouf, Dargan, Turner, & Klein-Marcuschamer, 2014) and (Dunn, Mueller, Kwon, & Wang, 2013). The inclusion or exclusion of land-use change represents an important divider in the literature. The impacts from direct land-use change can significantly influence the result of the LCA and, thereby, the environmental performance of the bio-jet fuel. The effects of land-use change are case-specific, and the associated emissions can, in some cases, negate the environmental benefits of the bio-jet fuel.

The body of literature on synthetic fuels, also called Power-to-Liquids (PtL), is not as extensive, especially for PtL jet fuel. Part of the reason is that no large-scale PtL jet fuel plant is in operation, although several are planned, one of which will be situated at Porsgrunn in Norway (Krohn-Fagervoll, 2020). In 2016 the Ludwig-Bölkow-Systemtechnik Gmbh (LBST) wrote a report on behalf of the German Environment Agency, which looked at the potentials for PtL jet fuels to be a future supply of renewable aviation fuel. (Schmidt, Weindorf, Roth, Batteiger, & Riegel, 2016). The report compares PtL jet fuels with bio-jet fuel on GHG emissions, water demand, land use, and cost. The report shows that the PtL jet fuels, produced using renewable electricity, emits far less CO_2-eq/MJ than any of the bio-jet fuel options. Figures from the report can be found in other literature, where they are used to back up the claim of environmental performance (Roth & Schmidt, 2017), (Schmidt, Batteiger, Roth, Weindorf, & Raksha, 2018), (ICAO, 2020). However, the LBST report assumes that the electricity from renewable sources used in the production of hydrogen and direct air capture (DAC) of CO_2 have no associated GHG emissions. It also excludes emissions from construction, which leaves only GHG emissions occurring in transportation, distribution, and dispensing (Schmidt et al., 2016). These assumptions do not represent the full life cycle and show the importance of investigating PtL jet fuel using the LCA framework.

Several studies look at other PtL fuels than jet fuel or individual production segments, like hydrogen and synthetic gas (syngas) production. They still provide useful information about the production of PtL jet fuel, as parts of the production are covered. The study by (van der Giesen, Kleijn, & Kramer, 2014) performs a well-to-wake LCA of synthetic hydrocarbons produced using PV electricity, hydrogen produced from alkaline electrolysis, and CO_2 captured from a concentrated source. The studies by (Schreiber, Peschel, Hentschel, & Zapp, 2020) and (Lozanovski & Brandstetter, 2015) perform life cycle assessments on high-temperature co-electrolysis, which produce syngas in a single step, using different electricity sources. (Schreiber et al., 2020) compare power-to-syngas with steam methane reforming, while (Lozanovski & Brandstetter, 2015) use the syngas to produce synthetic hydrocarbons in a PtL demonstration plant in Germany called Sunfire. LCAs covering various hydrogen production methods using renewable energy sources have, amongst others, been conducted by (Koroneos, Dompros, Roumbas, & Moussiopoulos, 2004), (Utgikar & Thiesen, 2006) and (Cetinkaya, Dincer, & Naterer, 2012).

1.2.2 Future aircraft fleet development and emissions

On a more aggregated level, many publications calculate the CO_2 emissions of the global aircraft fleet. There are mainly two approaches used when doing so. The first approach, used by (Sausen & Schumann, 2000) and continued by (D. S. Lee et al., 2009) and (D. S. Lee et al., 2020), estimate total CO_2 emissions based on the global jet fuel sales and the stoichiometric relationship between CO_2 and jet fuel in combustion. The second approach requires more collection of data by using civil aviation inventories to calculate emissions. This approach have been used by (Baughcum, Henderson, & Tritz, 1996), (Schmitt & Brunner, 1992), (Wilkerson et al., 2010), (J. J. Lee, Lukachko, Waitz, & Schafer, 2001), (Kim et al., 2007), (Schaefer, Jung, & Pabst, 2013), (Graver, Zhang, & Rutherford, 2019a) and (Graver, Zhang, & Rutherford, 2020). There is an established discrepancy between the two calculation methods of around 10% (D. S. Lee et al., 2020). Emission calculations using fuel sales are higher than when using civil aviation inventories. By default, fuel sales include all emissions by non-scheduled traffic and military operations, which are mostly excluded from aviation inventories due to lack of available data or because it is outside the scope of the study. In a survey by (Hoesly et al., 2018), the two approaches are combined to capture the emissions of the entire aircraft fleet, including non-scheduled and military operations, as well as covering the fleet turnover effects and technical developments, providing a holistic understanding of the CO_2 emissions of the fleet.

Simulations of the future development of the aircraft fleet and the associated CO_2 largely depend on projections and scenarios used in the modeling. A report by (IATA, 2019) is a good example. Here, three future air travel demand scenarios are included and ten scenarios for future technical development, creating a large span of future developments. The baseline scenario of (IATA, 2019), which project future development based on historical trends in GDP, flying cost, and demographics is a good match to the fleet development found in (Schaefer et al., 2013). Combined, they form a reference for future fleet development and associated emissions. The two largest aircraft manufacturers, Boeing and Airbus, release yearly reports on the current state and future forecast of the aircraft fleet (Boeing, 2020b), (Airbus, 2019a). Several studies also give estimations on future development of CO_2 emissions from aviation, without simulating the development of the aircraft fleet (Schmitt & Brunner, 1992), (Eyers et al., 2004), (Owen & Lee, 2006) and (Owen, Lee, & Lim, 2010).

1.2.3 Research gap

According to the International Energy Agency's net-zero by 2050 report, the largest share of emission reductions for the aviation sector must come from the use of alternative jet fuels (IEA, 2021). A firm understanding of the different jet fuel options and their associated life cycle emissions is therefore required. The scarce amount of life cycle assessment conducted on PtL jet fuels calls for more research on this topic. Many of the studies mentioned above simulate future aircraft fleet development and associated CO_2 emissions from aviation on a global scale for different future scenarios. However, using LCA results directly in a model of the aircraft fleet and its associated emissions would better the understanding of alternative jet fuels' emission reduction potential on a fleet-wide scale. The resolution of the simulation results of such a model will determine the accuracy of mitigation measures imposed on the aviation sector, which calls for a more refined segmentation of the aircraft fleet.

1.3 Research objective and report structure

In this master thesis, the main objective is to perform a comparative LCA of conventional fossil jet fuel and two synthetic PtL jet fuels. The aircraft stock cohort model developed during the project pre-phase of the thesis will incorporate the well-to-wake CO_2 emissions from the LCA results. The model provides information about possible transformation pathways for the aviation sector by simulating the aircraft fleet development and associated emissions. A set of generic aircraft representations can be derived from the Base of Aircraft Data (BADA) to provide a higher level of detail for the aircraft stock cohort model.

The thesis is divided into eight chapters. The first chapter introduces the background and motivation of the thesis, state of the art, and the research objective and report structure. The LCA methodology is briefly introduced in the second chapter, followed by descriptions of the three product systems assessed. In the third chapter, the method of creating the generic aircraft representations is described. In chapter four, the original aircraft stock cohort model from the project pre-phase is updated by including the generic aircraft representations and the LCA results. Chapter five and six are the two results chapters and present the LCA results and the aircraft stock cohort results. The seventh chapter contains the discussion, followed by the conclusion in chapter eight.

2 LCA methodology and case description

The LCA methodology and case description chapter of this thesis is divided into two sections. In the first section, the LCA methodology used is briefly presented. The second section contains the case descriptions of the three aviation jet fuels that have been analyzed. It presents the functional unit, the system boundaries, the allocation procedure, the data collection, and flowcharts of the product systems.

2.1 Life cycle assessment

Life cycle assessment is an analytic method used to assess the environmental impacts of a product, process, system or service, through the course of its lifetime (ISO, 2006a). The assessment addresses the environmental impacts of all life cycle stages of a product, from the acquisition of raw materials, through production and use, to the end of life treatment, recycling, and final disposal (ISO, 2006b). The LCA framework consists of four phases: Goal and scope definition, life cycle inventory analysis, life cycle impact assessment, and life cycle interpretation. In figure 2.1.1 below, a schematic flowchart of how the four phases interact with each other is presented. The following sections will describe the contents of each phase of the LCA.

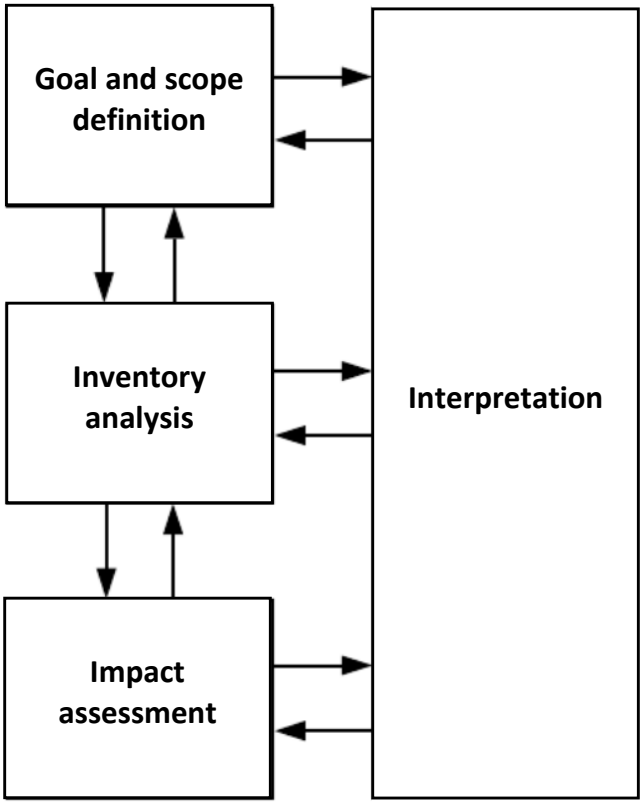

Figure 2.1.1: Framework of the LCA (ISO, 2006a).

2.1.1 Goal and scope definition

The goal and scope definition is the first phase of a life cycle assessment. The goal should clearly state the reason for conducting the LCA, and its possible applications, as well as the intended audience of the study (ISO, 2006b). It should also inform whether or not the results will be used to make comparative statements available to the public. The scope definition describes the extent of the LCA in terms of the product system being analyzed, the functional unit, the system boundaries, and allocation procedures (ISO, 2006b). It also defines the requirements for the data used, which impact categories to investigate and describe the assumptions and limitations of the study.

Functional unit

The functional unit of a life cycle assessment should reflect the function of the analyzed system and act as the reference of which all inputs, outputs, and environmental impacts of the product system are normalized to (ISO, 2006b). A functional unit can be related to energy, weight, distance, or other parameters to reflect the function of the product system. The functional unit quantifies the analyzed product system's performance and should be comparable to similar assessments conducted (ISO, 2006b). The functional unit should be presented in, and be consistent with, the goal and scope definition of the LCA.

System boundaries

The system boundaries specify which processes are included in the LCA and the level of detail to which these processes should be examined (ISO, 2006b). The system boundaries shall be in line with the defined goal and scope of the study and are often presented as a flowchart of the product system. In life cycle assessments, the system boundaries create a divider between the product system and the environment, between the significant and insignificant processes, and between the assessed product system and other product systems (Li, Zhang, Liu, Ke, & Alting, 2014). The system boundaries are often referred to as cradle-to-grave, cradle-to-gate, or cradle-to-cradle. A cradle-to-grave assessment covers the full life cycle from manufacturing through the use phase to the final disposal. Cradle-to-gate is a partial assessment covering processes from manufacture to the gate of the factory. Cradle-to-cradle is a version of the cradle-to-grave assessment where the final disposal is substituted by recycling of the product (Iyyanki, 2017). More specific terms are often used when performing LCA on fuels. Well-to-tank assessments also referred to as well-to-wheel for road transport and well-to-wing for aircraft, are examples of cradle-to-gate system boundaries. Well-to-wake system boundaries include all impacts from extraction and production of the fuel to the fuel is combusted.

Allocation procedures

Inputs and outputs of a product system need to be allocated to the different products being produced. An allocation procedure is required when a process is shared between two or more distinct product systems. Allocation should be avoided whenever possible by splitting the process in question into sub-processes or expanding the product system to include the co-products of the process (ISO, 2006b). The allocation procedure should be chosen to reflect the nature of the product systems. Three of the most common allocation procedures are mass allocation, energy allocation, and economic allocation.

2.1.2 Life cycle inventory analysis

In the life cycle inventory (LCI) analysis phase, all the necessary data is collected and validated for every process included within the system boundaries of the life cycle assessment. The data collection procedure and any calculations performed on the data should be clearly described. The life cycle inventory presents flow charts of the system to be modeled. Input and outputs of the processes are described, together with interrelations between the different processes in terms of flows of energy, materials, substances, and emissions (ISO, 2006b). The LCI analysis quantifies the amounts of materials and land used, in addition to emissions of environmental stressors like CO_2, NO_X, SO_2, etc. Considering the iterative nature of the LCA framework introduced previously in figure 2.1.1, the life cycle inventory analysis is also used to reevaluate the boundaries of the system established in the goal and scope definition.

The Ecoinvent database

Conducting a life cycle inventory analysis requires vast amounts of data to cover the complete supply chain, which calls for the use of background databases. Data needed in the background system to perform a complete LCI analysis is difficult and time-consuming to obtain. Therefore, background databases that contain important information to perform a complete LCI analysis are used. The Ecoinvent background database is currently the largest transparent LCI database in the world (Iyyanki, 2017). It covers all environmental flows of relevance for conducting a LCA, material and energy inputs, and market and transformation processes (Ecoinvent, 2020).

2.1.3 Life cycle impact assessment

The life cycle impact assessment (LCIA) is the fourth phase of the life cycle assessment, which assesses the environmental impacts of the product system relative to the chosen functional unit. Every life cycle impact assessment must include a selection of impact categories, classification, and characterization. The LCIA transforms the results of the life cycle inventory results to the impact categories selected (ISO, 2006b). In line with the framework of the LCA, this phase should evaluate whether the life cycle inventory results provide a sufficient base for performing a life cycle impact assessment, compliant with the goal and scope definition of the study.

LCA software

Many LCA software have been developed to assist the practitioner in performing the LCA. Some of the frequently used software include GaBi and SimaPro. The practitioner incorporates the data collected and the interrelations between the processes in the product system into the LCA software. The software performs a life cycle impact assessment using the input data from the practitioner and a background database, resulting in categorized environmental impacts.

2.1.4 Life cycle interpretation

The life cycle interpretation is the final stage of the life cycle assessment. In this phase, the completeness, sensitivity, and consistency of the assessment are evaluated, and significant issues are identified (ISO, 2006b). Interrelations between the different life cycle phases ensure that the three other phases contribute to identifying the significant issues. The life cycle interpretation phase is also where the conclusions of the LCA are drawn, limitations of the study are described, and possible recommendations are given.

2.2 Case description

The objective of conducting the LCA is to compare the environmental performance of fossil jet fuel and synthetic PtL jet fuel, specifically their climate change contributions. In the first subsections, the scope of the LCA will be presented in terms of functional unit, system boundaries, and allocation procedure. Descriptions of the three analyzed systems with accompanying flowcharts are then presented. The analyzed systems are fossil jet fuel, PtL jet fuel produced using alkaline electrolysis, and PtL jet fuel using high-temperature co-electrolysis. Limitations of the systems, assumptions made, and data sources will also be presented as part of the system descriptions. The final sections will state the tools used in the analysis, outline the life cycle impact assessment methodology used, and highlight the most important impact categories.

2.2.1 Functional unit

The functional unit of the LCA is 1 MJ of jet fuel produced and combusted. All three analyzed systems use the same functional unit. This functional unit is chosen as it makes it easy to compare the climate change contributions of the three systems with each other and previous research on alternative aviation fuels.

2.2.2 System boundaries

The life cycle assessment conducted is a well-to-wake analysis. This term is commonly used to describe the system boundaries of life cycle assessments of aviation fuels. For fossil jet fuel, a well-to-wake analysis should assess all processes from the extraction of crude oil to the combustion of fossil jet fuel in the aircraft engine. In contrast, the PtL systems extract CO_2 from the air and generate hydrogen from water instead of extracting crude oil from a well. For all the processes within the system boundaries, the associated extraction of materials, operation, manufacturing, construction and demolition should be included. The LCA conducted in this thesis does not include end-of-life treatment due to a lack of available data. However, components with a shorter lifetime than the rest of the system are replaced. Most processes are geographically limited to Germany and Europe, with some exceptions, such as crude oil recovery and raw material extraction. The lifetime of all three systems is set to 20 years.

2.2.3 Allocation procedure

There are two main allocation procedures to consider when investigating the environmental impacts of jet fuels. Mass allocation divides the process contribution on the co-products based on their mass fractions. In contrast, energy allocation divides the process contribution based on the energy fractions of the co-products. Testing both allocation methods shows little difference in the overall impacts. Therefore, a conservative approach using mass allocation is chosen to ensure no underestimation of emissions.

2.2.4 LCA software and background database

This life cycle assessment makes use of the LCA software ARDA to perform the computations. It is a NTNU developed software that uses Matlab to carry out the calculations and Excel to set up the product system's requirements and emissions. The Ecoinvent 3.2 database is used as the background database in the assessment.

2.2.5 Fossil jet fuel

The first product system to be analyzed is fossil jet fuel. Currently, more than 99% of total fuel consumption by the aircraft fleet is fossil jet fuel (EPRS, 2020). Therefore, the LCA of fossil jet fuel acts as a natural reference case for comparison with alternative jet fuels and provides an indication of the quality of the LCA set up by comparing the life cycle impacts to well-established values for fossil jet fuel. The fossil jet fuel product system's life cycle consists of six main steps as illustrated in the flowchart presented in figure 2.2.1 below. The first step covers the recovery and extraction of crude oil. In the second and third steps, oil is transported to a refining facility, where it is distilled to different fossil products. Jet fuel is then transported from the refinery to temporary storage before being combusted by the aircraft.

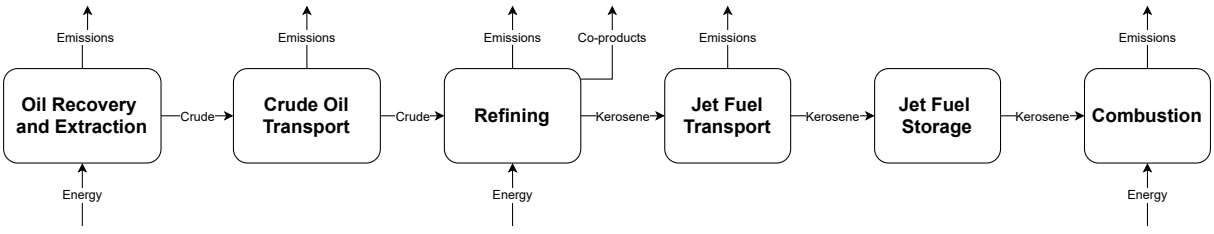

Figure 2.2.1: Flow sheet of the fossil jet fuel product system.

Ecoinvent provides geographically specific processes for oil recovery and extraction. Since the product system, in this case, is placed in Germany, the share of the different oil recovery and extraction processes were percent wise distributed based on the crude oil import and production numbers for Germany given by the federal ministry for economic affairs and energy (BMWi, 2021a). The distribution is presented in table 2.2.1 below.

Table 2.2.1: Annual crude oil imports to Germany averaged over three years (2015-2017) and grouped into available regions in Ecoinvent.

Ecoinvent region	Crude oil imports [Mt/y]	% of total
Great Britain	9.2	9.9
Rest of World	17.5	18.7
Nederland	2.4	2.6
Norway	11.3	12.1
USA	0.6	0.6
Nigeria	5.1	5.5
Region Africa	8.9	9.5
Russland	34.0	36.4
Region Middle East	4.5	4.8

For crude oil transport and jet fuel transport and storage, average values for transport distances in EU and US are used respectively (De Jong et al., 2017). Jet fuel refining is also given as an Ecoinvent process, reducing some of the data collection needed to perform the LCA of this product system. An average kerosene refinery efficiency of 92.2% was used when performing the LCA (M. Wang, Lee, & Molburg, 2004). Emissions from combustion of fossil kerosene jet fuel is well known, with CO_2 holding the largest share of the emissions at 3.16 kg CO_2/kg jet fuel combusted (Braun-Unkhoff, Riedel, & Wahl, 2017).

2.2.6 PtL jet fuel using alkaline electrolysis and wind power

The first power-to-liquid (PtL) product system analyzed uses alkaline electrolysis to produce hydrogen and mixes it with carbon monoxide made from carbon dioxide captured from the air to create syngas. The syngas is then processed in a gas-to-liquid (GtL) plant through a Fischer-Tropsch (FT) process, creating finished products like synthetic jet fuel. The FT process was chosen because it has the highest technical readiness level of the possible pathways and is already ASTM approved to be used in commercial aircraft as a 50% blend with fossil jet fuel (de Jong et al., 2017). An alkaline electrolyzer is used in hydrogen production. It is a state-of-the-art electrolyzer, which is commercially available on an industrial scale (Dincer & Acar, 2015). Wind power was chosen as the electricity source because the plant location is set to Germany, where wind power has the biggest share of the renewable energy production (BMWi, 2021b).

The analyzed PtL system is largely adopted from a paper by (van der Giesen et al., 2014) and is presented as a flow sheet with belonging input requirement per unit output for each process in figure 2.2.2 below. The direct air capture unit used is from Climeworks AG, one of the leading developers of DAC units across the globe (Schreiber et al., 2020). The efficiency of the alkaline electrolyzer of this PtL system is a conservative 59%. Due to a lack of data on combustion emissions from PtL jet fuels, the combustion data for fossil jet fuel is used. This assumption will be accurate for CO_2 emission. Still, it can lead to an overestimation in emissions of, for instance, SO_2 as fossil jet fuel has a higher sulfur content than synthetic jet fuels (Hileman & Stratton, 2014).

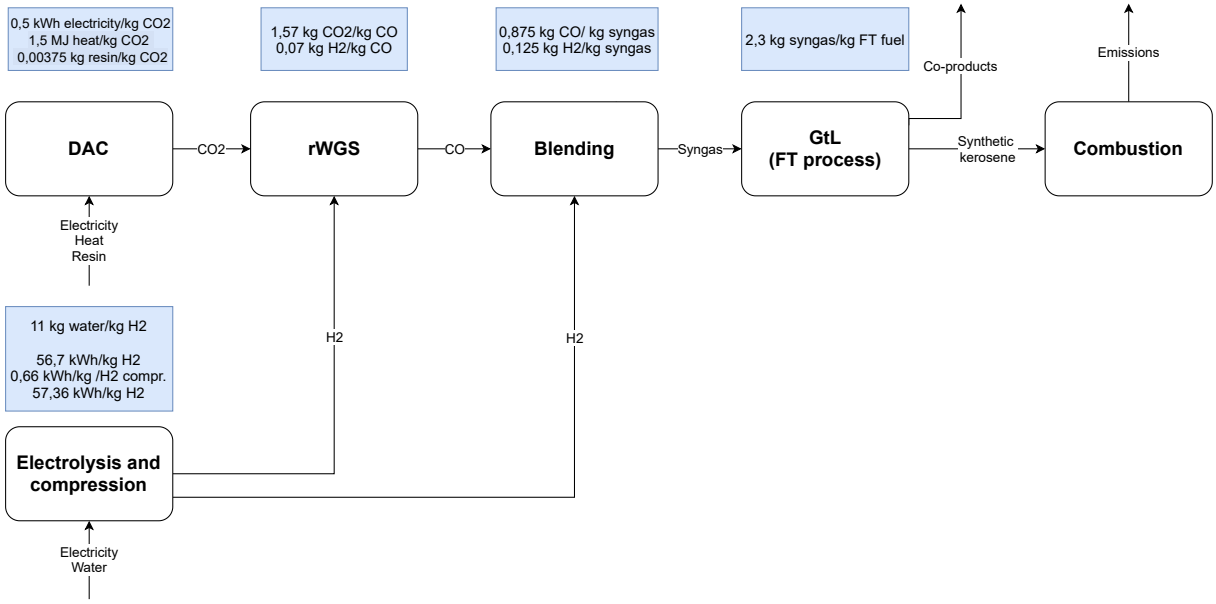

Figure 2.2.2: Flow sheet of the PTL jet fuel system with alkaline electrolysis using wind power. The blue boxes presents the input requirement per unit output for each process.

Construction is accounted for in all steps of production. The data used can be found in appendix C. The lifetime of the PtL system is set to 20 years, which is equal to the lifetime of the DAC unit. Parts with a shorter life span, like the electrolyzer, are replaced when they reach the end of life.

2.2.7 PtL jet fuel using high-temperature co-electrolysis and wind power

The second power-to-liquid product system that is analyzed differs from the previous one by using high-temperature (HT) co-electrolysis to produce syngas directly from H_2 and CO_2. CO_2 is still captured using the same DAC unit as the previous PtL system, and the syngas is processed in the same GtL plant. HT co-electrolysis uses solid oxide electrolyzer cells. These cells are at a lower technology readiness level than alkaline electrolysis (Dincer & Acar, 2015). The HT co-electrolysis is included in this LCA to compare available technology with a system of higher efficiency that would likely be available in the near future but have not been built on a commercial scale as of yet (Schreiber et al., 2020).

This PtL system is primarily adopted from (Schreiber et al., 2020) and a flow sheet of the system with belonging input requirements per unit of output of each process is presented in figure 2.2.3 below. The analyzed HT co-electrolyzer is 150 kW and produces syngas using water and CO_2 as inputs with an efficiency of 75%, which is noticeably higher than the hydrogen production efficiency of the alkaline electrolysis of 59%. The GtL plant is the same as the for the alkaline PtL system and is based on numbers from an operating GtL plant located in Qatar (van der Giesen et al., 2014).

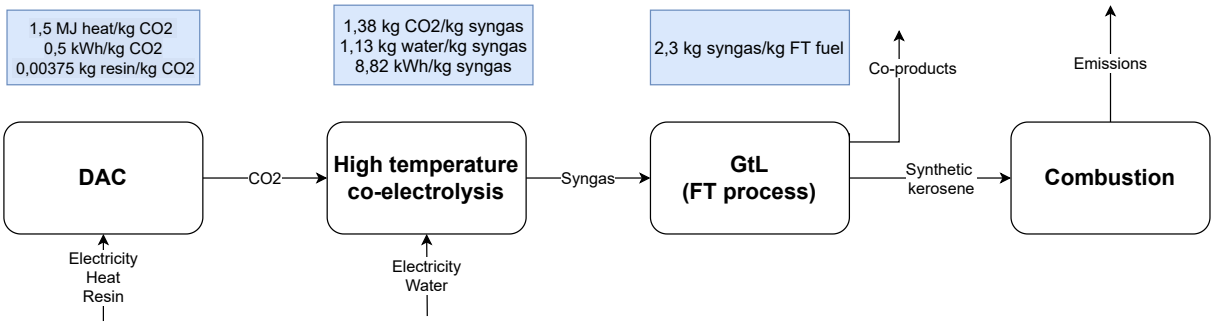

Figure 2.2.3: Flow sheet of the PtL jet fuel system with high temperature co-electrolysis using wind power. The blue boxes presents the input requirement per unit output for each process.

Construction is accounted for in all steps of production. The data used can be found in appendix C. The lifetime of the PtL system is set equal to the alkaline PtL system at 20 years. Parts with a shorter lifespan are replaced when they reach the end of life.

2.2.8 LCIA methodology and impact categories assessed in the analysis

The method used to transform the life cycle inventory analysis results into a limited number of impact categories is called the ReCiPe method. In the life cycle impact assessment, the environmental stressors calculated in the LCI analysis are transformed to 18 midpoint impact categories using the ReCiPe method (Goedkoop et al., 2009). The 18 midpoint impact categories cover a wide range of environmental impacts and are presented in table 2.2.2 below with their respective abbreviations and units. The ReCiPe method further converts the impacts at the midpoint level to impacts at the endpoint level. The endpoint categories cover damages to human health, ecosystem diversity, and resource availability (Goedkoop et al., 2009). The main impact category to be assessed in this thesis is the global warming potential (GWP) impact category. The GWP quantifies the climate change contribution of the product system, which is the main objective to assess in this LCA.

Table 2.2.2: Overview of midpoint impact categories (Goedkoop et al., 2009)

Impact Category	Abbreviation	Unit
Agricultural land occupation potential	ALOP	m^2*year
Global warming potential	GWP	kg CO_2 eq
Fossil depletion potential	FDP	kg oil eq
Freshwater ecotoxicity potential	FETP	kg 1,4-DB eq
Freshwater eutrophication potential	FEP	kg P eq
Human toxicity potential	HTP	kg 1,4-DB eq
Ionising radiation potential	IRP	kg U^{235} eq
Marine ecotoxicity potential	METP	kg 1,4-DB eq
Marine eutrophication potential	MEP	kg N eq
Mineral depletion potential	MDP	kg Fe eq
Land transformation potential	LTP	m^2
Ozone depletion potential	ODP	kg CFC-11 eq
Particulate matter formation potential	PMFP	kg PM_{10} eq
Photochemical oxidant formation potential	POFP	kg NMVOC
Terrestrial acidification potential	TAP	kg SO_2 eq
Terrestrial ecotoxicity potential	TETP	kg 1,4-DB eq
Urban land occupation potential	ULOP	m^2*year
Water depletion potential	WDP	m^3

3 | Generic aircraft representations

In this second method chapter, the method used for creating generic aircraft representations of the existing aircraft fleet is presented and explained together with the assumptions and choices made in the process. The goal of creating generic aircraft representations of the current aircraft fleet is to update the aircraft stock cohort model to cover a larger number of aircraft types. This update will provide a higher resolution of the aircraft fleet, the air travel demand, fuel consumption, and CO_2 emissions. The chapter is divided into three sections. First, the BADA database containing information on individual aircraft is introduced. The second section establishes how the aircraft have been clustered using the K-means algorithm, and the third section presents the final generic aircraft representations.

3.1 BADA database

The data used to create the generic aircraft representations comes from the Base of Aircraft Data (BADA) provided by the European Organisation for the Safety of Air Navigation, also known as Eurocontrol (Eurocontrol, 2019, 2020). Access to the BADA database is obtained through a license agreement, as the data is unavailable to the public. Information about the aircraft is provided as sets of ASCII files for 250 different aircraft. The files contain all technical data of the aircraft and its engines. In total, there are 89 parameters per aircraft, such as the reference mass of the aircraft, the maximum carrying capacity of the aircraft, the surface area of the wing, the maximum operating speed, thrust specific fuel consumption coefficients, etc. Some files contain information on military aircraft and have been excluded, as it is beyond the scope of this work, reducing the aircraft types to 242.

3.2 K-means clustering

Creating new subsets of an existing data set through clustering is a common approach, which many clustering algorithms can perform. K-means is one of the most well-known clustering algorithms, which partitions data into subsets by minimizing the clustering

error through an iterative process (Likas, Vlassis, & Verbeek, 2003). It is available as an integrated function in Matlab and allows the user to choose the desired K number of clusters that the data set should be divided into. The algorithm starts with K arbitrary points, which represent the initial cluster centers. From this starting point, the algorithm iteratively moves the cluster centers to minimize the clustering error, in Euclidean distance, between the cluster center and the data points in the cluster. The procedure leaves the data set divided into K clusters, where the cluster center represents the average value of the cluster and is called a centroid. K-means is considered a very applicable and fast algorithm but is sensitive to the initial positioning of the cluster centers (Likas et al., 2003).

3.2.1 Clustering parameters

There are 89 parameters per aircraft in the BADA database, which can be used as inputs for the K-means clustering algorithm. The parameters used to cluster the aircraft should show a spread in the data for the different aircraft, such that the clusters represent aircraft with distinct characteristics. Clustering parameters should also be relevant to the aircraft stock cohort model, dividing the fleet into specific fleet segments. To examine the data spread, standard deviation and mean absolute deviation were calculated for all parameters. The clustering parameters were then chosen based on relevance and spread of data among the different aircraft. This selection resulted in five clustering parameters: reference mass, maximum takeoff mass, max payload mass, aircraft cruise speed, and the engine type. These parameters contain information about the size of the aircraft, the carrying capacity of passengers or freight, aerodynamic properties of the aircraft, and fuel consumption.

3.2.2 Number of clusters

The number of clusters can be chosen when using the K-means algorithm. A procedure called the elbow method can be used to indicate the optimal number of clusters. The elbow method calculates the percentage of variance explained for different numbers of clusters to find the number K, where adding another cluster does not improve the modeling of the data (Bholowalia & Kumar, 2014). This point should be represented as an "elbow" when the percentage of variance is plotted as a function of the number of clusters. Figure 3.2.1 below presents the elbow-plot for the clustering parameters chosen in the previous section. In this case, the "elbow" is a more gradual transition than an obvious breaking point, but the figure still indicates that the optimal number of clusters is somewhere between 5-10. Beyond 10 clusters, there is little room for improvement and rather increases computational cost. The elbow method was used together with some testing of different values for K to choose the final number of clusters to be $K = 8$.

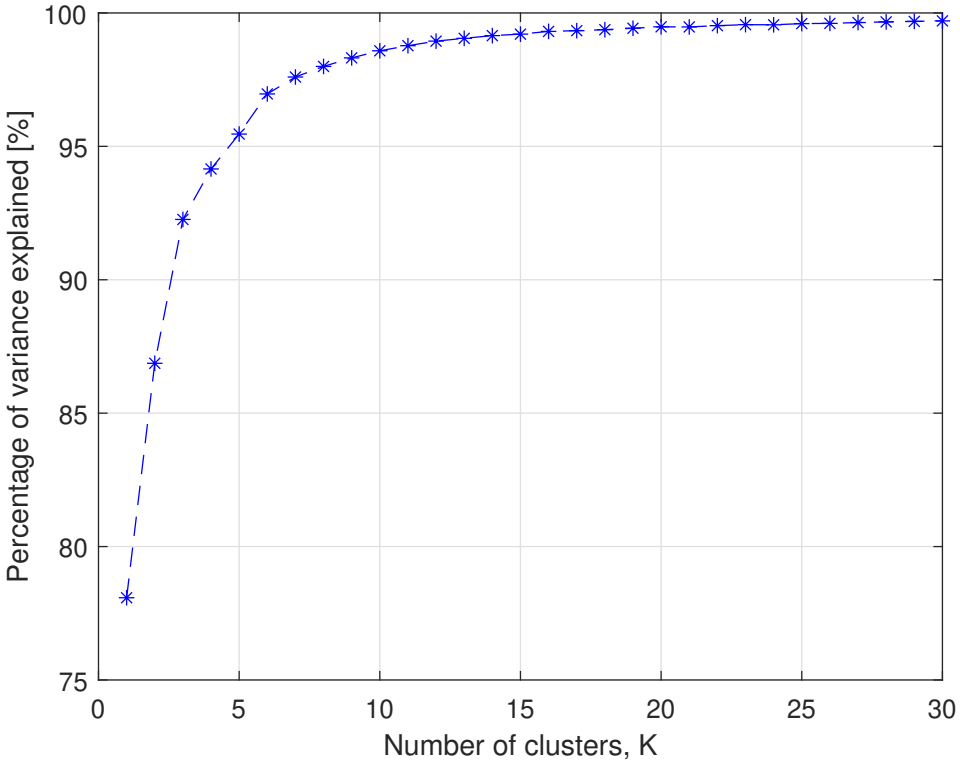

Figure 3.2.1: Percentage of variance as a function of the number of clusters. This is referred to as an elbow-plot, where the elbow of the graph indicate the optimal number of clusters.

3.2.3 Final clusters

The final clusters are created with the K-means algorithm in Matlab using the clustering parameters described in section 3.2.1 and $K = 8$ as the number of clusters. Figure 3.2.2 below present the clustering graphically for some of the clustering parameters. All the data is plotted with the reference mass of the aircraft on the x-axis and with maximum takeoff mass, maximum payload mass, aircraft cruise speed on the y-axis of rows one, two, and three, respectively. The left column displays the unclustered data, while the right column presents the same data color-coded to show the eight clusters of aircraft clearly. The figure shows that the K-means algorithm can divide the 242 aircraft into eight clusters with similar properties. It also shows the relationship between the different properties of the aircraft. Reference mass and maximum takeoff mass are linearly related. Higher reference mass also leads to higher carrying capacity in the form of maximum payload mass. The aircraft cruise speed increases with increasing reference mass for lighter aircraft before flattening out at a level of around Mach 0.8.

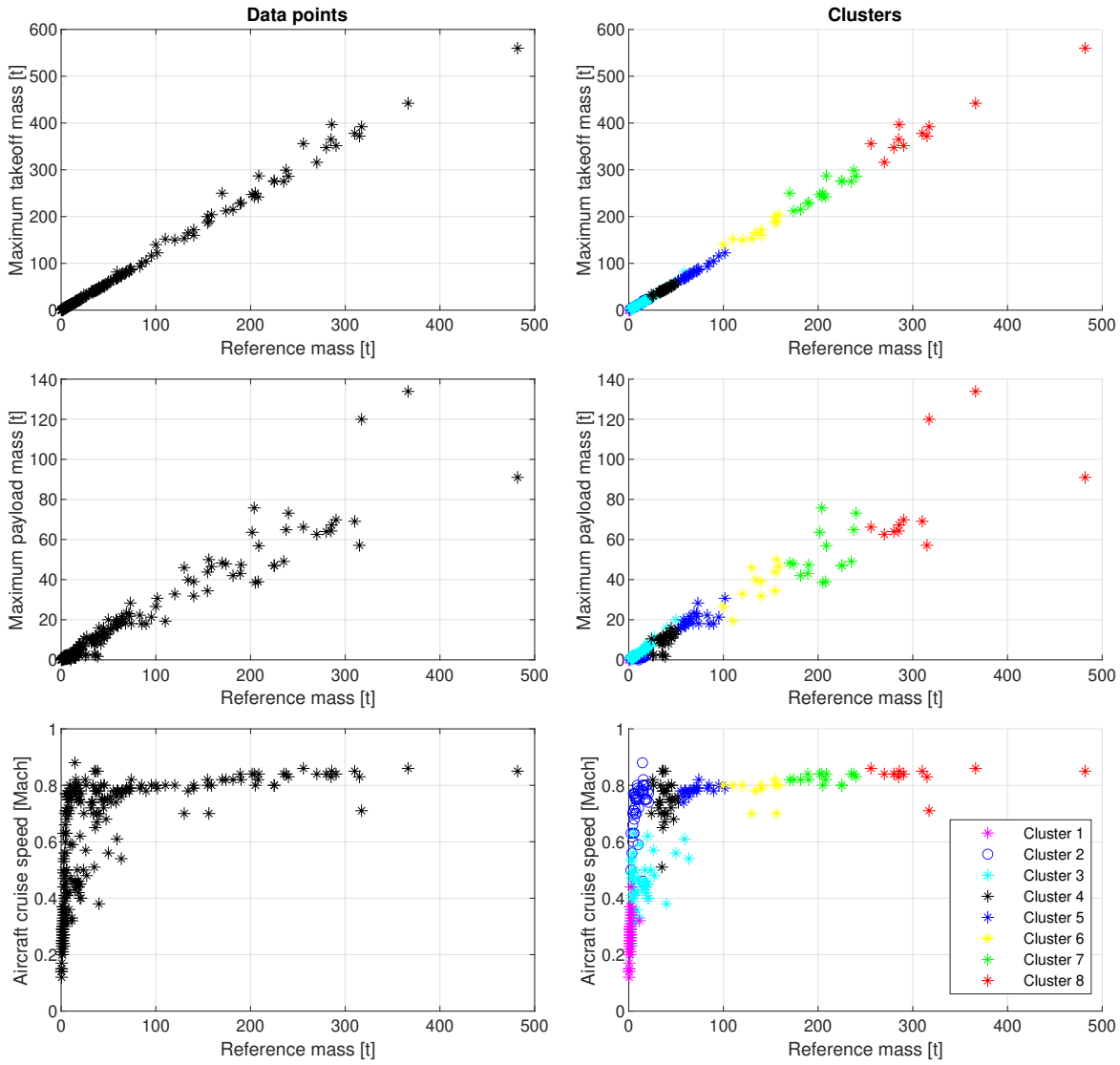

Figure 3.2.2: Clustering of aircraft based on reference mass [t], maximum takeoff mass [t], maximum payload mass [t], cruise speed [Mach] and engine type using the K-means algorithm. The left column display unclustered data while the right column display the color coded clustered data.

The parameters' range within the clusters and the clusters' centroids for each parameter are displayed below in table 3.2.1 for the clustering parameters. It shows the range within the different clusters and the average value calculated by the K-means algorithm. The clusters are sorted based on the reference mass. The engine type is not shown in this table as it is not a parameter giving a range or an average value when clustered. Cluster 1 are piston aircraft, cluster 3 are turboprop aircraft, while the rest are jet aircraft. The parameters show that carrying capacity increase with the increase in reference mass, while the cruise speed is more dependent on the engine type, as can be seen from the low cruising speed clusters 1 and 3.

Table 3.2.1: Range and centroids for the clustering parameters for all eight clusters. The range is displayed first, followed by the centroid value in parenthesis.

Cluster number	Reference mass [t] range, (centroid)	Max takeoff mass [t] range, (centroid)	Max payload mass [t] range, (centroid)	Cruise speed [Mach] range, (centroid)
Cluster 1	0-11 (1.7)	0-13 (1.9)	0-2 (0.5)	0.12-0.44 (0.26)
Cluster 2	2-21 (10.4)	3-24 (12.1)	0-6 (1.6)	0.46-0.88 (0.73)
Cluster 3	2-64 (13.1)	2-82 (15.4)	0-20 (4.4)	0.23-0.63 (0.44)
Cluster 4	24-53 (38.5)	30-63 (45.0)	2-16 (10.0)	0.51-0.85 (0.75)
Cluster 5	55-102 (71.2)	65-123 (83.9)	16-31 (20.5)	0.74-0.82 (0.78)
Cluster 6	100-159 (136.2)	140-204 (170.2)	19-50 (37.3)	0.70-0.82 (0.78)
Cluster 7	170-240 (206.3)	212-299 (254.4)	39-76 (52.3)	0.80-0.84 (0.82)
Cluster 8	256-482 (314.3)	316-560 (388.8)	57-134 (78.7)	0.71-0.86 (0.83)

The normalized standard deviation was calculated for every aircraft parameter to better understand the spread of data within each cluster. The normalized standard deviations of the clustering parameters and the parameters used to calculate fuel consumption for every cluster can be found in table A.5.1 in the appendix. These values show that the overall normalized standard deviations for the clustering parameters are lower than one or slightly over one, as expected. The parameters used for calculating fuel consumption in cruise configuration have not been used as clustering parameters. Still, they show an overall low normalized standard deviation, indicating that the clustering also provides a reasonable grouping of aircraft in these parameters. The exception from this pattern is the normalized standard deviations of the C_{f2} coefficient, which is noticeably higher for some of the clusters. However, it does not significantly impact the fuel consumption calculated due to how the coefficient is included in the equations.

3.3 Generic aircraft representations

The average value of each aircraft parameter for all the aircraft in the clusters must be calculated to take the step from clustered aircraft to generic aircraft representations. Centroids represent average values of the cluster but do not account for the number of aircraft in the fleet for each aircraft type in the cluster. The average values in each cluster should be weighted by the number of aircraft of each aircraft type in the existing aircraft fleet. This data is not a part of the BADA database provided and had to be looked up manually for each of the 242 aircraft to calculate representative average values for the aircraft parameters in each cluster. The number of aircraft of each aircraft type was retrieved from an open-source aircraft database (Planespotters, 2021). For any aircraft

types not covered by the database, the number of aircraft had to be assumed to provide a contribution to the calculated average values. Based on the five aircraft types available in the database with the lowest number of aircraft per aircraft type, ranging from 5-17 aircraft, the aircraft types not covered by the database were moderately set to 10 aircraft. Missing fleet data was mainly the case for very small aircraft and will have minor effects on the overall results when updating the aircraft stock cohort model.

Cluster 5 turned out to cover over 17 000 aircraft in the fleet despite only containing 20 aircraft types and was split in two when creating the generic aircraft representations to get a more appropriate distribution of the existing fleet. Using a higher number K in the clustering algorithm would not fix this problem but rather divide clusters 1-3 into several clusters. The generic aircraft representations from cluster 5 are denoted 5A and 5B to indicate the manual division of the cluster, where 5A cover aircraft in cluster 5 of reference mass 55-65 tonnes and 5B cover aircraft of reference mass 66-102 tonnes. The resulting nine generic aircraft representations have weighted average values calculated for all 89 aircraft parameters. These values and are presented below in table 3.3.1 in the form of the average values of the five clustering parameters.

Table 3.3.1: Eight generic aircraft representations made from the eight clusters. For every generic aircraft representation the engine type, the reference mass, the maximum takeoff mass, the maximum payload and the cruise speed is presented.

Generic aircraft representation	Engine type	Reference mass [t]	Max takeoff mass [t]	Max payload [t]	Cruise speed [Mach]
Aircraft 1	Piston	1.69	1.85	0.51	0.26
Aircraft 2	Jet	17.17	19.28	3.89	0.75
Aircraft 3	Turboprop	17.92	20.36	6.04	0.48
Aircraft 4	Jet	40.80	48.06	12.16	0.75
Aircraft 5A	Jet	63.35	75.53	19.96	0.78
Aircraft 5B	Jet	77.41	90.41	21.39	0.79
Aircraft 6	Jet	145.39	176.54	39.62	0.80
Aircraft 7	Jet	198.89	246.75	52.46	0.83
Aircraft 8	Jet	317.34	393.67	77.16	0.84

Comparing tables 3.3.1 and 3.2.1 shows that the weighted average values of the generic aircraft representation differ most from the cluster centroid values for the reference mass, the maximum takeoff mass, and the maximum payload mass, indicating the need for a weighted average. The cruise speed of the aircraft representations is closer to the clusters' centroid values due to the slight variation in the cruise speed of different aircraft types.

The relationship between the generic aircraft representations and the aircraft fleet is easier to understand through a visual display. In figure 3.3.1 below, two pie charts describing this relationship are presented. The chart to the left shows how the number of different aircraft types in the fleet is distributed on the generic aircraft representations. On the other hand, the chart on the right displays the number of aircraft covered in the fleet by the generic aircraft representations. The pie charts show that the smaller generic aircraft representations A1, A2, and A3 cover many aircraft types but small shares of the total number of aircraft in the fleet. In contrast, aircraft representations A5A and A5B only cover 9 and 11 aircraft types, respectively, but represent over half the number of aircraft in the fleet.

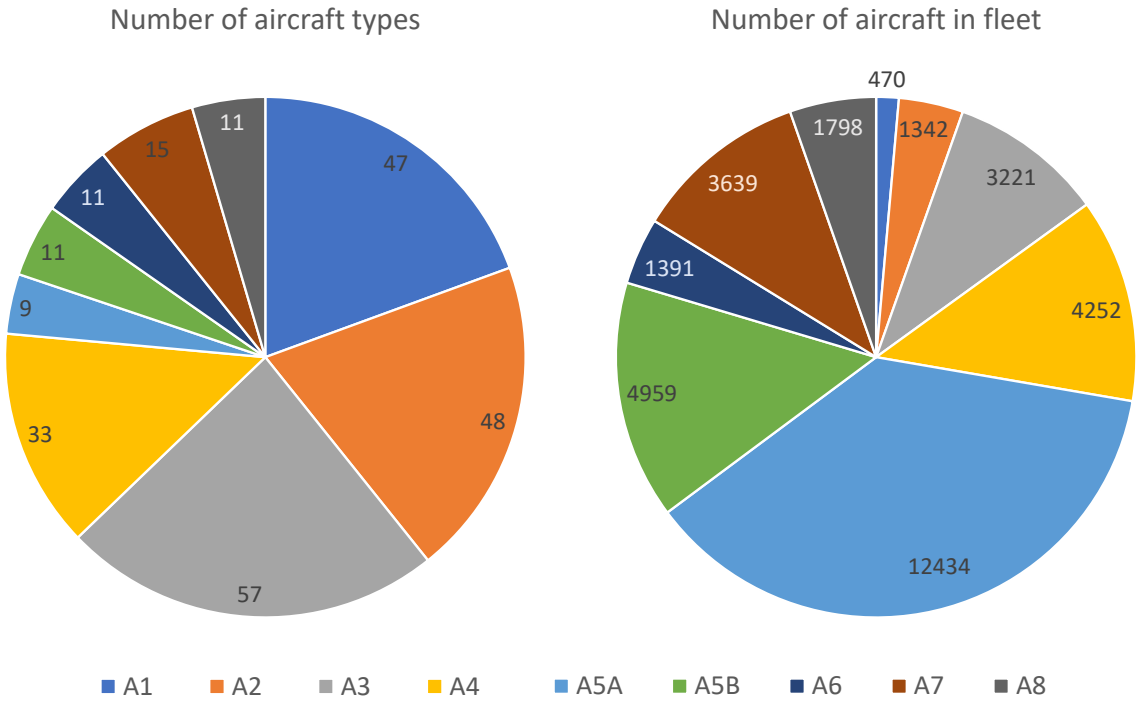

Figure 3.3.1: Pie charts showing the number of aircraft types and the number of aircraft in the fleet covered by the nine generic aircraft representations

The three aircraft types holding the biggest shares of each generic aircraft representations are presented in table 3.3.2 below to provide further information about the nine generic aircraft representations. The table also displays the engine type, the number of aircraft types covered, and the number of aircraft covered in the fleet by each generic aircraft representation. Aircraft 3 is the generic aircraft representation that covers the most aircraft types, while aircraft 5A is the one that covers the largest number of aircraft in the existing fleet. The final column shows that the range of the typical aircraft covered by the generic aircraft representation increases with the aircraft's increasing size and weight.

Table 3.3.2: Engine type, number of aircraft types covered, number of aircraft covered in fleet, typical aircraft types covered and their ranges for each of the nine generic aircraft representations.

Generic aircraft representation	Engine type	Aircraft types covered	Aircraft covered in fleet	Typical aircraft covered	Range of typical aircraft [km]
Aircraft 1	Piston	47	470	Cessna-162 SR20 P2006T	870 1 160 1 374
Aircraft 2	Jet	48	1342	CRJ-200 CRJ-100 Yak-40	2 275 2 417 1 800
Aircraft 3	Turboprop	57	3221	Dash-8-Q400 DHC-8-100 DHC-8-300	2 040 1 890 1 560
Aircraft 4	Jet	33	4252	ERJ-170-100-IGW ERJ-190-100-IGW B737-300	3 334 3 426 4 176
Aircraft 5A	Jet	9	12434	B737-800 A320-231 A319-131	5 665 5 700 6 940
Aircraft 5B	Jet	11	4959	A320-271N A321-251N A321-111	6 500 6 500 5 930
Aircraft 6	Jet	11	1391	B767-300ER A300B4-622 B767-200	10 415 7 500 7200
Aircraft 7	Jet	15	3639	A330-301 A330-243 B787-9	11 750 13 400 13 950
Aircraft 8	Jet	11	1798	B777-300ER B747-400 A380-841	13 649 13 450 14 800

4 Update of the aircraft stock cohort model

This third and final method chapter presents how the generic aircraft representations and the results of the LCA are implemented in the existing aircraft stock cohort model. The chapter is divided into three sections. In the first section, an overarching description of the development of the aircraft stock cohort model and how it works is provided. The second section explains the implementation of the generic aircraft representations, while the third section covers the implementation of the LCA results in the aircraft stock cohort model.

4.1 The original aircraft stock cohort model

A stock cohort model is a robust accounting tool to keep track of the size and age composition of segments in a fleet, and it can provide valuable insights into fleet dynamics, and development (Fridstrøm, Østli, & Johansen, 2016). In the project pre-phase of this master thesis, an aircraft stock cohort model was created and calibrated. It simulates the aircraft fleet growth, deliveries, and retirements of aircraft and calculates fuel use and CO_2 emissions based on historical and projected air travel demand. An overarching description of how the model has been developed and how it works will follow in the next paragraphs. For a more detailed explanation, the complete method of establishing the aircraft stock cohort model can be found in the project pre-phase report by (Enes, 2020), while a shortened version of the method can be found in appendix B.

4.1.1 Framework of the aircraft stock cohort model

The framework of the aircraft stock cohort model is largely adopted from a stock cohort model of the Norwegian passenger car fleet (Fridstrøm et al., 2016). The aircraft fleet is divided into four aircraft types and 45 age classes in the original aircraft stock cohort model. The four aircraft types are regional, narrow-body, wide-body, and freighter aircraft, which can be 0-44 years old. In the project pre-phase of the thesis, the historical simulation period was set to 1990-2018, while the simulation period for future development went from

2019-2050. Information on the aircraft in the fleet must be updated for each year of the simulation. Every aircraft in the fleet is moved up one age class when going from one year to the next. The number of aircraft to be removed from the fleet is then calculated using a scrapping rate and the age composition of the fleet. Similarly, the number of new aircraft introduced to the fleet is then calculated based on the number of aircraft remaining in the fleet and the number of aircraft needed to cover the air travel demand. The air travel demand is a crucial piece of input data to the model, as it acts as a driving force for fleet development. A flow sheet of the model taken from the project pre-phase report by (Enes, 2020) can be seen in figure B.1.1 in appendix B.

4.1.2 Calculations and assumptions

Many aircraft parameters in the fleet are changing over time, which needs to be addressed by the aircraft stock cohort model. The aircraft size is calculated by dividing the number of aircraft of each type by the air travel demand to be covered by that aircraft type, which provides a development of the aircraft's sizes in the model. Air travel demand covered per aircraft type is calculated using a transformation matrix, which splits the global air travel demand from 21 ICAO routes to demand per aircraft type. This matrix is based on assumptions on which aircraft types cover routes of different lengths. All intercontinental flights are covered by wide-body aircraft in these assumptions, while the remaining capacity of wide-body aircraft is distributed on other routes. Regional aircraft only cover flights within the same continent, and narrow-body aircraft cover all the remaining air travel demand. The resulting transformation matrix can be seen in table B.2.1 in appendix B.

For the historical simulations, the fuel efficiency of the aircraft fleet is based on previous studies. The fuel efficiency development of the fleet had to be slightly adjusted for the earliest years of the simulation to calibrate the model. For the simulations of future development, the fleet fuel efficiency development was set to a conservative 1% improvement per year to reflect a moderate technological development of the future aircraft fleet. The fuel consumption is calculated from the fleet fuel efficiency and the air travel demand. Combustion CO_2 emissions follow directly from the fuel consumption trough the CO_2 coefficient of 3.16 kg CO2/kg jet fuel (D. S. Lee et al., 2020).

4.1.3 Data collection

In the project pre-phase of the thesis, large amounts of data were collected to create the aircraft stock cohort model. For the historical part of the model, data on global air traffic, air traffic by route, global freight, and the number of aircraft in the fleet of the four aircraft types were obtained. The future simulations were based on future projections of air travel demand from Boeing, Airbus, ICAO, and IATA and four SSP-RCP scenarios. In total, this resulted in eight sets of simulation results of the development from 2019-2050. Data on fuel efficiencies of new aircraft were also collected in the project work. For years where data was unavailable, it was constructed using interpolation and extrapolation. An overview of the collected data, taken from (Enes, 2020), can be found in table B.3.1 in appendix B.

4.2 Implementation of generic aircraft representations

The original aircraft stock cohort model divides the fleet into four aircraft types: regional, narrow-body, wide-body, and freighter aircraft. Each aircraft type has its fuel efficiency, which changes over time as the fleet develops. The nine new generic aircraft representations will update both the number of aircraft types in the fleet and their respective fuel efficiencies.

4.2.1 Generic aircraft representations in the aircraft fleet

In the process of creating the generic aircraft representations, the number of aircraft of each aircraft type were acquired, as mentioned in section 4.2.1, providing detailed information about the aircraft fleet as of April 2021. This fleet was divided into the four aircraft types of the original aircraft stock cohort model, using that regional aircraft have less than 100 seats (Curtis, Rhoades, & Waguespack Jr, 2013), narrow-body aircraft have one aisle and more than 100 seats, and wide-body aircraft have two aisles. The number of freighter aircraft of different sizes was given in (Boeing, 2020d) for the year 2019 and could thereby be distributed on the aircraft representations. The resulting table 4.2.1 below shows how the four aircraft types from the original aircraft stock cohort model are distributed on the nine generic aircraft representations of the updated model. This distribution is used to split the four aircraft types of the original aircraft stock cohort model into the nine generic aircraft types of the new model, providing a higher level of detail in the simulation results.

Table 4.2.1: The original four aircraft types percent wise distributed on the generic aircraft representations.

Generic aircraft representation	Share of regional	Share of narrow-body	Share of wide-body	Share of freighter
Aircraft 1	6,9 %	0,0 %	0,0 %	0,0 %
Aircraft 2	19,6 %	0,0 %	0,0 %	0,0 %
Aircraft 3	47,0 %	0,0 %	0,0 %	0,0 %
Aircraft 4	26,5 %	12,3 %	0,0 %	0,0 %
Aircraft 5A	0,0 %	62,5 %	0,0 %	0,0 %
Aircraft 5B	0,0 %	24,9 %	0,0 %	0,0 %
Aircraft 6	0,0 %	0,3 %	19,7 %	37,3 %
Aircraft 7	0,0 %	0,0 %	53,8 %	32,3 %
Aircraft 8	0,0 %	0,0 %	26,6 %	30,3 %

4.2.2 Fuel consumption of generic aircraft representations

Dividing the fleet into a larger number of aircraft types requires new fuel efficiencies for the aircraft used in the simulations. Therefore, the fuel consumption in cruise configuration is calculated for each of the nine generic aircraft representations using the data provided by the BADA database. The method of calculating the fuel consumption is retrieved from the user manual accompanying the BADA database and is summarized in the following equations for jet aircraft (Eurocontrol, 2019).

The fuel consumption of a cruising jet aircraft is given as

$$f_{cr} = \eta * Thr_{cr} * C_{fcr} \tag{4.2.1}$$

where f_{cr} [kg/min] is the fuel consumption, η [kg/(min*kN)] is the thrust specific fuel consumption, Thr [kN] is the thrust and C_{fcr} is a constant given in the BADA data.

The thrust specific fuel consumption is given as

$$\eta = C_{f1} * (1 + \frac{V_{TAS}}{C_{f2}}) \tag{4.2.2}$$

where C_{f1} [kg/(min*kN)] and C_{f2} [knots] are thrust specific fuel coefficients given in the BADA data and V_{TAS} [knots] is the true airspeed.

The true airspeed can be calculated as

$$V_{TAS} = M * \sqrt{k * R * T} \tag{4.2.3}$$

where M is the Mach number in cruise, k is the adiabatic index of air, R [$m^2/(K*s^2)$] is the real gas constant of air, and T [K] is the air temperature.

The only variable missing in equation 4.2.1 is thrust. In cruise configuration, the thrust equals the drag of the aircraft and is given as

$$D = \frac{C_D * \rho * {V_{TAS}}^2 * S}{2} \tag{4.2.4}$$

where D [N] is drag, C_D is the drag coefficient, ρ [kg/m^3] is the air density, V_{TAS} [knots] is the true airspeed and S [m^2] is the wing surface area given in the BADA data.

The drag coefficient is given as

$$C_D = C_{D0,CR} + C_{D2,CR} * (C_L)^2 \tag{4.2.5}$$

where $C_{D0,CR}$ is the parasitic drag coefficient, $C_{D2,CR}$ is the induced drag coefficient, and C_L is the lift coefficient.

The lift coefficient is given as

$$C_L = \frac{2 * m * g_0}{\rho * {V_{TAS}}^2 * S * cos(\phi)} \tag{4.2.6}$$

where m [kg] is the mass of the aircraft, g_0 [m/s^2] is the gravitational acceleration, ρ [kg/m^3] is the air density, V_{TAS} [knots] is the true airspeed, S [m^2] is the wing surface area and ϕ [deg] is the bank angle.

These equations hold for all jet aircraft and can, with slight alterations, also be used for aircraft with turboprop or piston engines. The air density and temperature depend on the altitude of the aircraft. Typical cruising altitude for commercial aircraft is between 30 000-38 000 ft with a corresponding air pressure of 0.3-0.2 atm respectively (Sforza, 2014). For all the calculations performed, a cruising altitude of 35 000 ft was assumed, with corresponding air density and temperature under standard U.S. atmospheric conditions of 0.38 kg/m^3 and 219 K respectively (ToolBox, 2003).

The original aircraft stock cohort model uses fuel consumption as grams of jet fuel consumed per revenue passenger kilometer (RPK). Fuel consumption was calculated per RPK by dividing the fuel consumption per kilometer by the average number of passengers carried by the generic aircraft representations. This calculation was performed to implement the fuel consumption of the generic aircraft representations in the original model. The average number of passengers carried is found by multiplying the average number of seats of each aircraft representation with the average payload factor of 82.4% from 2019 (ICAO, 2019d). The number of seats for different aircraft is retrieved from the manufacturers websites (Boeing, 2020a), (Airbus, 2021). Aircraft representations A6-A8 have a large spread in the number of seats in the aircraft they cover. Therefore, the number of seats for every

aircraft type covered by aircraft representation A6-A8 is looked up and included in the calculated average. For the remaining six aircraft representations, only the three aircraft types holding the biggest fleet shares for each aircraft representation are used to calculate the average seating. The resulting cruise fuel consumption is displayed in table 4.2.2 below for all nine generic aircraft representations and shows that fuel consumption in kg/min and kg/km increase with increasing aircraft size for jet aircraft.

Table 4.2.2: Fuel consumption in cruise configuration of all nine generic aircraft representations given per unit time, distance, and RPK.

Generic aircraft representation	Fuel consumption [kg/min]	Fuel consumption [kg/km]	Fuel consumption [g/RPK]
Aircraft 1	0.94	0.20	30.68
Aircraft 2	14.91	1.11	27.04
Aircraft 3	29.02	3.42	61.96
Aircraft 4	22.29	1.68	15.30
Aircraft 5A	44.11	3.18	22.73
Aircraft 5B	58.86	4.20	26.41
Aircraft 6	85.70	6.04	30.43
Aircraft 7	195.88	13.26	43.86
Aircraft 8	251.55	16.78	40.96

4.3 Implementation of LCA results

Implementing the LCA result into the aircraft stock cohort model is straightforward. To calculate CO_2 emissions, the aircraft stock cohort model first calculates the fuel consumption, which is then multiplied by a CO_2 coefficient to give the CO_2 emissions. For combustion emissions from an aircraft engine, the CO_2 coefficient is 3.16 kg CO_2/kg jet fuel (D. S. Lee et al., 2020). Changing the CO_2 coefficient in the aircraft stock cohort model to the values of the CO_2 stressor from the performed LCA will show how the CO_2 emissions from the aircraft fleet change with different jet fuels.

Having established the method, assumptions, and choices made in the LCA analysis, the making of the generic aircraft representations, and in updating the aircraft stock cohort model, this concludes the method chapters of this thesis. The following two chapters will present the results from the LCA and the simulation results from the updated aircraft stock cohort model.

5 | LCA results

The LCA results chapter of this report is the first of two results chapters and is divided into four sections. In the first section, the total environmental impacts of the three jet fuel systems are presented. The second section presents a contribution analysis of the six environmental stressors for each of the three systems. In the third section, the global warming potential impact category is investigated. The final section presents a sensitivity analysis of the global warming potential of the PtL alkaline system using wind power.

5.1 Total environmental impacts

The total well-to-wake environmental impacts are calculated for the 18 impact categories and the six stressors per MJ fuel. A selection of the impact categories is presented as absolute values in table 5.1.1 below. The entire table with all impact categories included can be found in table A.1.1 in the appendix. Fossil jet fuel impacts are given in the third column, followed by the two PtL systems. The PtL results are color-coded to show whether the impacts are lower or higher than the fossil jet fuel for the same impact category, indicated by the green and red colors, respectively. Explanations of the abbreviations used in the table are presented previously in chapter 2.2.2.

Table 5.1.1 shows that in the global warming potential (GWP) impact category, both the PtL systems are lower compared to fossil jet fuel. The GWP is the most crucial impact category to assess since the scope of the thesis defines climate change contribution to be the main comparison criteria to other fuels. Fossil jet fuel emits 94.0 g CO_2-eq/MJ over its life cycle. In comparison, PtL jet fuel using alkaline electrolysis and wind power emits 22.2 g CO_2-eq/MJ, while PtL jet fuel using high-temperature co-electrolysis and wind power emits 19.9 g CO_2-eq/MJ over its life cycle. The PtL jet fuels perform better in terms of GWP because CO_2 is captured from the air as part of the production process. This DAC capture generates negative emissions of CO_2, equivalent to the CO_2 emissions from the combustion of the fuel. The negative emissions and the combustion emissions cancel out, leaving only emissions related to the remaining production processes and energy use of the DAC unit.

The PtL jet fuels have a lower fossil depletion potential (FDP) of 6.4-6.8 g oil-eq/MJ than the fossil jet fuel's FDP of 57.8 g oil-eq/MJ. This difference is expected considering that the FDP impact category measures the reduction of oil reserves. Producing fossil jet fuel depletes oil reserves, and the FDP value can therefore be viewed as a measure of how many kg crude oil is needed to make one MJ of fossil jet fuel. In contrast, the production of PtL jet fuel using electricity from renewable sources will only use fossil fuels in the plant's construction, making the FDP impacts of PtL jet fuel one magnitude lower than the fossil jet fuel value. Similarly, the PtL jet fuel has a higher water depletion potential (WDP) of 1.7-1.8 liter/MJ than fossil jet fuel's WDP of 0.8 liters/MJ. PtL jet fuels have a much higher water consumption due to the water used to produce hydrogen through electrolysis.

The freshwater ecotoxicity potential (FETP), the marine ecotoxicity potential (METP), the terrestrial ecotoxicity potential (TETP), and the human toxicity potential (HTP) are related through being measured in kg 1.4-DB-eq/MJ. Emissions of 1,4 dichlorobenzene cause impacts in the categories mentioned to freshwater, marine water, industrial soil, and urban air, respectively (Goedkoop et al., 2009). Where the emissions occur will determine which of the impact categories get the most significant impacts. For all three jet fuels, the largest emissions of 1.4-DB-eq/MJ is in the HTP category. This finding is expected because fuel combustion in the aircraft causes emissions to urban air. The PtL jet fuels have higher FETP and METP than fossil jet fuel, indicating higher emissions of 1.4-DB-eq/MJ to both fresh and marine waters than fossil jet fuel. For the TETP impact category, the PtL jet fuel has lower emissions than fossil jet fuel, but all three values are insignificantly small compared to the human toxicity potential.

The agricultural land occupation (ALOP) and the urban land occupation (ULOP) are given as m^2*year/MJ. In this assessment, no land-use requirements have been specified, meaning that the impacts in the ALOP and ULOP categories are embedded in the background processes from Ecoinvent. The table shows that both PtL jet fuels create slightly higher impacts in the ALOP and ULOP impact categories. This result can stem from the use of electricity from wind power in the production of the PtL jet fuels due to windmills' land occupation requirements. The land occupation most likely stems from refinery and processing facilities used in the production process for fossil jet fuel.

Both PtL jet fuels have higher impacts than fossil jet fuel in the mineral depletion potential (MDP) impact category. The PtL jet fuels have a MDP of 13.9-15.7 g Fe-eq/MJ compared to 1.3 g Fe-eq/MJ for fossil jet fuel. This difference likely stems from the minerals used to produce electrolyzers for the hydrogen generation process of the PtL jet fuels. In contrast, the two PtL jet fuels have lower impacts than fossil jet fuel in the terrestrial acidification potential (TAP). The TAP impact category is quantified in kg SO_2-eq/MJ, a substance that reacts with water and creates sulfurous acid. Emissions of SO_2 usually stem from the

burning of fossil fuels. In this assessment, the combustion emissions of the three jet fuels are assumed equal, meaning that the difference in SO_2 emissions comes from the burning of fossil fuels in the recovery, extraction, and transport of crude oil.

Table 5.1.1: Total well-to-wake environmental impacts per MJ jet fuel for fossil jet fuel, PtL jet fuel produced using alkaline electrolyzer and wind power, and PtL jet fuel produced using high-temperature co-electrolysis and wind power. The results are given in absolute values, and the PtL results are colored green if they are lower and red if they are higher than the fossil jet fuel for the same impact category.

Impact Category	Unit	Fossil Jet Fuel	PtL alkaline electrolysis, wind power	PtL HT co-electrolysis, wind power
GWP	kg CO_2 eq	9,40E-02	2,22E-02	1,99E-02
FDP	kg oil eq	5,78E-02	6,76E-03	6,38E-03
WDP	m^3	8,37E-04	1,83E-03	1,68E-03
FETP	kg 1,4-DB eq	2,05E-04	6,36E-03	5,42E-03
METP	kg 1,4-DB eq	1,80E-04	5,56E-03	4,74E-03
TETP	kg 1,4-DB eq	1,71E-05	2,17E-06	1,99E-06
HTP	kg 1,4-DB eq	4,89E-03	1,86E-02	1,68E-02
ALOP	m^2year	3,89E-04	5,74E-04	5,66E-04
ULOP	m^2year	3,89E-04	8,80E-04	7,51E-04
MDP	kg Fe eq	1,30E-03	1,57E-02	1,30E-02
TAP	kg SO_2 eq	3,87E-04	2,00E-04	1,96E-04

The six stressors representing emissions of CO_2, CH_4, N_2O, NO_X, particle matter (PM), and SO_X are presented in table 5.1.2 below. It follows the same layout and color-coding as the previous table. As expected after examining the GWP impact category, the CO_2 emissions of the PtL jet fuels are lower than the fossil jet fuel. Comparing the CO_2 emissions with the GWP shows that 97% of the fossil jet fuel's GWP and 92% of the PtL jet fuel's GWP stems from CO_2 emissions. The remaining GWP stems from much smaller emissions of the more potent greenhouse gases, CH_4 and N_2O. Fossil jet fuel emits more CH_4, NO_X and SO_X per MJ than the PtL jet fuels, while the PtL jet fuels emit more PM per MJ than the fossil jet fuel. Emissions of N_2O are close to identical for all three jet fuels. Pinpointing why the stressors are the way they are is difficult and calls for a more in-depth investigation of the emissions by looking at the process contributions.

Table 5.1.2: Total well-to-wake emissions per MJ jet fuel for fossil jet fuel, PtL jet fuel produced using alkaline electrolyzer and wind power, and PtL jet fuel produced using high-temperature co-electrolysis and wind power. The results are given in absolute values, and the PtL results are colored green if they are lower and red if they are higher than the fossil jet fuel for the same stressor.

Stressor	Unit	Fossil Jet Fuel	PtL alkaline electrolysis, wind power	PtL HT co-electrolysis, wind power
CO_2	kg CO_2	9,13E-02	2,05E-02	1,83E-02
CH_4	kg CH_4	1,14E-04	6,89E-05	6,39E-05
N_2O	kg N_2O	5,45E-07	5,69E-07	5,47E-07
NO_X	kg NO_X	2,57E-04	2,02E-04	1,97E-04
PM	kg PM	3,02E-05	6,77E-05	5,81E-05
SO_X	kg SO_X	2,42E-04	8,46E-05	8,41E-05

5.2 Contribution analysis of stressors

A contribution analysis is performed and presented to understand better which processes have the highest associated emissions for the six stressors. The contribution analysis of fossil jet fuel will be given first, followed by the PtL jet fuel produced using alkaline electrolysis and wind power and the PtL jet fuel produced using high-temperature co-electrolysis and wind power.

5.2.1 Contribution analysis for fossil jet fuel

The process contributions to the six stressors are presented as a 100% bar chart in figure 5.2.1 below. The six stressor bars in the chart are color-coded to show the percent-wise distribution of the process contributions to the different stressors. Total emissions are given in absolute values on the right-hand side of the figure, per MJ jet fuel, to provide information about the size of the emissions. For fossil jet fuel, the figure shows that 77% of the life cycle CO_2 emissions come from the combustion of jet fuel in the aircraft engine, 11% comes from the refining process, and 8% from oil recovery and extraction. The rest of the CO_2 emissions come from jet fuel transport and crude oil transport. Even though 77% of the CO_2 emissions come from the burning of fossil jet fuel, a large share of the remaining 23% percent also stems from the burning of fossil fuels, as the remaining contributing processes largely depend on the use of fossil fuels.

The CH_4 emissions mainly come from oil recovery and extraction and refining, contributing with 55% and 38% respectively. These processes are expected to have the largest contributions as oil production is a significant emitter of methane, responsible for 40% of methane emissions from the energy industry (Worldoil, 2021). The N_2O emissions are more evenly distributed on the processes, with the largest contributions coming from oil recovery and extraction and refining, followed by jet fuel transport and crude oil transport. The burning of fossil fuels is a source of N_2O emissions, indicating that the four processes mentioned are dependent on fossil fuels.

The NO_X emissions are mainly caused by combustion in aircraft, with a 60% contribution, followed by oil recovery and extraction and refining, both contributing with 14% each. These emissions also mainly come from the burning of fossil fuels. For PM emissions, refining and oil recovery and extraction are the two processes contributing most to the total emissions with 32% and 40%. Significant contributions also come from jet fuel transport and crude oil transport with 16% and 11%. PM emissions can come from industrial processes, burning of fossil fuels, and dust from roads. The SO_X emissions mainly stem from refining with a 36% contribution and oil recovery and extraction with a 48% contribution. SO_X emissions are caused by the burning of fossil fuels containing sulfur. The figure shows that 9% of the total SO_X emissions of 0.24 g SO_X/MJ comes from combustion in the aircraft, which equals combustion emissions of 0.02 g SO_X/MJ fossil jet fuel.

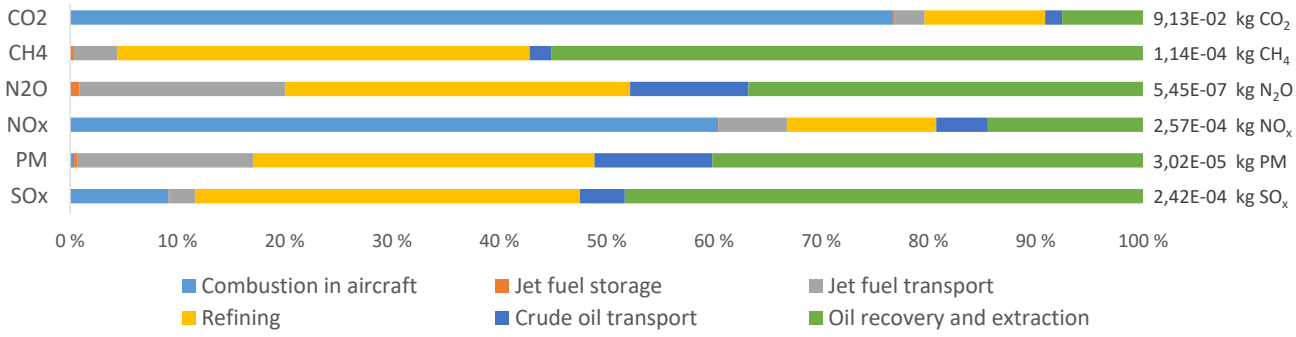

Figure 5.2.1: Contribution analysis of stessors for fossil jet fuel. The absolute value per MJ jet fuel for each stressor is displayed to the right of the figure, while the bars show the percent wise distribution of the emissions on the different processes.

5.2.2 Contribution analysis for PtL jet fuel using alkaline electrolysis and wind power

The process contributions to the six stressors for the PtL jet fuel produced using alkaline electrolysis and wind power are presented as a 100% bar chart in figure 5.2.2 below. Compared to the fossil jet fuel, the CO_2 stressor stands out by having a process contributing with negative emissions, in the form of direct air capture (DAC) of CO_2. Contributions of the DAC unit is split into two processes to distinguish the negative emissions from the CO_2 captured from the positive CO_2 emissions from energy use in the DAC unit. The captured CO_2 is emitted in the combustion of jet fuel, making the two contributions of the same magnitude. Even though the combustion CO_2 emissions are canceled out by the CO_2 captured, the net CO_2 emissions are still positive due to the CO_2 emissions of the remaining five processes. These five processes are responsible for the total net emissions of 20.5 g CO_2/MJ. Isolating these processes shows that 46% of the net CO_2 emissions stems from hydrogen production, 33% from energy use in the DAC unit, 16% from the construction of the DAC unit, and 4% from the construction of the electrolyzer. The most significant contributions to the net CO_2 emissions come from hydrogen production and the DAC unit's energy use. Both processes require large amounts of electricity, indicating that the source of electricity used will have a significant impact on the total CO_2 emissions. In this case, the electricity used is from wind power, which has a low carbon intensity. CO_2 emissions from hydrogen production come from the use of this electricity. The DAC unit uses both electricity from wind power and industrial heat. Therefore, the CO_2 emissions from the DAC energy use process come both from the electricity use and the burning of natural gas in a combined-heat-and-power plant supplying the heat. Construction-related emissions add up to 20% of the net CO_2 emissions or 4.1 g CO_2/MJ, indicating an energy-intensive and comprehensive construction phase for both the DAC unit and the electrolyzer.

For CH_4 emissions, the hydrogen production contributes 48% of the total, energy use of the DAC contributes 34%, construction of the DAC with 14%, and construction of the electrolyzer with 4%. As mentioned previously, both hydrogen production and CO_2 capture use a lot of electricity generated from wind power. Construction of the windmills leads to CH_4 emissions due to the production of epoxy resin used in the blades of the windmill (Mishnaevsky Jr & Favorsky, 2011). Even though the percent-wise contribution of the two processes is high, the absolute value of the CH_4 emission is 0.07 g CH_4/MJ, which is much lower than the CO_2 emission value of 20.5 g CO_2/MJ. In addition to the electricity and heat use, some of the CH_4 emission from the DAC energy use process comes from producing the anionic resin used by the DAC unit.

The N_2O emissions follow roughly the same process distribution as the CH_4 emissions, but with an even lower absolute emission value. Hydrogen production and energy use of

the DAC unit are the most significant contributors to N_2O emissions with 52% and 29% contributions, respectively. The N_2O emissions from hydrogen production stem from steel and glass fiber production used in the windmills that generate the electricity used. N_2O emissions are a bi-product in the combustion of fossil fuels. Therefore, a large part of the N_2O emissions from the DAC energy use process comes from the heat used in the CO_2 capture process, which comes from a combined-heat-and-power natural gas plant. The NO_X emissions mainly come from the combustion of PtL jet fuel in the aircraft, with a 77% contribution of the total. This contribution equals the amount of the combustion NO_X emission of fossil jet fuel because the PtL jet fuel and the fossil jet fuel are assumed to have the same fuel characteristics. The relative contribution from combustion is higher for the PtL jet fuel due to a lower absolute value for the total NO_X emission.

For PM emissions, the most significant process is hydrogen production, followed by the construction of the DAC unit. Hydrogen production requires lots of electricity, indicating that the PM emissions from hydrogen production are related to the electricity source. Setting up windmills requires new roads to get the windmills in place, which can be a significant source of PM emissions. Construction-related PM emissions can come from producing and refining the many different materials needed for the construction and the work done in the construction phase on-site. The largest contribution to SO_x emissions comes from hydrogen production, followed by combustion in the aircraft, construction of the DAC unit, and energy use in the DAC unit. Fuels containing sulfur lead to SO_x emissions, and in this case, the PtL jet fuel is assumed to have the same composition as fossil jet fuel. SO_X emissions from hydrogen production, construction, and energy use of the DAC unit stem from fuel burn and material production needed for constructing the windmills and the DAC unit.

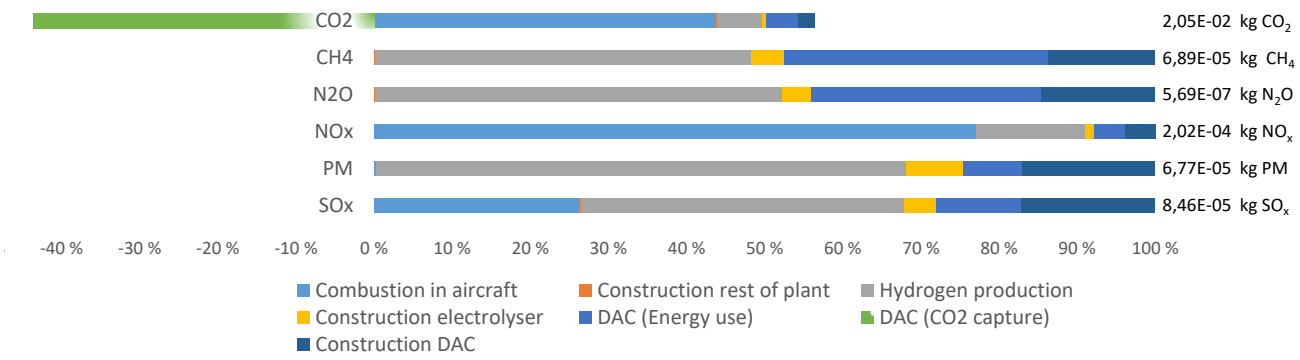

Figure 5.2.2: Contribution analysis of stressors for PtL jet fuel produced using alkaline electrolyser and wind power. The absolute value per MJ jet fuel for each stressor is displayed to the right of the figure, while the bars show the percent wise distribution of the emissions on the different processes.

5.2.3 Contribution analysis for PtL jet fuel using high-temperature co-electrolysis and wind power

The process contributions to the six stressors for the PtL jet fuel produced with high-temperature co-electrolysis using wind power are presented as a 100% bar chart in figure 5.2.3 below. As seen for the PtL alkaline jet fuel, the CO_2 emissions from combustion and the negative CO_2 emissions from the DAC cancel each other out. However, the net CO_2 emissions are lower for the PtL HT jet fuel compared to the PtL alkaline jet fuel due to higher system efficiency in the high-temperature co-electrolysis. Isolating the remaining five processes that make up the net CO_2 emissions, syngas production, and energy use for the DAC are the largest contributors to net CO_2 emissions due to the high electricity demand of the processes.

The five remaining stressors also show similar process distributions as the PtL alkaline jet fuel. Still, they have lower absolute emission levels due to higher efficiency in the high-temperature co-electrolysis. Since the systems are quite similar, the reasoning of where the process emissions stems from for the PtL alkaline jet fuel will hold for the PtL HT jet fuel. The most noticeable difference between the two PtL stressor contribution figures is the construction of rest of plant contributions for the PtL HT jet fuel. This difference mainly comes from the construction data available for the two PtL production systems. The construction data of both systems can be found in appendix C and show that the high-temperature co-electrolysis plant provides detailed information on the materials and energy used to construct the plant itself. In contrast, the PtL alkaline system only provides construction data for the individual components.

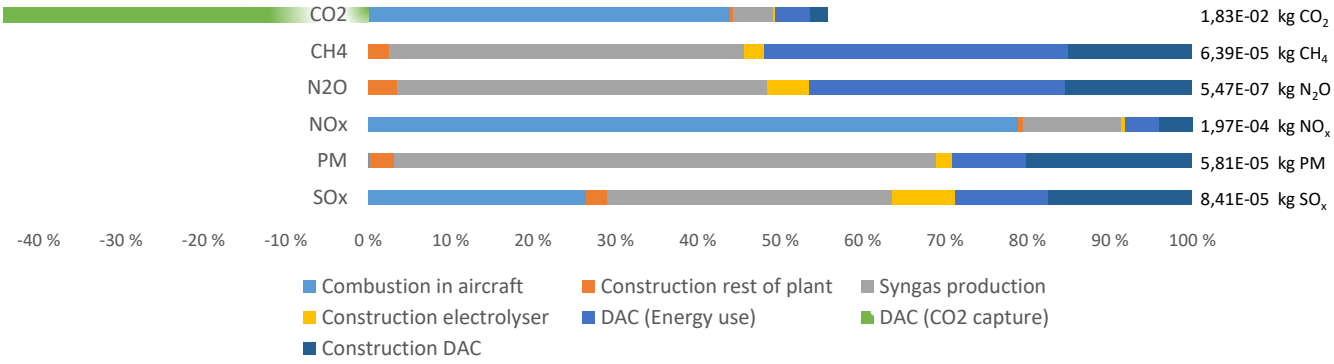

Figure 5.2.3: Contribution analysis of stressors for PtL jet fuel produced using HT co-electorlysis and wind power. The absolute value per MJ jet fuel for each stressor is displayed to the right of the figure, while the bars show the percent wise distribution of the emissions on the different processes.

5.3 Global warming potential

The main scope of the LCA part of this thesis is to compare the climate change contributions of PtL jet fuel and fossil jet fuel. This comparison makes the global warming potential (GWP) the most important impact category to investigate and is thoroughly assessed in this section. The following subsections present the results for this impact category and display how the impacts change with different allocation methods and electricity sources.

5.3.1 Allocation

In the fossil system, the refining process transforms crude oil into different fuels. The PtL systems transform syngas to synthetic crude and refine the syncrude to different fuels in a gas-to-liquid (GtL) plant. All three systems produce more than one product in the refining step of the jet fuel life cycle, which calls for an allocation approach. In figure 5.3.1 below, the total GWP for all three systems is presented for both mass and energy allocation. For both PtL systems, the mass allocation leads to a higher GWP of around 1.5 g CO_2-eq/MJ jet fuel compared to using energy allocation. When looking at fossil jet fuel, the two allocation methods give results of the same magnitude. The differences in GWP between the two allocation methods are small because the mass percentage and the energy percentage of jet fuel of the total product slate are roughly the same. To take a conservative approach, the presented impacts in all other figures in this chapter use the mass allocation approach, ensuring no underestimation of emissions due to the choice of allocation method.

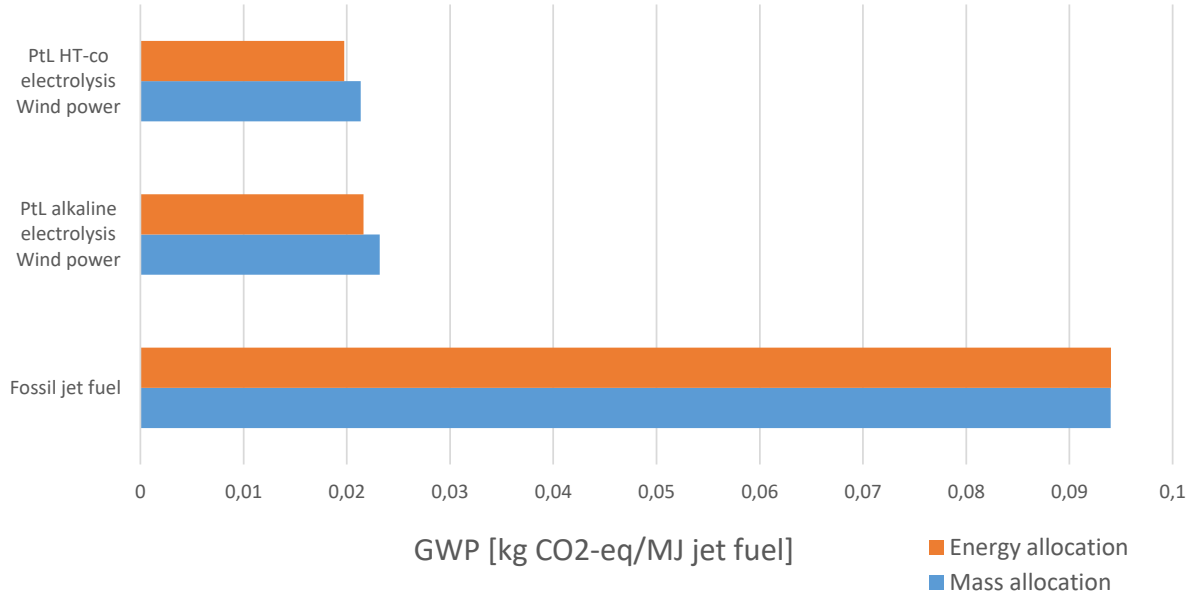

Figure 5.3.1: Total GWP impact from all three systems, using mass and energy allocation

5.3.2 GWP of fossil jet fuel

The GWP of fossil jet fuel has been calculated to serve as a comparison to the two PtL jet fuel systems. In figure 5.3.2 below, the GWP of fossil jet fuel is presented as a stacked bar chart consisting of the different process contributions. The total GWP of fossil jet fuel is 94.0 g CO_2-eq/MJ, an emission level in agreement with the established range of EU fossil jet fuel well-to-wake emissions of 80.4-105.7 g CO_2-eq/MJ, depending on crude oil composition (EC, 2015). The figure shows that the combustion in the aircraft engine has the largest contribution to the overall GWP at 70.0 g CO_2-eq/MJ, followed by refining at 11.3 g CO_2-eq/MJ and oil recovery and extraction at 8.4 g CO_2-eq/MJ. Smaller contributions come from crude oil and jet fuel transport at 1.5 and 2.6 g CO_2-eq/MJ, respectively, while jet fuel storage has close to zero contribution.

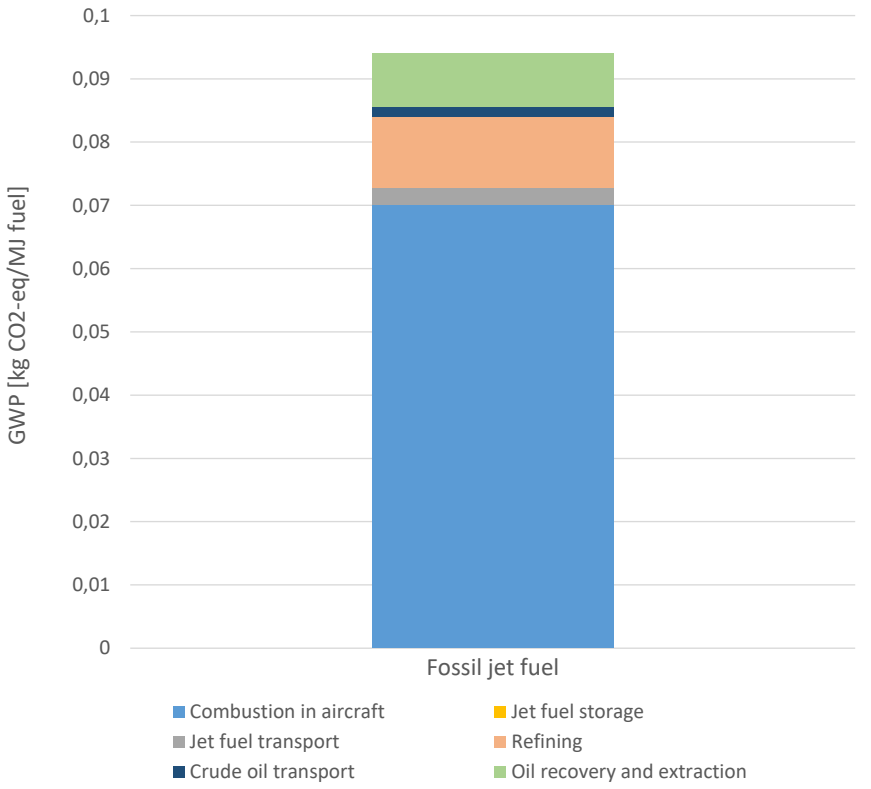

Figure 5.3.2: Total GWP for fossil jet fuel, divided into process contributions.

5.3.3 GWP of PtL systems for different electricity sources

The production of hydrogen and the extraction of CO_2 from the air required in the production of PtL jet fuel requires large amounts of electricity. Therefore, GHG emissions from the PtL systems largely depend on the carbon intensity of the electricity source. In figure 5.3.3, the GWP of both PtL systems is presented for four different electricity sources, with the GWP of fossil fuel displayed at the right-hand side to serve as a point of reference. The electricity sources investigated are the German electricity mix, photovoltaic panels, wind power, and hydropower. Each column represents the GWP using one electricity source and is divided into process contributions. The red dot on each column represents the net GWP when adding together positive and negative emissions.

The CO_2 captured by the DAC unit and the CO_2 emitted in combustion cancel out for all PtL cases, meaning that the differences lie primarily in the energy used by the DAC unit and the hydrogen production. The HT co-electrolysis system has a lower GWP than the alkaline system for all electricity sources due to a higher system efficiency for the HT co-electrolysis. The GWP is much higher for both PtL systems than for the fossil jet fuel when using the German electricity mix. This is because over 45% of German electricity production uses fossil fuels (BNetzA, 2021). All the renewable electricity sources result in lower GWP impacts compared to the fossil jet fuel case. For the PtL alkaline system, using PV electricity results in a GWP of 71.7 g CO_2-eq/MJ jet fuel. The same system gets a GWP of 22.2 g CO_2-eq/MJ jet fuel and 15.6 g CO_2-eq/MJ jet fuel using wind power and hydropower, respectively. For the PtL HT co-electrolysis system, using PV electricity, wind power, and hydropower results in GWP of 61.7, 19.9, and 14.3 g CO_2-eq/MJ jet fuel. Comparing these numbers to the fossil jet fuel GWP of 94.0 g CO_2-eq/MJ jet fuel shows that using electricity from wind power or hydropower provides substantial reductions in GWP compared to fossil jet fuel. In contrast, smaller reductions can be achieved using PV electricity.

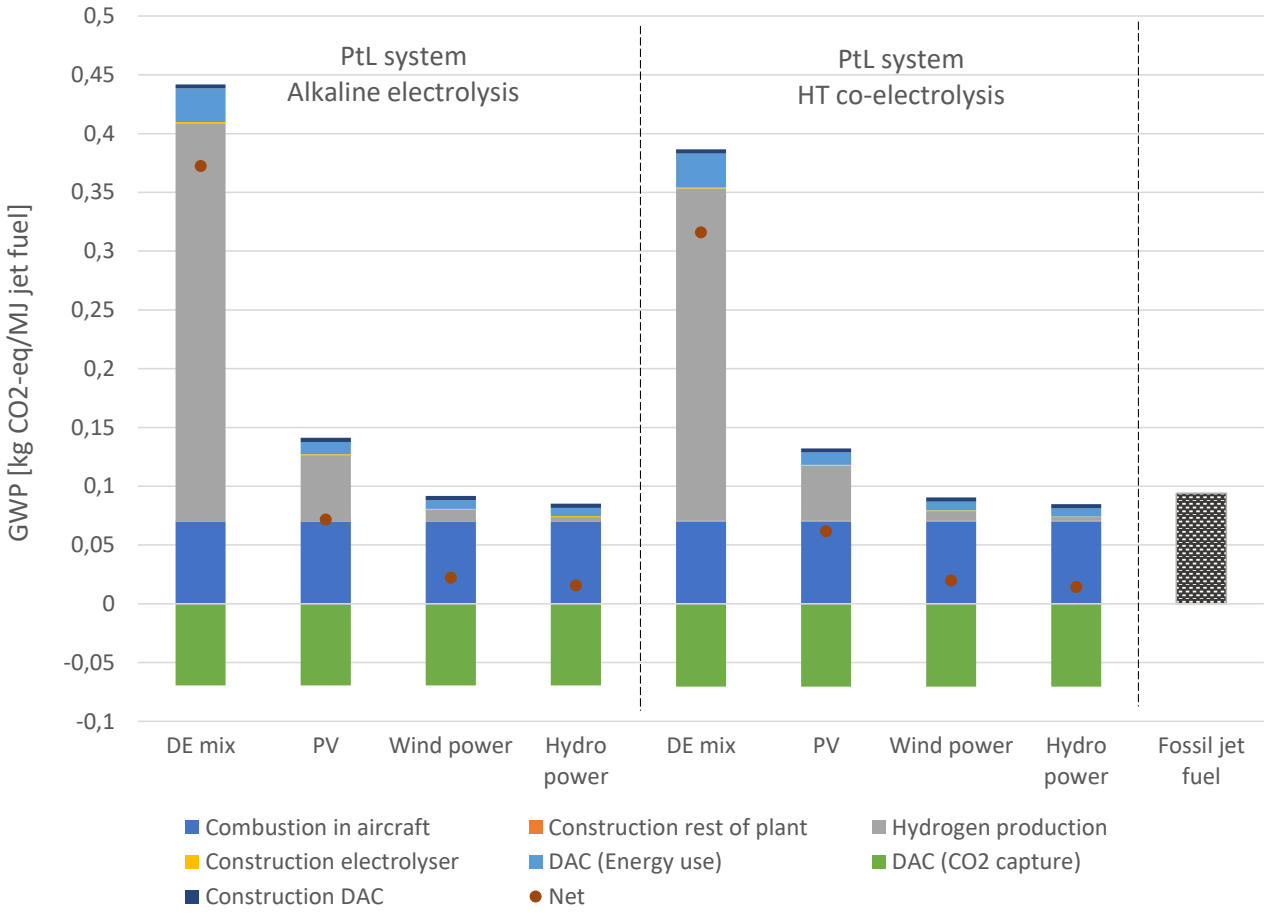

Figure 5.3.3: GWP of both PtL systems for four differnt electricity sources, divided into process contributions. Negative emissions represent CO_2 capture. The red dot represent the net GWP. Total GWP of fossil jet fuel is displayed on the right hand side of the figure to serve as comparison to the PtL systems.

5.4 Sensitivity analysis

A sensitivity analysis has been carried out on the PtL system using alkaline electrolysis and wind power for the GWP impact category. The sensitivity analysis aims to understand better how sensitive the system is to changes in different assumptions made in the LCA, thereby indicating how robust the LCA results are. In figure 5.4.1 below, the results of the sensitivity analysis are presented in the form of a tornado chart. It shows how the GWP, given in g CO_2-eq/MJ, varies when changing the system parameters and assumptions. The blue bars represent an increase in GWP, while the orange bars represent a decrease in GWP, relative to the GWP of the PtL system using alkaline electrolysis and wind power, which has a GWP of 22.2 g CO_2-eq/MJ.

Figure 5.4.1 indicates that the GWP of the PtL system is most sensitive to change in electricity source. This sensitivity is expected because both hydrogen production through electrolysis and direct air capture of CO_2 require a lot of electricity. Of the tested electricity sources, the most considerable reduction in GWP comes from changing electricity source from wind power to hydropower, resulting in a decrease from 22.2 g CO_2-eq/MJ to 15.6 g CO_2-eq/MJ. The largest increase comes from changing electricity source to the German electricity mix resulting in an increase from 22.2 g CO_2-eq/MJ to 372.4 g CO_2-eq/MJ. The PtL systems hydrogen production efficiency of 59% was varied with ± 20pp to 79%, close to the best alkaline electrolysis can perform (Santos, Sequeira, & Figueiredo, 2013), and down to the very low efficiency of 39%. Higher efficiency of 79% reduces the GWP to 19.8 g CO_2-eq/MJ jet fuel, showing that the electricity source used is more important than the efficiency of the hydrogen production. The figure further shows that using HT co-electrolysis with a solid oxide electrolyzer would reduce the GWP compared to the alkaline electrolyzer. This difference has been seen previously in figure 5.3.3.

Figure 5.3.3 also shows that changing the H2/CO ratio of the syngas by ± 0.2 to 1.8 and 2.2 has a noticeable effect, resulting in GWP levels of 20.0 and 25.4 g CO_2-eq/MJ, respectively. Even though reducing the H2/CO ratio of the syngas appears to reduce GWP, the model cannot paint the complete picture of this change. Lower H2/CO ratio requires less hydrogen production, lower energy use, and lower emissions from syngas production. However, the GtL plant is designed to process syngas at a H2/CO ratio of 2. Change in this ratio will change the efficiency of the GtL plant, but there is no available data on how this efficiency would change with the H2/CO ratio of the syngas. Changing the efficiency of the Fischer-Tropsch process in the GtL plant from the original 80% down to 70% increase the GWP of the jet fuel to 24.8 g CO_2-eq/MJ from the 22.2 CO_2-eq/MJ reference, indicating that the gains of reducing the H2/CO ratio could be evened out by efficiency loss in the GtL plant. Two different allocation methods have been assessed for this case. The energy allocation method leads to a slightly lower GWP than mass allocation. Changing the energy use of the DAC unit and the compressor have little to no effect because of the low carbon intensity of wind power. If the electricity used was the German mix or other carbon-intensive electricity sources, these changes would have given bigger variations in the GWP.

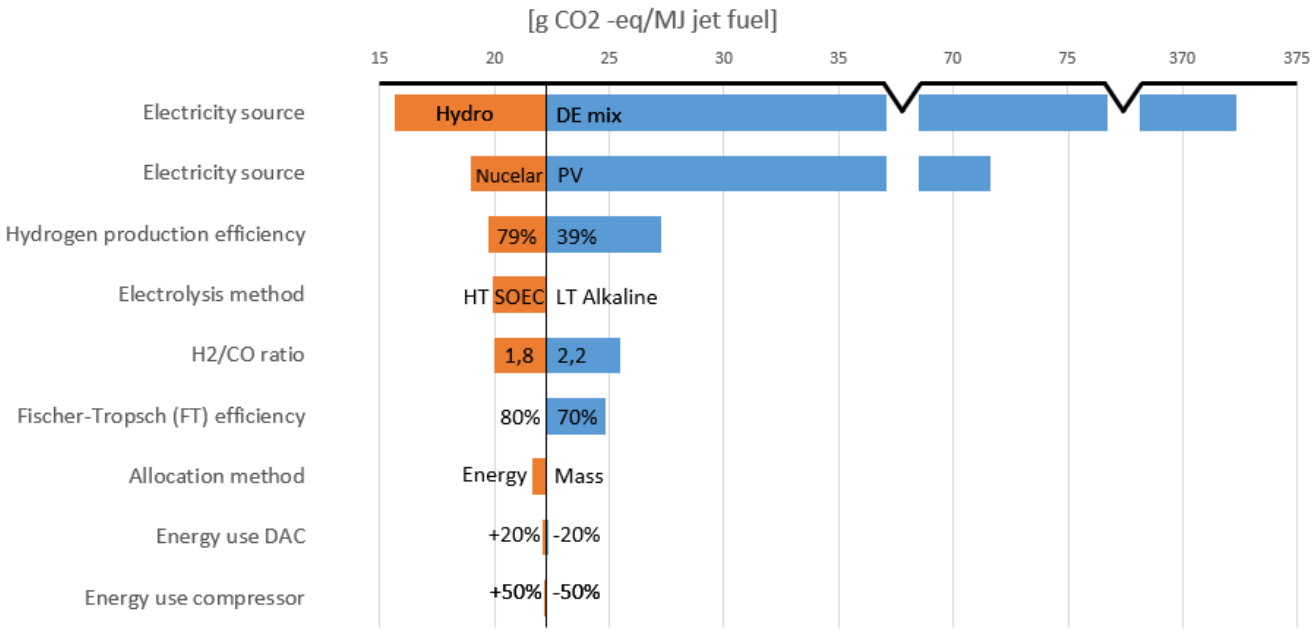

Figure 5.4.1: Sensitivity analysis of the GWP of PtL jet fuel produced using alkaline electrolysis and wind power. Blue bars represent an increase in GWP, while orange bars represent a decrease in GWP, relative to the reference of 22.2 [g CO_2-eq/MJ]. The percentages in hydrogen production efficiency and FT efficiency were altered to the percentages displayed in the figure, while energy use of the DAC and the compressor were altered by $\pm$ 20% and $\pm$ 50% respectively.

6 | Aircraft stock cohort model results

In this second of two results chapters, the simulation results of the updated aircraft stock cohort model are presented. The first three sections compare the simulation results obtained before and after including the generic aircraft representations for the air travel demand, the aircraft fleet, the fleet's fuel consumption, and the associated CO_2 emissions. The two final sections present the combustion and life cycle emissions of fossil jet fuel, as well as the CO_2 emissions in 2050 for different jet fuel blends.

The aircraft stock cohort model produces eight sets of simulation results using projections of air travel from the industries and projections of CO_2 emissions from SSP-RCP scenarios, as mentioned in chapter 4.1.3. The four industry projections of air travel demand come from Boeing, Airbus, ICAO, and IATA and result in four sets of simulation results. Only the key simulation results from one of the projections are included in this thesis to limit the results presented. Boeing's air travel demand projection was chosen as it represents the middle ground of the four projections. In addition, it provides the highest level of detail in future air travel, as can be seen from the data collection in table B.3.1 in the appendix. The model simulates the deliveries and retirements of aircraft to and from the fleet to keep track of the aircraft fleet development. Figures of the deliveries and retirements of aircraft are not included in this results chapter. Still, they can be found in figures A.6.1 and A.7.1 in the appendix, respectively.

6.1 Air travel demand

In the aircraft stock cohort model, the air travel demand is the driving force that dictates the aircraft fleet development and fuel use. The simulation results of the air travel demand are presented below in figure 6.1.1. It is a figure in two parts, where the upper half presents the simulation results of the aircraft stock cohort model before the update, and the bottom half presents the simulation results after the update. The same arrangement will be found in the two following figures as well, and they will be referred to as figure a and figure b, respectively. Figure 6.1.1.a presents the air travel demand from the original aircraft stock cohort model, while figure 6.1.1.b presents the air travel demand of the updated model.

Figure 6.1.1.b show the same increase in the total air travel demand as figure 6.1.1.a. The total air travel demand of the original and the updated model are equal because the air travel demand in figure 6.1.1.b is given from a percent wise distribution of the total air travel demand from figure 6.1.1.a, as described by table 4.2.1. The table shows that regional aircraft are distributed between aircraft representations A1-A4, narrow-body aircraft between A4-A6, and wide-body and freighter aircraft between A6-A8.

In figure 6.1.1.a, freighter demand is converted from trillion FTK to trillion RPK to make it more comparable with the passenger demand. In figure 6.1.1.b, freight is baked into the demand of the nine aircraft representations using the assumption that 50% of freight is designated freight, while 50% is covered as belly freight. This assumption means that the designated 50% of the freight in figure 6.1.1.a is distributed on aircraft representations A6-A8, where all designated freighter aircraft are placed. Therefore, the A6-A8 air travel demand in figure 6.1.1.b is substantially larger than the wide-body demand in figure 6.1.1.a because it includes large parts of the freight demand. The remaining 50% is belly freight and is distributed on all nine aircraft representations based on their shares of the total capacity.

Figure 6.1.1 shows that the total air travel demand triples from 2019 to 2050 and that the demand increases for all aircraft types. In figure 6.1.1.a, narrow-body demand experienced the most significant growth, followed by wide-body demand, freighter demand, and finally regional demand, which contributes very little to the overall increase. The demand covered by aircraft representation A5A shows the largest growth from 2019-2050, increasing from 3.1 to 10.3 Trillion RPK, covering 28% of the total demand in 2019 and 31% in 2050. Similarly, the growth in demand covered by aircraft representation A5B increase from 1.2 to 4.1 trillion RPK, covering 11% of the total in 2019 and 12% of the total in 2050. Demand covered by aircraft representations A6-A8 nearly triples over the simulated period, with aircraft A7 having the largest contribution, increasing from 2.8 to 7.9 trillion RPK. Despite this increase, the share of the total demand covered by aircraft representations A6-A8 decreases from 52% in 2019 to 48% in 2050. The three smallest aircraft representations' shares of the total demand are small compared to the rest and are barely visible in the figure. The enormous growth in air travel demand shows no sign of behavioral changes from the passengers. However, it indicates that aircraft representations A5A and A5B will be increasingly important in the future. These narrow-body aircraft are flexible in their applications and will cover more of the total air travel demand by expanding their current routes. This expansion happens at the expense of the larger aircraft representations, covering a smaller share of the total demand in the future.

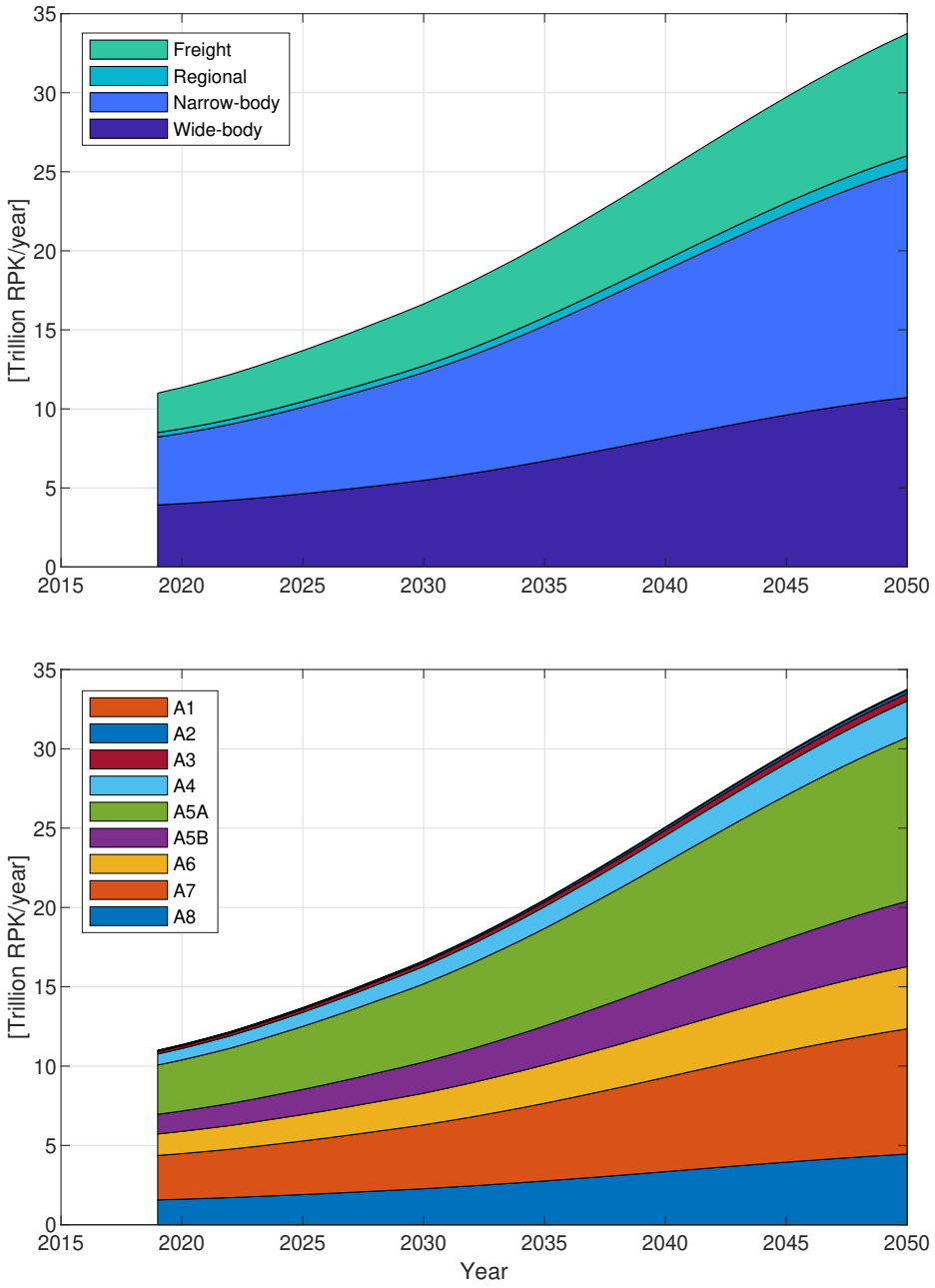

Figure 6.1.1: Simulation results of the air travel demand [Trillion RPK/year] development from 2019-2050. Figure 6.1.1.a in the upper half presents the simulation results of the aircraft stock cohort model before the update and covers four aircraft types. Figure 6.1.1.b in the lower half presents the simulation results of the updated model and cover all nine generic aircraft representations.

6.2 Aircraft fleet

The simulation results of the aircraft fleet development from 2019-2050 is presented in figure 6.2.1 below. Figure 6.2.1.a presents the fleet simulation of the original aircraft stock cohort model, while figure 6.2.1.b presents the simulation results of the updated model. Like for the air travel demand in figure 6.1.1, the results in figure 6.2.1.b are a distribution of the total fleet size in figure 6.2.1.a, meaning that the total aircraft fleet size is the same before and after the update. The difference between the results lies in the increase in resolution from four aircraft types in the original model to nine generic aircraft representations in the updated model.

In figure 6.2.1.a, it is clear that the largest fleet growth stems from the increase of narrow-body aircraft. Figure 6.2.1.b shows that most of the fleet growth more specifically comes from A5A aircraft, a generic aircraft representation only covering nine aircraft types (e.g., B737-800 and A320-231). In the simulated period, the A5A subfleet increase with over 19 000 aircraft, representing 43% of the total fleet in 2050. The second-largest contributor to overall fleet growth is the A5B aircraft representation, a slightly heavier narrow-body aircraft representation than the A5A, growing from 3 648 to 11 246 aircraft in the simulated period. The A6 generic aircraft representation covers mostly wide-body aircraft, while A7 and A8 cover wide-bodies exclusively. Aircraft representations A6-A8 in figure 6.2.1.b make up a larger share of the fleet than the wide-body aircraft in figure 6.2.1.a because the freighter aircraft in figure 6.2.1.a are distributed between aircraft A6-A8 in figure 6.2.1.b. Figure 6.2.1.b shows that the number of aircraft A6-A8 in the fleet all roughly double from 2019 to 2050. The largest wide-body increase, in terms of the number of aircraft, stems from aircraft A7. It is the second-largest aircraft representation, and it increases from 3 324 to 6 611 aircraft in the simulated period. The A4 aircraft representation also contributes to substantial growth of the overall fleet size, increasing from 3 283 to 7 245 aircraft over the simulated period. A1-A3 remains nearly constant in the same period.

Comparing the demand figure 6.1.1 with the aircraft fleet figure 6.2.1 shows the vast difference in carrying capacity of the different aircraft representations. In 2050, the three largest aircraft representations together make up 21% of the total aircraft fleet, while they cover 48% of the total demand. Due to their limited size, A5A aircraft only cover 31% of the total demand in 2050, despite representing 43% of the total number of aircraft in the 2050 aircraft fleet. The simulated fleet development from the aircraft stock cohort model shows that aircraft representations A5A and A5B are the aircraft of the future, with a combined fleet coverage of 60% in 2050. Aircraft representations A5A and A5B represent aircraft like the B737-800 and the B737-900ER, respectively. These aircraft are popular amongst airliners due to the flexibility in their application as they are relatively small in size, compared to wide-body aircraft, but can still cover distances of 5000-7000 km.

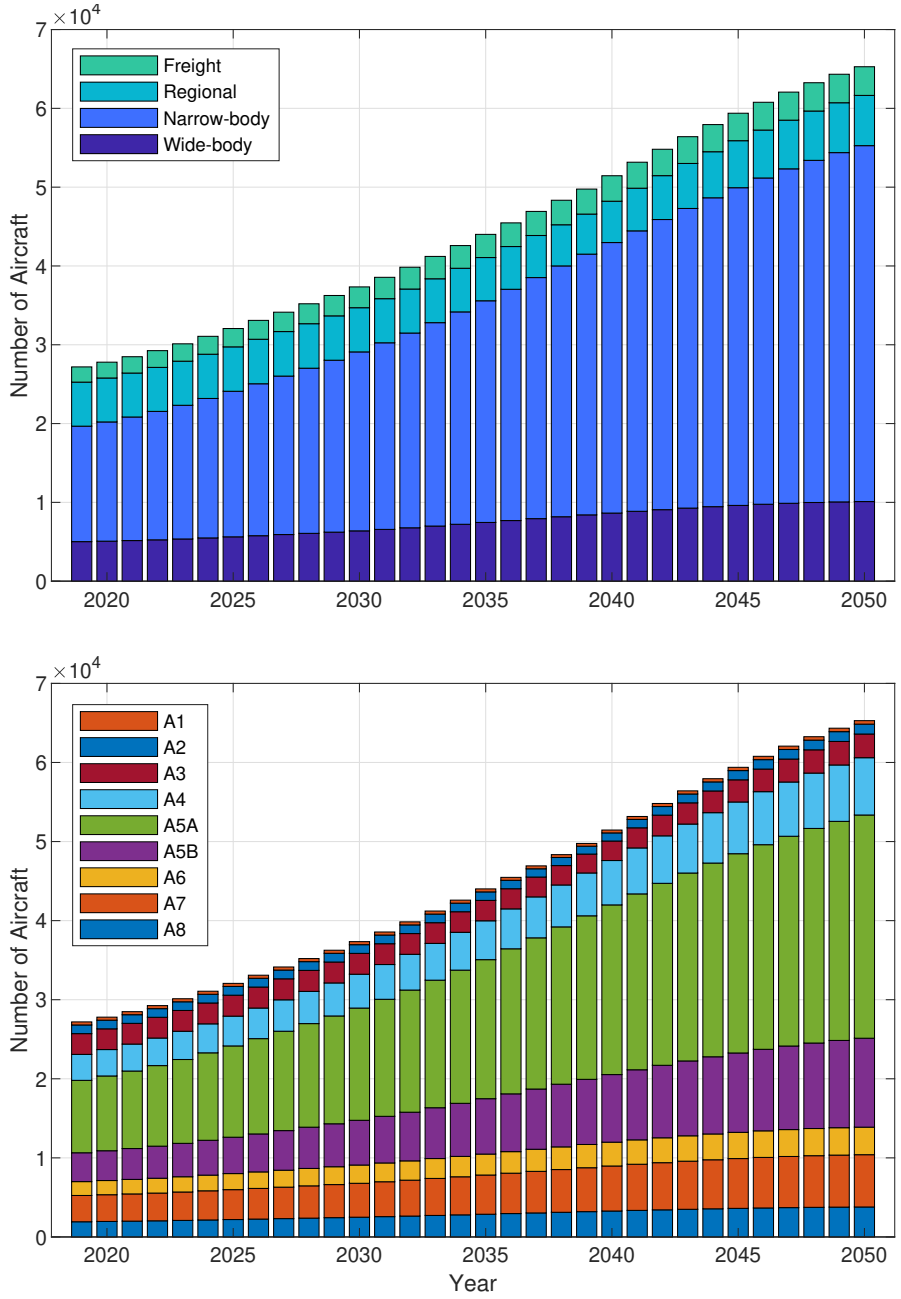

Figure 6.2.1: Simulation results of the aircraft fleet development from 2019-2050. Figure 6.2.1.a in the upper half presents the simulation results of the aircraft stock cohort model before the update and covers four aircraft types. Figure 6.2.1.b presents the simulation results of the updated model and cover all nine generic aircraft representations.

6.3 Fuel consumption and CO_2 emissions

The simulation results of the aircraft fleet's fuel consumption are presented in figure 6.3.1 below. The fuel consumption calculated with the original aircraft stock cohort model is presented in figure 6.3.1.a. Figure 6.3.1.b presents the fuel consumption after updating the model with the generic aircraft representations, and their belonging calculated fuel efficiencies, presented previously in table 4.2.2. For the original model, the total fuel consumption of the aircraft fleet grows from 285 to 644 Mt/year in the period from 2019 to 2050. In the simulation results of the updated model, the total fuel consumption grows from 311 to 681 Mt/year in the same period. The updated model's fuel consumption is 26 Mt/year higher in 2019 and 37 Mt/year higher in 2050 than the original model. In the updated model, calculated fuel consumption is moderately higher than for the original model. This difference is caused by the calculated fuel efficiencies of the three largest aircraft representations being slightly higher than the fuel efficiency used for wide-body aircraft in the original model, taken from the literature (Graver et al., 2020).

CO_2 emissions from combustion are proportional with the aircraft fuel consumption trough a factor of 3.16 kg CO_2/kg fuel, for fossil jet fuel (D. S. Lee et al., 2020). Therefore, by adding an extra y-axis on the right-hand side, the CO_2 emissions are also presented in figure 6.3.1. In the simulation results of the updated aircraft stock cohort model, the level of total CO_2 emissions of the aircraft fleet more than doubles, from 983 Mt CO_2/year in 2019 to 2152 Mt CO_2/year in 2050. The difference in the simulation results of the original and the updated model, as mentioned for the fuel consumption in the previous paragraph, applies to the CO_2 emissions as well. Total CO_2 emissions from the aircraft fleet increase by 219% from 2019-2050. In comparison, the air travel demand increase by 307% in the same period. The higher increase in air travel demand than in CO_2 emissions is due to the increasing fuel efficiency of the aircraft fleet. Every year in the simulation period, the fleet's fuel efficiency is improved by 1%, resulting in an increasingly fuel efficient fleet going towards 2050. A graph investigating the effect of adjusting the rate of fuel efficiency improvement can be found in figure A.9.1 in the appendix. It shows that an annual improvement of 3% leads to an emission reduction of 256 Mt/CO2 in 2050, compared to a 0% annual improvement.

Figure 6.3.1.a shows that the fuel consumption, and thereby CO_2 emissions, grows for all aircraft types. In 2050, narrow-body aircraft hold the largest share of fuel consumption, followed by wide-body aircraft, designated freighter aircraft, and regional aircraft. Figure 6.3.1.b also shows a growth in fuel consumption for all aircraft types. Here, aircraft A6-A8 make up 57% of the fuel consumption and CO_2 emissions of the entire fleet. This is because the fuel consumption by designated freighter aircraft in figure 6.3.1.a is covered by aircraft A6-A8, as explained previously in section 6.2. Aircraft A7 consequently has the largest

growth in fuel consumption and CO_2 emissions from 2019-2050, as it covers some of the growth in fuel consumption of both wide-body and freighter aircraft. The second-largest growth in fuel consumption is by aircraft A5A, which covers a large share of the total narrow-body fuel consumption, reaching 24% of the total fleet's consumption in 2050.

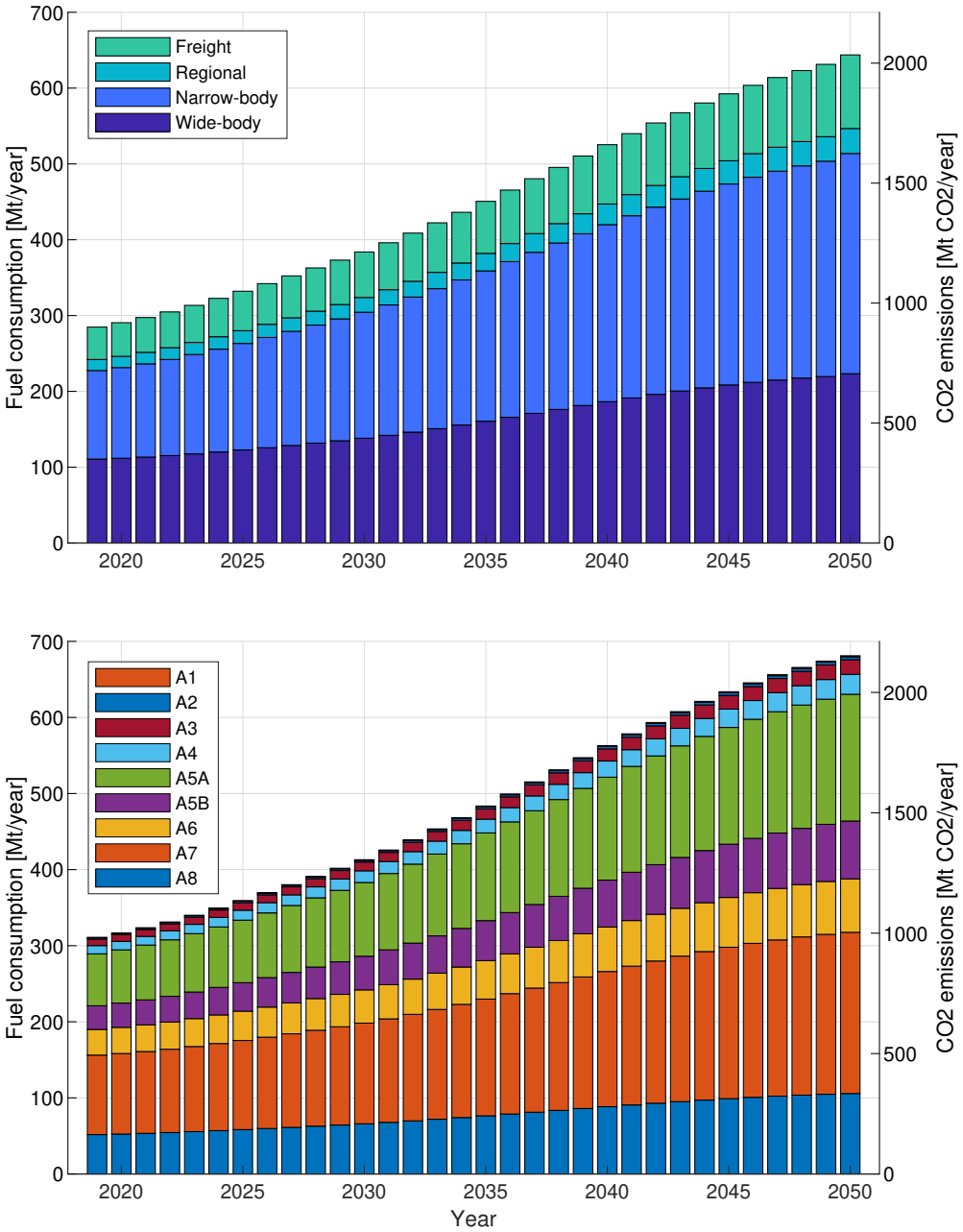

Figure 6.3.1: Simulation results of the fuel consumption [Mt/year] and CO_2 emission [Mt CO_2 /year] development from 2019-2050. Figure 6.3.1.a in the upper half presents the simulation results of the aircraft stock cohort model before the update and covers four aircraft types. Figure 6.3.1.b presents the simulation results of the updated model and cover all nine generic aircraft representations.

6.4 CO_2 emissions from fossil jet fuel

In figure 6.4.1 below, the total aircraft fleet's CO_2 emissions, when using only fossil jet fuel, is compared to four different SSP-RCP future scenarios for combustion CO_2 emissions from aviation. The figure also presents the total CO_2 emissions of the aircraft fleet when including well-to-wake life cycle CO_2 emissions of fossil jet fuel, illustrated as a red line. The life cycle CO_2 emissions are based on the LCA results in chapter 5, and are 30% higher than the CO_2 emissions from combustion only.

The SSP-RCP scenarios are retrieved from the CIMP6 emissions database (Gidden et al., 2019; Riahi et al., 2017; Rogelj et al., 2018). Scenarios SSP1-19 and SSP1-26 indicate the emissions pathways for aviation where global warming is limited to 1.5°C and below 2°C, respectively. SSP2-45 represent an intermediate scenario, while SSP5-85 represent a high emissions scenario (IPCC, 2014a). If the demand presented previously, in figure 6.1.1, is covered by fossil jet fuel, the combustion CO_2 emissions will follow the trajectory of the blue line. The blue line trajectory is very close to the high emission scenario SSP5-85 and represents far higher emission levels than the desired SSP1-19 and SSP1-26 scenarios. In 2050, the CO_2 combustion emissions are 1410 and 1920 Mt CO_2/year higher than SSP1-26 and SSP1-19 respectively.

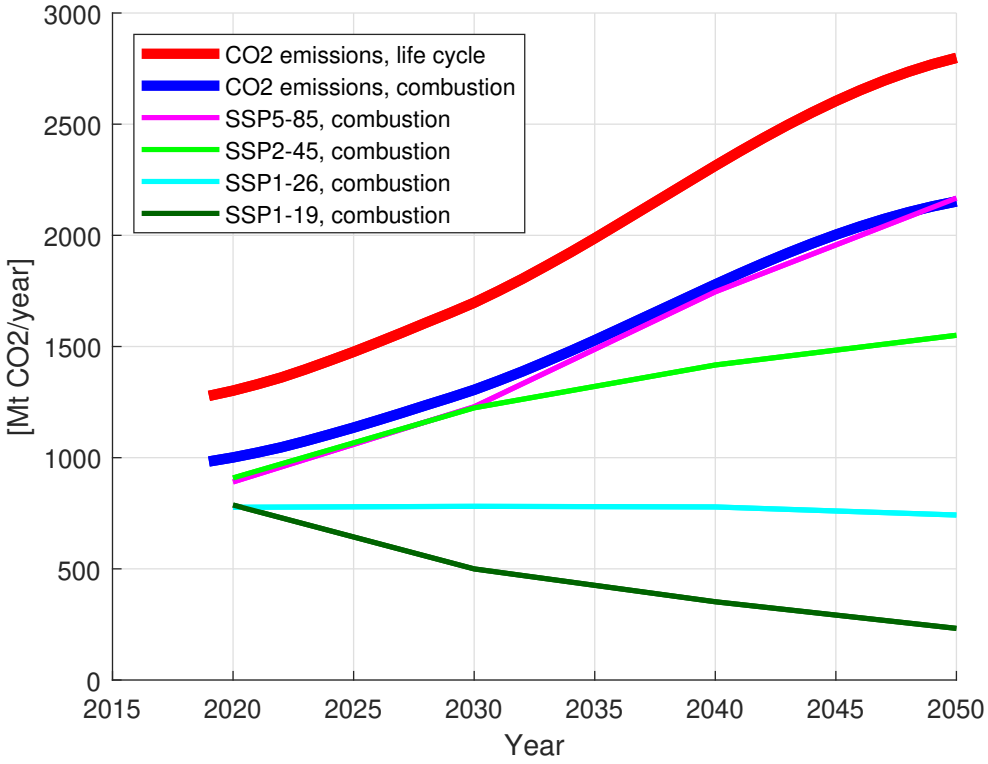

Figure 6.4.1: Simulation results of the total CO_2 combustion emissions [Mt CO_2 /year] and the total CO_2 life cyle emissions [Mt CO_2 /year] of the aircraft fleet when using only fossil jet fuel, compared to four SSP-RCP scenarios [Mt CO_2 /year], from 2019-2050.

6.5 CO_2 emissions in 2050

The CO_2 emissions of different fuel blends used by the aircraft fleet are presented in figure 6.5.1 below. The blue columns represent the total CO_2 emissions when the aircraft fleet uses certain shares of PtL jet fuel produced with alkaline electrolysis, given in the x-axis, while the rest is fossil jet fuel. Similarly for the red columns, which represent shares of PtL jet fuel produced using HT co-electrolysis. The dotted lines represent the four SSP-RCP scenario's CO_2 emission levels for aviation in 2050. Taking the forth column as an example, the blue column shows that the aircraft fleet emits 1009 Mt CO_2 /year in 2050 if it uses 75% PtL alkaline jet fuel and 25% fossil jet fuel. Likewise, the fourth red column shows that the aircraft fleet emits 959 Mt CO_2 /year in 2050 if it uses 75% PtL HT jet fuel and 25% fossil jet fuel. Both of the 75% blends place the CO_2 emissions of the aircraft fleet between the emission levels of scenarios SSP1-26 and SSP2-45.

Comparing column one, using only fossil jet fuel, and column five, using only PtL jet fuel, shows a potential reduction in CO_2 emissions of 1524-1591 Mt CO_2/year in 2050. The 67 Mt CO_2/year difference between the PtL jet fuels in column five stems from the LCA results in chapter 5, showing that the PtL jet fuel produced with the HT co-electrolysis emits slightly less CO_2 per MJ jet fuel well-to-wake. For the two alternative jet fuels analyzed, it is only the 100% blend that reduces the emissions level in 2050 down to below the emission level of the SSP1-26 scenario, in line with the 2°C target. The 100% PtL jet fuel blend would give lower CO_2 emissions from the aircraft fleet in 2050 than in 2019, while the 75% blend would give close to equal CO_2 emissions in 2050 as in 2019 at around 1000 Mt CO_2 /year. Using 50% or 75% PtL jet fuel places the total CO_2 emissions of the fleet in 2050 between SSP1-26 and SSP2-45. A blend of 0-25% PtL jet fuel places the CO_2 emissions between scenarios SSP2-45 and SSP5-85.

Figure 6.5.1 provide information about the CO_2 emission levels of different PtL and fossil jet fuel blends in 2050. However, it does not contain information about different pathways of reaching the defined blends. Such pathways are hard to predict and easily become speculative and are not pursued in this thesis. If the aircraft fleet in 2050 were to use 100% PtL jet fuel, the rate and timing at which the PtL were introduced would not change the 2050 emissions. It would, however, affect the accumulated CO_2 emissions in the time period going towards 2050. To illustrate this, the explorative figure A.8.1 can be found in the appendix, presenting two hypothetical scenarios of introducing PtL jet fuel to a 100% blend by 2050. The two hypothetical scenarios reach the same emission level in 2050, even though the starting years for phasing in PtL jet fuel are 15 years apart. These 15 years lead to a difference in cumulative CO_2 emissions of 17 542 Mt CO_2/year.

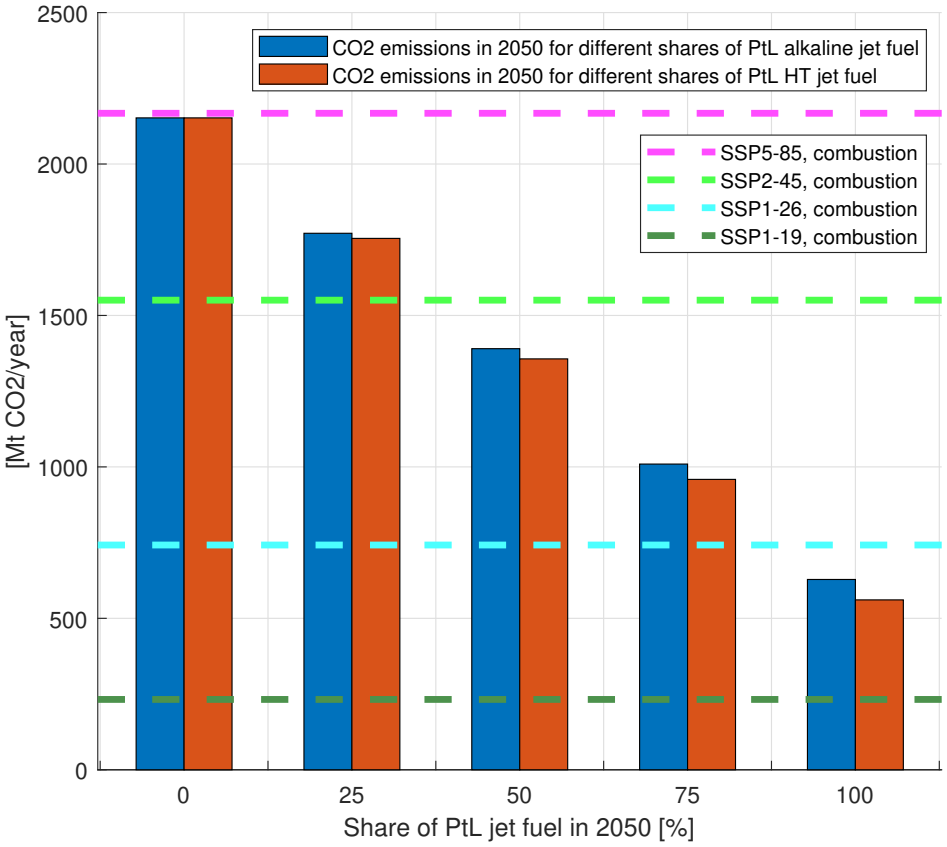

Figure 6.5.1: Simulation results of the total CO_2 emissions [Mt CO_2 /year] of the aircraft fleet, when replacing different shares of fossil jet fuel with PtL jet fuel, in 2050. Blue and red columns represent the CO_2 emissions of the aircraft fleet, for different shares of fossil fuel being replaced by PtL alkaline and PtL HT jet fuel respectively. The dotted lines represent the aviation combustion CO_2 emissions in 2050, for the four SSP-RCP scenarios.

This chapter shows that the air travel demand, the aircraft fleet, and the CO_2 emissions all will increase drastically towards 2050 if no changes are made and when following a business as usual development. Introducing the generic aircraft representations to the aircraft stock cohort model gives a more detailed understanding of the aircraft fleet. Aircraft representation A5A stands out with its large fleet share as the aircraft of the future. Its size and range make it a versatile aircraft that can expand its applications in the coming years. The implementation of the PtL jet fuels' LCA results shows a large emission reduction potential. Future emission levels of aviation can be significantly reduced by substituting fossil jet fuel with PtL jet fuel or other alternative jet fuels. The figures in this chapter provide information about the link between fuel consumption and CO_2 emissions and how they are related to the aircraft fleet and the air travel demand. Exploring these interrelations can provide useful information on the effects of various mitigation measures.

7 | Discussion

The discussion chapter of the thesis is divided into four sections. It starts off by addressing the strength and limitations of the study. The second section compares the results to previous literature to assess the quality of the LCA results and the aircraft stock cohort model. In the third section, the results are discussed, and the implications of the findings are looked into. The final section contains possibilities for future work.

7.1 Strengths and limitations of the study

In this thesis, a life cycle assessment of three different jet fuels has been conducted. The results have been used to update an aircraft stock cohort model, which was developed in the project pre-phase of the thesis. Introducing the LCA results into the aircraft stock cohort is a strength of the thesis, as it brings a global context to the LCA results. It allows for calculating fleet-wide emissions and potential emission reductions of the entire aviation sector instead of just comparing the jet fuels' environmental performance on a per MJ basis. The two PtL jet fuels only differ when it comes to the technology used to produce the syngas. Comparing these two technologies of different readiness levels provides information about the environmental performance of PtL jet fuel today and some information about expected performance in the near future.

Nine generic aircraft representations were created using the BADA database and included in the aircraft stock cohort model to increase the resolution of the simulation results. A higher resolution of the aircraft fleet, air travel demand, fuel consumption, and CO_2 emissions provide a better understanding of how the fleet composition affects the emissions of the sector. Detailed information about the development of the aircraft fleet, air travel demand, and fuel consumption makes it easier to uncover where the most significant emission reduction potential of the aircraft fleet lies.

The data used in the LCA of the PtL jet fuels are taken from the two studies by (van der Giesen et al., 2014) and (Schreiber et al., 2020). There are limited previous studies conducting well-to-wake LCAs of PtL jet fuel. These two studies were chosen as the basis of the LCA as they provided the most complete data sets with their analysis. For

the aircraft stock cohort model, an overview of the data used to build the model and run the simulations can be found in table B.3.1 in the appendix. Data on the historical aircraft fleet and the historical and projected air travel demand are collected from several sources and compared. The most important input of the model is the projected air travel demand. Projections from Boeing, Airbus, ICAO, and IATA were collected and compared. Boeing and ICAO have projections of the same magnitude, while Airbus is slightly higher and IATA slightly lower. The air travel projection from Boeing was chosen in this thesis because it represents the middle ground of the four industries, and the projection had a higher resolution than the other three.

The fuel consumption coefficient was only calculated for cruise configuration. The publicly available air travel data used in the aircraft stock cohort model is quite aggregate, making it difficult to divide the demand into different flight phases. Assuming all air travel demand is covered in cruise configuration can lead to underestimation and overestimation of fuel consumption. The potential underestimation is most present for short-haul flights. Flying a short distance leads to higher average fuel consumption because the take-off procedure is so energy-intensive. The potential overestimation is most present for long-haul flights. Flying long distances requires a fuller fuel tank than shorter distances. A fuller tank equals a heavier aircraft and higher average fuel consumption. In the paper by (Egelhofer, Marizy, & Bickerstaff, 2008), a long-range aircraft's fuel consumption was calculated as a function of distance. For a 1000 km flight, the average fuel consumption was higher than 10.0 kg/km. It was 8.5 kg/km for flights between 4000-5000 and 9.7 kg/km for flights of 15 000 km. Some of the potential overestimation and underestimation will cancel each other out, reducing the overall uncertainty.

The fuel consumption coefficient was calculated as g fuel/RPK, such that the original aircraft stock cohort model could be used. These fuel consumption coefficients are subject to some uncertainty because they have been calculated using a fixed fleet-wide average passenger load factor, which in reality varies with geographical location and over time. Calculations performed on 54 global routes in 2018 showed a range in the average passenger load factor of 60-83% (Graver et al., 2019a). From 1950-2018, the average passenger load factor has increased from 61-82% (A4A, 2018b). A continued increase of the average passenger load factor will not be reflected in the model and would result in an overestimation of emissions. However, there is a cap to this overestimation, as the average passenger load factor can maximum reach 100%.

Detailed data of the number of aircraft of each aircraft type in the fleet was retrieved for April of 2021. This data was used to distribute the four aircraft types of the original aircraft stock cohort model to the nine aircraft representations of the updated model. Using the aircraft fleet as of April 2021 to distribute the four aircraft types of the original

model to the nine aircraft representations will affect the simulation results of the number of aircraft in the fleet. The development going towards 2050 will be accurate for the total number of aircraft. However, the number of aircraft of each aircraft representation is distributed the same way for all years towards 2050. This way of distributing the aircraft means that, for instance, the number of aircraft A5A will increase when the number of narrow-body aircraft increases, but the number of A5A aircraft will represent the same share of the number of narrow-body aircraft for every year simulated. Therefore, the uncertainty of the distribution of each aircraft representation's number of aircraft in the total fleet will increase as the simulation moves towards 2050.

7.2 Quality of the results and comparison to other studies

In this section, the LCA results and the simulation results of the aircraft stock cohort model are compared to previous studies found in the literature. This comparison is essential to establish the robustness of the results and the quality of the LCA and the aircraft stock cohort model. The LCA results will be evaluated first, followed by the aircraft stock cohort results.

7.2.1 Quality and comparison of the LCA results

The LCA results are divided into three different jet fuels: fossil jet fuel, PtL alkaline jet fuel, and PtL HT jet fuel. For all three jet fuels, the combustion emissions are given by stoichiometric reactions, meaning that the difference in results will mainly come from emissions associated with the production of the fuels. The fossil jet fuel results showed a GWP of 94 g CO_2-eq/MJ, where 70 g CO_2-eq/MJ came from combustion and 24 g CO_2-eq/MJ from the remaining well-to-tank processes. This GWP value is well within the established range of EU fossil jet fuel well-to-wake emissions of 80-106 g CO_2-eq/MJ, which largely depends on the composition of the crude oil used in the production (EC, 2015). In addition to crude oil composition, the well-to-tank emissions depend on transport distances and refineries used. Therefore, previous literature shows a spread in the well-to-tank GWP of fossil jet fuel. This spread can be exemplified by looking at two different studies that, among other things, carried out a LCA of fossil jet fuel. The first uses crude oil from the Middle East and refineries in Europe, resulting in a well-to-tank GWP of just over 50 g CO_2-eq/MJ (Koroneos, Dompros, Roumbas, & Moussiopoulos, 2005). In the second study, life cycle inventory data from the Australian production system was used, which resulted in a well-to-tank GWP of only 12 g CO_2-eq/MJ (Cox et al., 2014).

The LCA results for the PtL jet fuels also have to be compared to the available results of previous studies on synthetic fuels. Both PtL systems are largely adopted from two previous studies, as described in chapters 2.2.6 and 2.2.7. The PtL alkaline system uses the system setup of (van der Giesen et al., 2014), but replaces the carbon capture from concentrated source with a DAC unit from (Schreiber et al., 2020). The PtL HT system uses the same system set up but replaces the hydrogen and syngas production with a high-temperature co-electrolysis from (Schreiber et al., 2020). Since (van der Giesen et al., 2014) investigate synthetic hydrocarbons in general produced with CO_2 captured from a concentrated source, and (Schreiber et al., 2020) look at just the syngas production using different electricity sources, the results are only comparable to a certain degree.

In the paper by (van der Giesen et al., 2014), the synthetic hydrocarbon well-to-wake GWP is calculated to 120 g CO_2-eq/MJ when using PV electricity. In that case, the CO_2 comes from a natural gas combustion plant and therefore does not give a negative contribution to the overall emissions. In this thesis, the well-to-wake GWP of PtL alkaline jet fuel produced using PV electricity is 72 g CO_2-eq/MJ. The difference between the two comes from the negative emissions from the DAC carbon capture for the PtL alkaline jet fuel. When excluding these negative emissions, the GWP becomes 141 g CO_2-eq/MJ. This GWP value is slightly higher than the result of (van der Giesen et al., 2014), a difference that can be explained by higher energy use in capturing CO_2 with the DAC unit compared to the concentrated source. In the paper by (Schreiber et al., 2020), syngas production using high-temperature co-electrolysis with German electricity mix emits 6.5 kg CO_2-eq/kg syngas or 276 g CO_2-eq/MJ. This value can be compared to the GWP of syngas production only, for PtL HT jet fuel using German electricity mix, of 283 g CO_2-eq/MJ. The difference between the two results is only 2.5%. The similar values of GWP between the LCA results of this thesis and the two studies indicate that the LCA is correctly performed and that the results are sound.

A LCA analysis of the Sunfire PtL demonstration plant in Germany, which produces synthetic diesel using DAC of CO_2 and hydrogen from high-temperature co-electrolysis, is performed by (Lozanovski & Brandstetter, 2015). The report compares the GHG emissions when producing the fuel using electricity from the German grid, PV, wind power, and hydropower, making it very comparable to the LCA results of this thesis. The overall results from (Lozanovski & Brandstetter, 2015) show the same as found in this thesis; using electricity from the German grid results in higher emissions than the fossil reference, while renewable sources give lower emissions than the fossil reference. Like in this thesis, the hydropower option performs best, closely followed by wind power and then PV with noticeably higher emissions. The GWP values of the fuel from the Sunfire plant were 32, 34, 51, and 300 g CO_2/MJ using hydropower, wind power, PV, and German grid electricity, respectively. In this thesis, the PtL HT jet fuel using the same sources of electricity gave

the GWP values 14, 20, 61, and 316 g CO_2/MJ, respectively. To explain the differences in these numbers, looking closer at the process contributions is necessary. The Sunfire plant only provides process contributions for production using electricity from wind power and from the German grid. The DAC unit of the Sunfire plant contributes with 22 g CO_2/MJ in the wind power case and 33 g CO_2/MJ in the German grid case. In this thesis, the equivalent values are 7 g CO_2/MJ and 29 g CO_2/MJ. The Sunfire plant uses a DAC unit which requires more thermal energy relative to electricity than the one used in this thesis. Therefore, the emissions in the DAC unit of the Sunfire plant are less dependent on the electricity source and have higher relative emissions when using electricity sources of low carbon intensity. If the Sunfire plant had the same GHG emissions from the DAC unit as the one in this thesis, the Sunfire wind power case would have a GWP of 19 g CO_2/MJ, which is very close to the equivalent GWP of 20 g CO_2/MJ in this thesis.

7.2.2 Quality and comparison of aircraft stock cohort results

Since the aircraft fleet size depends on the air travel demand, the projections used will affect the simulation results. In the project pre-phase of the thesis, the aircraft stock cohort model used projections of future air travel demand from Boeing, Airbus, ICAO, and IATA to run separate simulations, which resulted in fleet sizes in good agreement with the projected future aircraft fleets of the respective industries. The demand used in this thesis is taken from (Boeing, 2020b). The fleet development simulation results show an expected growth from around 27 200 to 49 800 aircraft from 2019-2039. This increase is in good agreement with the fleet growth projected by Boeing, from 25 900 to 48 400 aircraft in the same period, especially when considering that Boeing does not include piston and turboprop aircraft in the fleet (Boeing, 2020b).

When comparing fleet development with other literature, the projection of air travel demand must be kept in mind. In IATA's aircraft technology roadmap to 2050, the fleet development is divided into three future scenarios based on air travel demand projections (IATA, 2019). The total fleet size of this thesis falls between the baseline scenario and the UP scenario because the projected air travel demand from Boeing lies between the IATA projections used in the baseline and the UP scenario. However, as the IATA fleet development uses a similar resolution in its simulation results as done in this thesis, it makes for a good comparison. IATA divides the fleet into eight segments based on passenger-carrying capacity. According to (IATA, 2019) the largest growth comes from aircraft with 151-210 seats, a size that coincides with the generic aircraft representation A5A and A5B, which are the two most significant contributors to fleet growth in the simulation results of this thesis. Similarly, the second largest contributor to fleet growth in the IATA report is aircraft with 101-150 seats. This size coincides with aircraft representation A4, the third-largest contributor to fleet size in this thesis.

In 2019, the first year of the simulation results, the total CO_2 emissions from the fleet are 983 Mt CO_2/year for the updated aircraft stock cohort model and 900 Mt CO_2/year for the original model. The difference between the two comes from the slightly higher calculated fuel consumption coefficients of aircraft representations A6-A8 in the updated model, as addressed in chapter 6.3. As mentioned in the state of the art, there are two main ways of calculating CO_2 emissions from the aircraft fleet, either by using jet fuel sales or civil aviation inventories. As one would expect due to the known discrepancy between the two methods, both the original and updated model calculate lower CO_2 emissions than the estimations from (D. S. Lee et al., 2020) of 1034 Mt CO_2/year in 2018, based on jet fuel sales. In the paper by (Graver et al., 2020), the estimate of total CO_2 emissions of 2019 using a civil aviation inventory was 920 Mt CO_2, which places it between the results of the original and the updated model. Having identified the reasons behind the moderate differences between this thesis and previous studies, the starting point of the simulation results of CO_2 emissions is sound.

Future emissions of the aviation sector are difficult to predict, as they depend on projections and assumptions on future development. This dependency can be exemplified by the paper by (Owen et al., 2010), where the estimated CO_2 emissions of the fleet in 2050 span from 1000-2500 Mt CO_2/year in 2050. The previous sections have established that the simulation results of the aircraft stock cohort model are coherent to prior studies when using the same or similar input data. Through the model simulations, a given air travel demand results in a specific fleet size and a corresponding level of CO_2 emissions. Therefore, the aircraft stock cohort model is not a way of predicting the future but rather a tool to provide valuable information about the future development of the aircraft fleet and the associated emissions, given particular prerequisites.

7.3 Discussion of the results and implications of the findings

In this section, the LCA results and the aircraft stock cohort results are discussed, and the results' implications are investigated. The first two subsections look at the LCA results and the results of the aircraft stock cohort results specifically, while the remaining subsections put the results into a wider context.

7.3.1 LCA results

The total values of the GWP impact category and the CO_2 and CH_4 stressors are lower for the PtL jet fuels compared to fossil jet fuel. For PtL alkaline jet fuel, the GWP of 22.2 g CO_2-eq/MJ is 76.4% lower than the fossil jet fuel at 94.0 g CO_2-eq/MJ. Similarly, the PtL alkaline jet fuel's GWP at 19.9 g CO_2-eq/MJ is 78.8% lower than the fossil jet fuel. The large differences in GWP per MJ of fossil jet fuel and the PtL jet fuels show a significant emissions reduction potential in substituting fossil jet fuel by PtL jet fuels. This substitution could lead to large reductions of GHG emissions from the entire aviation sector if performed on a fleet-wide scale.

The stressors and the GWP impact category were examined more closely in this thesis. This examination provides the individual process's contributions to the total results, giving a better understanding of the origin of the emissions. The contribution analysis of the stressors showed that hydrogen production and direct air capture of CO_2, which are processes requiring large amounts of electricity, were the most significant contributors to the PtL jet fuels net GHG emissions. Therefore, changing the electricity source resulted in a considerable variation in the GWP of the PtL jet fuels. These variations clearly show that renewable energy sources like PV, wind power, or hydropower must be used when producing PtL jet fuels to get a lower GWP than fossil fuel. Production of PtL jet fuel using the German electricity mix results in over three times higher GWP than fossil jet fuel. Therefore, large-scale emissions reductions from the aircraft fleet require a sufficient supply of electricity from renewable sources.

7.3.2 Aircraft stock cohort results

The simulation results of the air travel demand show an enormous growth going towards 2050. The most significant increase comes from demand covered by A5A aircraft, which grows from 3.1-10.3 trillion RPK/year from 2019-2050 and covers 31% of the total demand in 2050. This growth indicates that the airlines are gaining confidence in the narrow-body aircraft as a versatile aircraft with the ability to cover many different routes. Air travel demand covered by A7 aircraft represents the second biggest growth going from 2.8-7.9

trillion RPK/year over the simulation period. The demand covered by A7 aircraft and A6 and A8 make up 48% of the total demand in 2050. This coverage shows the importance of the capacity of the larger aircraft representations to cover the growth in demand of both passenger travel and freight.

In a study by (Graver et al., 2020) the carbon intensity of seating classes were calculated for regional, narrow-body, and wide-body aircraft. The calculations showed that premium seating was more than twice as carbon-intensive as economy seating for regional aircraft, more than three times as carbon-intensive for narrow-body aircraft, and close to four times for wide-body aircraft. Considering that the wide-body aircraft represented by aircraft representations A6-A8 cover 48% of the demand, the difference in the carbon intensity of seating classes indicates a significant CO_2 emission reduction potential from more space-efficient seating. Replacing first class and business class seating with more space-efficient seating would allow aircraft to cover a larger demand in air travel using the same number of aircraft and flights.

The air travel demand in the simulation results follows a business as usual trajectory, continuing the growth trends of historical demand. Behavioral change of the passengers could change this air travel demand development. Increased environmental awareness could result in slower growth in demand and thereby a slower growth in fleet size and CO_2 emissions. In addition, if the passengers' choice of airlines becomes dependent on the airlines' environmental performance, it would create an economic incentive for airliners to reduce their climate contributions.

The simulation results of the aircraft fleet show how the fleet is divided based on technical properties. As expected, after looking at the air travel demand, the A5A aircraft stand out with the largest fleet share. The A5A aircraft represent 34% of the 2019 fleet and 43% of the 2050 fleet, despite only covering nine aircraft types in the total aircraft fleet. In 2050, the second-largest share of the aircraft fleet is held by A5B aircraft, at 17%. A5A and A5B are the two most similar aircraft representations of the nine and add up to 60% of the total fleet in 2050. This share provides a strong indication of the importance of this aircraft segment in the years to come. Comparing the number of aircraft in the fleet to the air travel demand covered by the different aircraft representations shows the importance of considering the aircraft size when looking at the total fleet. In 2050, the A5A and A5B aircraft represent 60% of the number of aircraft in the fleet but only cover 43% of the demand. This relationship is the other way around for the larger aircraft representations. Aircraft representations A6-A8 only represent 21% of the total number of aircraft in the fleet in 2050 but cover 48% of the total air travel demand.

The simulation results of the fuel consumption and CO_2 emissions of the fleet show how the fleet's fuel use and CO_2 emissions are distributed on the generic aircraft representations. Aircraft A7 is the holds the largest share of the total CO_2 emissions, followed by aircraft A5A. The most significant contributors to total CO_2 emissions also hold the best opportunity for large-scale emission reduction. In 2050, the simulation results show that 93% of the total CO_2 emissions comes from aircraft A5A-A8, while only 7% comes from aircraft A1-A4. In other words, large-scale emission reductions from the fleet will only be possible if the mitigation measures can target aircraft representations A5A-A8.

Electric aircraft is currently a topic of debate regarding the future of aviation and is frequently mentioned as a possible mitigation option. The largest commercially available electric aircraft today can seat nine passengers and has a range of 160 km (NBC, 2020). Half of all flights globally are shorter than 1 200 km, a range that electric aircraft are predicted to be able to cover in the near future according to (American, 2020). The number of short-haul flights makes electric aircraft a promising business opportunity. However, the energy density and weight of the batteries pose a challenge for longer flights, making it uncertain if electric aircraft ever will be able to cover distances over 2 200 km (Schäfer et al., 2019). The limitations in range and carrying capacity affect the mitigation potential of electric aircraft. Placing the electric aircraft ranges into the context of this thesis, the emission reduction potential is limited to the smallest aircraft representations and thereby targets the 7% of the total emissions caused by A1-A4, as mentioned in the previous paragraph. Therefore, the emission reduction potential of electric aircraft is limited and is not the sole solution to the problem. However, it can still be an important step toward reducing GHG emissions from the aviation sector.

Improved operations and technological development are also pointed to as important mitigation measures for the aviation sector (IATA, 2019). The main difference between the two measures is the implementation rate. Operational measures result in immediate emission reductions because they can be simultaneously implemented across the entire fleet. Implementation of technological development measures is subject to the fleet turnover rate. Introducing new and more energy-effective aircraft to the fleet results in better average fuel efficiency, but it takes a long time before the entire fleet has been replaced. The effect of different levels of technological development can be seen in figure A.9.1 in the appendix, which shows the spread in CO_2 emissions by changing the annual fuel efficiency improvement of the aircraft fleet.

Introducing the LCA results of the three jet fuels into the updated aircraft stock cohort model brings a global perspective to the results. The LCA results alone present the difference in environmental performance per MJ of the analyzed jet fuels. In contrast, the aircraft stock cohort results provide information about the emission reduction potential of

the entire aircraft fleet. The total fuel use of the fleet increases from 311 to 681 Mt/year from 2019-2050, with the corresponding CO_2 emissions from combustion of fossil jet fuel increasing from 983 to 2152 Mt CO_2/year in the same period. Replacing fossil jet fuel with PtL jet fuels reduces the emission level of the aircraft fleet significantly. If all fossil jet fuel were replaced by PtL alkaline or PtL HT jet fuel in 2050, it would reduce the total emissions of the aircraft fleet by 628 and 561 Mt CO_2/year, respectively. This emission reduction would place CO_2 emissions from the aircraft fleet in 2050 lower than today's level and between scenarios SSP1-19 and SSP1-26 and ensure that the aviation sector does its part in limiting global warming to below 2°C. A blend of 75% PtL jet fuel and 25% fossil jet fuel used by the fleet in 2050 would bring the emission levels down to today's level of around 1000 Mt CO_2/year, in line with the long term aspirational goal of remaining at 2020 emission levels. Based on this information, the emission reduction potential of PtL seems very promising. However, large-scale emission reduction assumes that the production of PtL jet fuel can meet the demand by the aircraft fleet in 2050.

7.3.3 PtL jet fuel production cost and electricity demand

The production cost of PtL jet fuel was addressed through a techno-economic analysis in a recent report by (Sherwin, 2021). It investigated a PtL production system, very similar to the PtL jet fuel system using alkaline electrolysis in this thesis. It found that PtL jet fuel produced using DAC of CO_2 and electricity from solar or wind power would cost between 4.41-4.66$/litre of gasoline-equivalent (lge), which is much higher than the average US jet fuel price from 2010-2019 of 0.59 $/lge (Sherwin, 2021). The current price gap makes reducing CO_2 from aviation by replacing fossil jet fuel with PtL jet fuel a costly way to mitigate emissions. However, the same report estimates that the PtL jet fuel price will be reduced due to reducing the cost of DAC and electrolyzer systems to 1.7-1.8 $/lge in the next decade and to below 1 $/lge by 2050. A price reduction of this magnitude would create possibilities for using PtL jet fuel to achieve large-scale emission reductions in the aviation sector.

For large-scale emission reductions by the aircraft fleet to be possible using PtL jet fuel, there has to be enough electricity from renewable sources available for jet fuel production. In 2050, the simulation results show a fleet fuel consumption of 681 Mt/year. Producing PtL jet fuel with alkaline electrolysis requires 0.6 kWh/MJ, which is equal to 25.9 kWh/kg or 25.9 TWh/Mt. The production of PtL jet fuel, using HT co-electrolysis, requires 21.9 TWh/Mt. Therefore, the fleet fuel consumption of 2050 requires 17 638 TWh/year or 14 914 TWh/year, if covered by PtL alkaline or PtL HT jet fuel, respectively. To put these numbers into perspective, the total energy production in Norway is normally around 153 TWh/year (NVE, 2021), meaning that producing the PtL jet fuel to cover the entire fleet would use 97-115 times Norway's annual electricity production.

In 2018, 6 995 Twh of electricity were produced from renewable sources worldwide and represent 26.2% of the global electricity production (Raturi, 2019). A recent report by the International Energy Agency (IEA) claims that if all national net-zero pledges are upheld towards 2050, renewable energy will make up 90% of the total electricity production of over 50 000 TWh in 2050 (IEA, 2021). Assuming a future development of the renewable electricity production in line with this report would lead to 45 000 TWh of renewable electricity generated in 2050. If 100% of the jet fuel consumed in 2050 is PtL alkaline jet fuel, it would require 39% of the total electricity produced from renewable energy sources. Similarly, if 100% is PtL HT jet fuel, it would require 33% of the total electricity from renewable sources. It is unrealistic for one sector to take up such a large share of global renewable electricity. The calculation is rather an exemplification of what it would take if the aviation sector were to put all their emission reduction effort into PtL jet fuels. However, these numbers emphasize the importance a seemingly small efficiency difference will have in large-scale production.

The IEA net-zero report also gives predictions about the role of alternative jet fuels in 2050. It states that 30% of jet fuel consumption in 2050 will be synthetic hydrogen-based fuels, while 45% will be bio-jet fuels (IEA, 2021). If 30% of all jet fuel is covered by PtL jet fuel in 2050, and the rest by fossil jet fuel, this would lead to an emission reduction of 457-477 Mt CO_2/year, depending on which of the two PtL jet fuels are used. Producing this fuel using HT co-electrolysis would require 4474 TWh, equivalent to 10% of the global electricity production from renewable sources in 2050. Using 10% of electricity produced from renewable sources to produce PtL jet fuel would provide significant emission reductions from the sector and seems more realistic in terms of electricity consumption on a global scale.

7.3.4 Biofuels and land use

Bio-jet fuel is another alternative jet fuel with the potential of mitigating emissions from the aviation sector. It has not been assessed in this thesis but can be compared to PtL jet fuel using previous studies conducted. There are many pathways and feedstocks that can be used to produce bio-jet fuels, which leads to a wide range of GWP of the different fuels. In the study by (Stratton et al., 2010), the HEFA pathway resulted in GWP values ranging from 30.1-50.7 g CO2-eq/MJ using different oils as feedstock. Compared to the GWP results of this study, the range falls between PtL jet fuels produced using wind power and PtL jet fuels produced using PV electricity. Using oils as feedstock for biofuels can be problematic, as it consumes feedstock that could be used as food, like soybean oil and rapeseed oil. Switchgrass is a feedstock of growing interest because it is an adaptable feedstock that is easy to integrate into existing agriculture and has a high productivity (David & Ragauskas, 2010). In the study by (Stratton et al., 2010), bio-jet fuel from

switchgrass had a GWP of 17.7 g CO2/MJ when excluding land use, placing it between the PtL jet fuels produced using electricity from wind power and hydropower in this thesis. These numbers show a significant emission reduction potential in replacing fossil jet fuel with bio-jet fuels.

Bio-jet fuels are often criticized for occupying large amounts of land for the cultivation of feedstocks. This issue is best explained using an example. The yield of bio-jet fuel produced using switchgrass as feedstock and the Fischer-Tropsch pathway becomes 2 500 l/(ha*year) or 1900 kg/(ha*year) (Stratton et al., 2010). If this specific type of bio-jet fuel covered 45% of the total fuel consumption of 681 Mt in 2050, it would require 1.6 Mkm^2, which is more than four times the surface area of Norway (Bank, 2021). Occupying land areas of this magnitude is problematic, especially if the land use is at the expanse of cropland. As land use is not adequately covered in this thesis, numbers from the literature are retrieved for PtL jet fuel. The LBST report from 2016 estimated the yield from PtL jet fuel using alkaline electrolysis and wind power to be 10 400-23 100 kg/(ha*year) (Schmidt et al., 2016). This yield results in land use of 0.1-0.3 Mkm^2, for the same amount of fuel, equivalent to 6-19% of the land area needed for the bio-jet fuel consumption.

It comes as no surprise that the amount of energy and land needed to mitigate the CO_2 emissions from aviation is vast. The current air travel demand, together with many other aspects of modern-day living, is a result of the availability of enormous amounts of energy in the form of fossil fuels. Fossil resources have allowed for nearly unlimited growth in energy demand by tapping into energy reserves accumulated over billions of years. The economic sectors have to phase out fossil resources to reduce their GHG emissions. This phase-out will lead to an imbalance between energy supply and demand if the energy demand exceeds the energy harvested from renewable sources. Using only renewable energy sources to cover the global energy demand constrains the energy use to a sustainable annual yield. The energy use enabled by fossil fuels is therefore not sustainable in the framework of a bioeconomy. This means that a new balance between supply and demand of energy, which does not rely on fossil fuels, is not necessarily compliant with the projected growth in air travel or other sectors' energy demand.

7.3.5 Carbon budget

The term carbon budget refers to an estimate of cumulative anthropogenic CO_2 emissions that can be emitted, going from pre-industrial times to the point where net zero anthropogenic CO_2 emissions are reached, which still limits global warming to a given level (Allen et al., 2018). Last years emission gap report from the United Nations Emissions Programme (UNEP) stated that the global carbon budget for limiting global warming to 1.5°C was 600 Gt CO_2, and similarly 1200 Gt CO_2 if limiting global warming to 2°C

(UNEP, 2020). The area below the blue line in figure 6.4.1 represents the cumulative CO_2 emissions of the aircraft fleet from 2019-2050, using fossil jet fuel. The cumulative emissions add up to 49 Gt CO_2, which is equivalent to 8.2% of the global carbon budget of limiting global warming to 1.5°C. For a sector currently responsible for 2.5% of annual global CO_2 emissions, this is too big a share of the global carbon budget and emphasizes the need for emission reductions in aviation in the coming years.

The carbon budget underlines the importance of when CO_2 emission reductions occur, not just the size of the emission reduction in a given year. Figure A.8.1 in the appendix exemplifies the difference in cumulative emissions for two hypothetical future scenarios for phasing in PtL jet fuel. Both scenarios end up using 100% PtL jet fuel in 2050, but the difference in cumulative emissions becomes significant. The scenario with an early phase in of PtL jet fuel, reaching a 50% blend in 2030, gave cumulative CO_2 emissions from 2019 to 2050 of 23.5 Gt CO_2. In the second scenario, the later phase-in of PtL jet fuel, reaching a 50% blend in 2045, gave cumulative emissions of 41.1 Gt CO_2. The difference between the scenarios represents 17.6 Gt CO_2 more spent from the aviation sector's and the global carbon budget. It has been established that using only PtL jet fuel in 2050 is an unrealistic future for the aviation sector. However, the argument on cumulative emissions holds for any mitigation measures being implemented and shows the importance of taking action sooner rather than later.

7.4 Future work

In future work, several aspects could be explored to build upon the LCA analysis conducted and the aircraft stock cohort model developed in this thesis. There are many possible ways of producing synthetic jet fuel using electricity. Investigating several PtL jet fuels, using other hydrogen and syngas production technologies, and different carbon capture solutions would establish which PtL production pathway is the most promising. Future work could also expand the types of jet fuel analyzed using the LCA framework to get comparable results for synthetic and non-synthetic alternative aviation fuels. The new LCA results can be implemented into the aircraft stock cohort model, allowing examination of the emission reduction potential on a fleet-wide scale for every new jet fuel analyzed.

The LCA results contain a lot of information beyond this thesis's scope, which can be investigated to a greater extent. Emissions of other substances than CO_2 and impact categories besides GWP could be more thoroughly examined. This examination would provide more information about jet fuels' different impacts on the environment. All the LCA results are given as various units per MJ of jet fuel. Therefore, all stressors and impact categories can be calculated into fleet-wide emissions and impacts by implementation in the aircraft stock cohort model.

Several future scenarios could be examined using the framework established in this thesis. Examining different scenarios of air travel demand, technological development, behavioral changes, or phase-in rates of alternative jet fuels could provide useful information about the possible future development of the aviation sector.

The generic aircraft representations are used in this thesis to give a higher resolution of the aircraft stock cohort models simulation result. A secondary purpose of creating the generic aircraft representations was to contribute to a more comprehensive model being developed. In that model, a grouping of aircraft, like the one presented in this thesis, is advantageous because it avoids processing data for every single aircraft type in the fleet. However, that model would likely require a larger number of generic aircraft representations than the updated aircraft stock cohort model. Therefore, a natural next step for the generic aircraft representations would be to re-cluster the aircraft fleet and make new generic aircraft representations that are an even better fit for the model being developed.

8 | Conclusion

The main objective thesis is to compare the environmental performance of fossil jet fuel with two variations of synthetic PtL jet fuel, using the LCA framework. The system boundaries are well-to-wake, and the functional unit is 1 MJ of jet fuel produced and combusted. The LCA provides information about 18 impact categories and six stressors, of which the GWP impact category and the six stressors are closely investigated. The LCA results showed a GWP of 94.0 g CO2-eq/MJ for fossil jet fuel, 22.2 g CO2-eq/MJ for PtL alkaline jet fuel, and 19.9 g CO2-eq/MJ for PtL HT jet fuel. Changing the source of electricity used in the PtL jet fuel production uncovered that using German grid electricity gave higher GWP than the fossil jet fuel while using renewable electricity sources results in lower GWP than fossil jet fuel. Hydropower resulted in the lowest GWP, followed by wind power and PV electricity. Both PtL jet fuels outperform fossil jet fuel in terms of GWP, creating a potential for using PtL jet fuel to reduce emissions from aviation, given that a sufficient level of electricity from renewable sources is available.

This thesis builds on the aircraft stock cohort model developed in the project pre-phase of the thesis. It uses a business as usual projection of future air travel demand to simulate the aircraft fleet development and its underlying dynamics, fuel consumption, and associated CO_2 emissions. Nine generic aircraft representations were derived using the BADA database and were included in the model to provide a higher resolution in the simulation results. The increased resolution uncovered that aircraft representation A5A is the most significant contributor to growth in air travel demand and fleet size towards 2050, increasing with 7.2 trillion RPK and over 19 000 aircraft in the simulation period, despite only covering nine aircraft types in the fleet. It also showed that even though aircraft representations A6-A8 in 2050 only represent 21% of the aircraft fleet, they cover 48% of the air travel demand and are responsible for 57% of total fuel consumption and CO_2 emissions from the fleet.

The aircraft stock cohort model included the LCA results to provide a fleet-wide perspective to the PtL jet fuels' emission reduction potential. If the fleet uses only PtL jet fuel in 2050, it will reduce CO_2 emission by 1524-1591 Mt CO_2 in 2050. This reduction would place the level of emissions lower than scenario SSP1-26, compliant with a future development of limiting global warming to below 2°C. However, a 100% share of PtL jet fuel would use

33-39% of global electricity produced from renewable sources due to the high electricity consumption in production with today's efficiencies. A PtL jet fuel share in line with the IEA's projection of 30% is more realistic, which would result in emission reductions of 457-477 Mt CO2 in 2050.

Both the LCA results and the aircraft stock cohort results are in good agreement with previous studies. The updated aircraft stock cohort model brings a global perspective to the LCA results and an increased level of detail in the simulation results, providing a basis for identifying the most effective mitigation measures. By including LCA results of other alternative jet fuels, using alternative air travel demand projections, or changing the fleet fuel efficiency development, the model can explore several future scenarios. Therefore, the updated model can provide valuable insights, for both policymakers and airlines, into the development of the aircraft fleet and the associated emissions.

This thesis has shown that even though the use of PtL jet fuel could be a step towards lowering the sector's emission, no mitigation measure can single-handedly take care of the problem at hand. Both technological and behavioral developments must be thoroughly assessed to provide direction for the future of aviation. If no action is taken, the sector's CO_2 emissions will far exceed the emission levels in line with limiting global warming to below 1.5°C and 2°C. Therefore, a significant transformation of the sector is needed to lower the future emissions from aviation substantially.

References

A4A. (2018a, 08). *Airlines for america | world airlines traffic and capacity.* https://www.airlines.org/dataset/world-airlines-traffic-and-capacity/#. ((Accessed on 11/22/2020))

A4A. (2018b). *World airlines traffic and capacity | airlines for america.* https://www.airlines.org/dataset/world-airlines-traffic-and-capacity/. ((Accessed on 06/09/2021))

Airbus. (2019a). *Global market forecast 2019-2038.* https://gmf.airbus.com/assets/pdf/Airbus_Global_Market_Forecast_2019-2038.pdf?v=1.0.1. ((Accessed on 11/18/2020))

Airbus. (2019b). *Global market forecast 2019-2038.* https://gmf.airbus.com/assets/pdf/Airbus_Global_Market_Forecast_2019-2038.pdf?v=1.0.1. ((Accessed on 11/23/2020))

Airbus. (2021). *A321neo - a320 family - airbus.* https://www.airbus.com/aircraft/passenger-aircraft/a320-family/a321neo.html. ((Accessed on 06/05/2021))

Allen, M., Babiker, M., Chen, Y., Coninck, H. d., Connors, S., Diemen, R. v., ... others (2018). Global warming of 1.5° c. summary for policymakers.

American, S. (2020). *Electric aviation could be closer than you think - scientific american.* https://www.scientificamerican.com/article/electric-aviation-could-be-closer-than-you-think/. ((Accessed on 06/02/2021))

ATAG. (2019). *Corsia explained : Aviation: Benefits beyond borders.* https://aviationbenefits.org/environmental-efficiency/climate-action/offsetting-emissions-corsia/corsia/corsia-explained/. ((Accessed on 05/31/2021))

Bailis, R. E., & Baka, J. E. (2010). Greenhouse gas emissions and land use change from jatropha curcas-based jet fuel in brazil. *Environmental science & technology*, *44*(22), 8684–8691.

Bank, W. (2021). *Land area (sq. km) - india | data.* https://data.worldbank.org/indicator/AG.LND.TOTL.K2?locations=IN. ((Accessed on 06/01/2021))

Baughcum, S. L., Henderson, S. C., & Tritz, T. G. (1996). Scheduled civil aircraft emission inventories for 1976 and 1984: Database development and analysis.

Bholowalia, P., & Kumar, A. (2014). Ebk-means: A clustering technique based on elbow method and k-means in wsn. *International Journal of Computer Applications*, *105*(9).

BMWi. (2021a). *Bmwi - federal ministry for economic affairs and energy - origin of german crude oil imports, 2015-2017.* https://www.bmwi.de/Redaktion/EN/Infografiken/woher-kommen-die-deutschen-rohoelimporte.html. ((Accessed on 04/06/2021))

BMWi. (2021b). *Smard | market data visuals.* https://www.smard.de/en/marktdaten?marketDataAttributes=%7B%22resolution%22:%22month%22,%22from%22:1547221524705,%22to%22:1610328992613,%22moduleIds%22:%5B5000410,3000189,3003792,3004076,3000186,3000188,3000194,3004073,3004072,3004075,3000198,3004074,3000207,1004066,1001226,1001225,1004067,1004068,1001228,1001224,1001223,1004069,1004071,1004070,1001227%5D,%22selectedCategory%22:5,%22activeChart%22:true,%22style%22:%22color%22,%22region%22:%22DE%22%7D. ((Accessed on 04/06/2021))

BNetzA. (2021). *Smard | market data visuals.* https://www.smard.de/en/marktdaten?marketDataAttributes=%7B%22resolution%22:%22month%22,%22from%22:1547221524705,%22to%22:1610328992613,%22moduleIds%22:%5B5000410,3000189,3003792,3004076,3000186,3000188,3000194,3004073,3004072,3004075,3000198,3004074,3000207,1004066,1001226,1001225,1004067,1004068,1001228,1001224,1001223,1004069,1004071,1004070,1001227%5D,%22selectedCategory%22:5,%22activeChart%22:true,%22style%22:%22color%22,%22region%22:%22DE%22%7D. ((Accessed on 05/19/2021))

Boeing. (2005). *Current market outlook 2005.* http://libraryonline.erau.edu/online-full-text/books-online/RAC109206.pdf. ((Accessed on 11/23/2020))

Boeing. (2009). *Current market outlook 2009-2028.* https://libraryonline.erau.edu/online-full-text/books-online/BoeingCurrentMarketOutlook2009to2028.pdf. ((Accessed on 11/23/2020))

Boeing. (2013). *Current market outlook 2013-2032.* https://speednews.com/documentaccess/103536_cmo2013.pdf. ((Accessed on 11/23/2020))

Boeing. (2014). *Current market outlook 2014-2033.* http://i2.cdn.turner.com/cnn/2015/images/09/02/boeing_current_market_outlook_2014.pdf. ((Accessed on 11/23/2020))

Boeing. (2016). *Current market outlook 2016-2035.* https://www.boeing.com/resources/boeingdotcom/commercial/about-our-market/assets/downloads/cmo_print_2016_final_updated.pdf. ((Accessed on 11/23/2020))

Boeing. (2018). *Workbook: Boeing commercial market outlook 2018-2037.* https://public.tableau.com/views/BoeingCommercialMarketOutlook2018-2037/CommercialMarketOutlook?:showVizHome=no. ((Accessed on 11/23/2020))

Boeing. (2020a). *Boeing: 787 dreamliner.* https://www.boeing.com/commercial/787/. ((Accessed on 06/05/2021))

Boeing. (2020b). *Commercial market outlook 2020-2039.* http://www.boeing.com/resources/boeingdotcom/market/assets/downloads/2020_CMO_PDF_Download.pdf. ((Accessed on 11/18/2020))

Boeing. (2020c). *Commercial market outlook 2020-2039.* http://www.boeing.com/resources/boeingdotcom/market/assets/downloads/2020_CMO_PDF_Download.pdf. ((Accessed on 11/23/2020))

Boeing. (2020d). *World air cargo forecast 2020–2039.* https://www.boeing.com/resources/boeingdotcom/market/assets/downloads/2020_WACF_PDF_Download.pdf. ((Accessed on 05/05/2021))

Braun-Unkhoff, M., Riedel, U., & Wahl, C. (2017). About the emissions of alternative jet fuels. *CEAS Aeronautical Journal*, *8*(1), 167–180.

Cetinkaya, E., Dincer, I., & Naterer, G. (2012). Life cycle assessment of various hydrogen production methods. *International journal of hydrogen energy*, *37*(3), 2071–2080.

Cox, K., Renouf, M., Dargan, A., Turner, C., & Klein-Marcuschamer, D. (2014). Environmental life cycle assessment (lca) of aviation biofuel from microalgae, pongamia pinnata, and sugarcane molasses. *Biofuels, Bioproducts and Biorefining*, *8*(4), 579–593.

Curtis, T., Rhoades, D. L., & Waguespack Jr, B. P. (2013). Regional jet aircraft competitiveness: challenges and opportunities. *World Review of Entrepreneurship, Management and Sustainable Development*, *9*(3), 307–319.

Czerny, A. I., Fu, X., Lei, Z., & Oum, T. H. (2021). Post pandemic aviation market recovery: Experience and lessons from china. *Journal of Air Transport Management*, *90*, 101971.

David, K., & Ragauskas, A. J. (2010). Switchgrass as an energy crop for biofuel production: a review of its ligno-cellulosic chemical properties. *Energy & Environmental Science*, *3*(9), 1182–1190.

De Jong, S., Antonissen, K., Hoefnagels, R., Lonza, L., Wang, M., Faaij, A., & Junginger, M. (2017). Life-cycle analysis of greenhouse gas emissions from renewable jet fuel production. *Biotechnology for biofuels*, *10*(1), 1–18.

de Jong, S., Hoefnagels, E., van Stralen, J., Londo, H., Slade, R., Faaij, A., & Junginger, H. (2017). *Renewable jet fuel in the european union: scenarios and preconditions for renewable jet fuel deployment towards 2030.* Copernicus Institute, Department IMEW, Energy & Resources.

Dincer, I., & Acar, C. (2015). Review and evaluation of hydrogen production methods for better sustainability. *International journal of hydrogen energy*, *40*(34), 11094–11111.

Dunn, J. B., Mueller, S., Kwon, H.-y., & Wang, M. Q. (2013). Land-use change and greenhouse gas emissions from corn and cellulosic ethanol. *Biotechnology for biofuels*,

6(1), 1–13.

EC. (2015). Study on actual ghg data for diesel, petrol, kerosene and natural gas. *European Commission, Directorate-General for Energy*.

Ecoinvent. (2020). *Why do i need the ecoinvent database when doing a life cycle assessment? – ecoinvent.* https://www.ecoinvent.org/support/faqs/first-time-users/why-do-i-need-the-ecoinvent-database-when-doing-a-life-cycle-assessment.html. ((Accessed on 06/07/2021))

Egelhofer, R., Marizy, C., & Bickerstaff, C. (2008). On how to consider climate change in aircraft design. *Meteorologische Zeitschrift*, *17*(2), 173–180.

Elgowainy, A., Han, J., Wang, M., Carter, N., Stratton, R., Hileman, J., ... others (2012). *Life-cycle analysis of alternative aviation fuels in greet* (Tech. Rep.). Argonne National Laboratory.

Enes, J. (2020). A model of the global aircraft fleet.
(Project work in the course TEP4570 at NTNU. The report is from the project pre-phase of the thesis in the course TEP4935.)

EPRS. (2020, EPRS). *Sustainable aviation fuels.* https://www.europarl.europa.eu/RegData/etudes/BRIE/2020/659361/EPRS_BRI(2020)659361_EN.pdf. ((Accessed on 05/28/2021))

Eurocontrol. (2019). User manual for the base of aircraft data (bada) revision 3.15. *EEC Technical/Scientific Report No. 19/03/18-45*, *2019*.

Eurocontrol. (2020, 06). *Base of aircraft data (bada) | eurocontrol.* https://www.eurocontrol.int/model/bada. ((Accessed on 06/04/2021))

Eyers, C., Norman, P., Middel, J., Plohr, M., Michot, S., Atkinson, K., & Christou, R. (2004). *Aero2k global aviation emissions inventories for 2002 and 2025* (Tech. Rep.). Technical Report QINETIC/04/01113 (QinetiQ, 2004).

Fortier, M.-O. P., Roberts, G. W., Stagg-Williams, S. M., & Sturm, B. S. (2014). Life cycle assessment of bio-jet fuel from hydrothermal liquefaction of microalgae. *Applied Energy*, *122*, 73–82.

Fridstrøm, L., Østli, V., & Johansen, K. W. (2016). A stock-flow cohort model of the national car fleet. *European Transport Research Review*, *8*(3), 1–15.

Gidden, M. J., Riahi, K., Smith, S. J., Fujimori, S., Luderer, G., Kriegler, E., ... Takahashi, K. (2019). Global emissions pathways under different socioeconomic scenarios for use in cmip6: a dataset of harmonized emissions trajectories through the end of the century. *Geoscientific Model Development*, *12*(4), 1443–1475. Retrieved from https://www.geosci-model-dev.net/12/1443/2019/ doi: 10.5194/gmd-12-1443-2019

Goedkoop, M., Heijungs, R., Huijbregts, M., De Schryver, A., Struijs, J., & Van Zelm, R. (2009). Recipe 2008. *A life cycle impact assessment method which comprises harmonised category indicators at the midpoint and the endpoint level*, *1*, 1–126.

Graver, B., Zhang, K., & Rutherford, D. (2019a). Co2 emissions from commercial aviation, 2018. *The International Council on Clean Transportation*.

Graver, B., Zhang, K., & Rutherford, D. (2019b). Co2 emissions from commercial aviation, 2018. *The International Council of Clean Transportation*.

Graver, B., Zhang, K., & Rutherford, D. (2020). Co2 emissions from commercial aviation, 2013, 2018, and 2019. *The International Council on Clean Transportation*.

Han, J., Elgowainy, A., Cai, H., & Wang, M. Q. (2013). Life-cycle analysis of bio-based aviation fuels. *Bioresource technology*, *150*, 447–456.

Hileman, J., & Stratton, R. (2014). Alternative jet fuel feasibility. *Transport Policy*, *34*, 52–62.

Hoesly, R. M., Smith, S. J., Feng, L., Klimont, Z., Janssens-Maenhout, G., Pitkanen, T., ... others (2018). Historical (1750-2014) anthropogenic emissions of reactive gases and aerosols from the community emission data system (ceds). *Geoscientific Model Development*, *11*, 369–408.

IATA. (2019). *Aircraft technology roadmap to 2050.* `https://www.iata.org/contentassets/8d19e716636a47c184e7221c77563c93/technology20roadmap20to20205020no20foreword.pdf`. ((Accessed on 11/18/2020))

ICAO. (2013). *Appendix 1. tables relating to the world of air transport in 2013.* `https://www.icao.int/annual-report-2013/Documents/Appendix_1_en.pdf`. ((Accessed on 11/24/2020))

ICAO. (2015). *Appendix 1. tables relating to the world of air transport in 2015.* `https://www.icao.int/annual-report-2015/Documents/Appendix_1_en.pdf`. ((Accessed on 11/24/2020))

ICAO. (2017). *Economic development, air cargo 2017 facts figures.* `https://www.icao.int/sustainability/economic-policy/PublishingImages/Pages/Facts-and-Figures/Download%20full%20document.pdf`. ((Accessed on 11/23/2020))

ICAO. (2018). *Icao long-term traffic forecasts.* `https://www.icao.int/sustainability/Documents/LTF_Charts-Results_2018edition.pdf`. ((Accessed on 11/23/2020))

ICAO. (2019a). *2019 environmental report, aviation and environment.* `https://www.icao.int/environmental-protection/Documents/ICAO-ENV-Report2019-F1-WEB%20(1).pdf`. ((Accessed on 11/23/2020))

ICAO. (2019b). *Climate change.* `https://www.icao.int/environmental-protection/pages/climate-change.aspx`. ((Accessed on 05/31/2021))

ICAO. (2019c). *Trends in emissions that affect climate change.* `https://www.icao.int/environmental-protection/Pages/ClimateChange_Trends.aspx`. ((Accessed on 05/31/2021))

ICAO. (2019d). *The world of air transport in 2019.* `https://www.icao.int/annual`

-report-2019/Pages/the-world-of-air-transport-in-2019.aspx. ((Accessed on 05/05/2021))

ICAO. (2020). *Power-to-liquid (ptl) for aviation.* https://www.icao.int/environmental-protection/GFAAF/Pages/Project.aspx?ProjectID=46. ((Accessed on 05/29/2021))

IEA. (2021, 05). *Net zero by 2050 - a roadmap for the global energy sector.* https://iea.blob.core.windows.net/assets/4719e321-6d3d-41a2-bd6b-461ad2f850a8/NetZeroby2050-ARoadmapfortheGlobalEnergySector.pdf. ((Accessed on 05/19/2021))

IPCC. (2014a). *Climate change 2014: Synthesis report. contribution of working groups i, ii and iii to the fifth assessment report of the intergovernmental panel on climate change [core writing team, r.k. pachauri and l.a. meyer (eds.)].* Geneva, Switzerland, 151 pp.

IPCC. (2014b). *Summary for policymakers. in: Climate change 2014: Mitigation of climate change. contribution of working group iii to the fifth assessment report of the intergovernmental panel on climate change.*

IPCC. (2018a). *Global warming of 1.5˚c. an ipcc special report on the impacts of global warming of 1.5˚c above pre-industrial levels and related global greenhouse gas emission pathways, in the context of strengthening the global response to the threat of climate change, sustainable development, and efforts to eradicate poverty.*

IPCC. (2018b). *Summary for policymakers. in: Global warming of 1.5˚c. an ipcc special report on the impacts of global warming of 1.5˚c above pre-industrial levels and related global greenhouse gas emission pathways, in the context of strengthening the global response to the threat of climate change, sustainable development, and efforts to eradicate poverty.*

ISO. (2006a). Iso 14040:2006 environmental management - lift cycle assessment - principles and framework. Geneva, Switzerland: International Organization for Standardization.

ISO. (2006b). Iso 14044:2006 environmental management - life cycle assessment - requirements and guidelines. Geneva, Switzerland: International Organization for Standardization.

Iyyanki, V. M. (2017). Chapter 5 life cycle assessment. *Environmental Management, Science and Engineering for Industry, Iyyanki V. MuralikrishnaValliManickam, Eds, Butterworth Henneman Elsevier, UK*, 57–75.

Kharina, A., & Rutherford, D. (2015). Fuel efficiency trends for new commercial jet aircraft: 1960 to 2014.

Kim, B. Y., Fleming, G. G., Lee, J. J., Waitz, I. A., Clarke, J.-P., Balasubramanian, S., ... others (2007). System for assessing aviation's global emissions (sage), part 1: Model description and inventory results. *Transportation Research Part D: Transport*

and Environment, *12*(5), 325–346.

Koroneos, C., Dompros, A., Roumbas, G., & Moussiopoulos, N. (2004). Life cycle assessment of hydrogen fuel production processes. *International journal of hydrogen energy*, *29*(14), 1443–1450.

Koroneos, C., Dompros, A., Roumbas, G., & Moussiopoulos, N. (2005). Advantages of the use of hydrogen fuel as compared to kerosene. *Resources, Conservation and Recycling*, *44*(2), 99–113.

Krohn-Fagervoll, S. (2020). *Planlegger å produsere flydrivstoff fra vann og co2 på herøya - heroyaindustripark.* `https://www.heroya-industripark.no/aktuelt/planlegger-aa-produsere-flydrivstoff-fra-vann-og-co2-paa-heroeya`. ((Accessed on 05/29/2021))

Lee, D. S., Fahey, D., Skowron, A., Allen, M., Burkhardt, U., Chen, Q., ... others (2020). The contribution of global aviation to anthropogenic climate forcing for 2000 to 2018. *Atmospheric Environment*, *244*, 117834.

Lee, D. S., Fahey, D. W., Forster, P. M., Newton, P. J., Wit, R. C., Lim, L. L., ... Sausen, R. (2009). Aviation and global climate change in the 21st century. *Atmospheric Environment*, *43*(22-23), 3520–3537.

Lee, J. J., Lukachko, S. P., Waitz, I. A., & Schafer, A. (2001). Historical and future trends in aircraft performance, cost, and emissions. *Annual Review of Energy and the Environment*, *26*(1), 167–200.

Li, T., Zhang, H., Liu, Z., Ke, Q., & Alting, L. (2014). A system boundary identification method for life cycle assessment. *The International Journal of Life Cycle Assessment*, *19*(3), 646–660.

Likas, A., Vlassis, N., & Verbeek, J. J. (2003). The global k-means clustering algorithm. *Pattern recognition*, *36*(2), 451–461.

Lozanovski, A., & Brandstetter, C. P. (2015). Herstellung von kraftstoffen aus co2 und h2o unter nutzung regenerativer energie. *Bundesministerium für Bildung und Forschung BMBF*.

Mishnaevsky Jr, L., & Favorsky, O. (2011). Composite materials in wind energy technology. *Thermal to Mechanical Energy Conversion: Engines and Requirements, EOLSS Publishers: Oxford, UK*.

NBC. (2020). *The largest electric plane yet completed its first flight — but it's the batteries that matter.* `https://www.nbcnews.com/science/science-news/largest-electric-plane-yet-completed-its-first-flight-it-s-n1221401`. ((Accessed on 06/02/2021))

NVE. (2021, 04). *Kraftproduksjon - nve.* `https://www.nve.no/energiforsyning/kraftproduksjon/?ref=mainmenu`. ((Accessed on 05/19/2021))

OW. (2018). *Global fleet mro market forecast commentary 2018–2028.* `https://www.oliverwyman.com/content/dam/oliver-wyman/v2/publications/`

2018/January/2018-2028_Global_Fleet_MRO_Market_Forecast_Commentary_Public_Final_web.pdf. ((Accessed on 11/23/2020))

OW. (2019). *Global fleet mro market forecast commentary 2019–2029.* https://www.oliverwyman.com/content/dam/oliver-wyman/v2/publications/2019/January/global-fleet-mro-market-forecast-commentary-2019-2029.pdf. ((Accessed on 11/23/2020))

Owen, B., & Lee, D. (2006). Allocation of international aviation emissions from scheduled air traffic-future cases, 2005 to 2050. *Centre for Air Transport and the Environment. Manchester Metropolitan University, United Kingdom*.

Owen, B., Lee, D. S., & Lim, L. (2010). *Flying into the future: aviation emissions scenarios to 2050.* ACS Publications.

O'Neill, B. C., Kriegler, E., Riahi, K., Ebi, K. L., Hallegatte, S., Carter, T. R., ... van Vuuren, D. P. (2014). A new scenario framework for climate change research: the concept of shared socioeconomic pathways. *Climatic change*, *122*(3), 387–400.

Planespotters. (2021). *Supported aircraft types.* https://www.planespotters.net/production-list/index. ((Accessed on 04/22/2021))

Raturi, A. K. (2019). Renewables 2019 global status report.

Riahi, K., van Vuuren, D. P., Kriegler, E., Edmonds, J., O'Neill, B. C., Fujimori, S., ... Tavoni, M. (2017, jan). The shared socioeconomic pathways and their energy, land use, and greenhouse gas emissions implications: An overview. *Global Environmental Change*, *42*, 153–168. doi: 10.1016/j.gloenvcha.2016.05.009

Rogelj, J., Popp, A., Calvin, K. V., Luderer, G., Emmerling, J., Gernaat, D., ... Tavoni, M. (2018, mar). Scenarios towards limiting global mean temperature increase below 1.5 °c. *Nature Climate Change*, *8*(4), 325–332. doi: 10.1038/s41558-018-0091-3

Roth, A., & Schmidt, P. (2017). *Power-to-liquids: A new pathway to renewable jet fuel.* https://www.icao.int/Meetings/altfuels17/Documents/20170208_ROTH_V1-0_submitted.pdf. ((Accessed on 05/29/2021))

Santos, D. M., Sequeira, C. A., & Figueiredo, J. L. (2013). Hydrogen production by alkaline water electrolysis. *Química Nova*, *36*(8), 1176–1193.

Sausen, R., & Schumann, U. (2000). Estimates of the climate response to aircraft co2 and nox emissions scenarios. *Climatic Change*, *44*(1-2), 27–58.

Schaefer, M., Jung, M., & Pabst, H. (2013). The regional distribution of air traffic emissions in the past, present and future.

Schäfer, A. W., Barrett, S. R., Doyme, K., Dray, L. M., Gnadt, A. R., Self, R., ... Torija, A. J. (2019). Technological, economic and environmental prospects of all-electric aircraft. *Nature Energy*, *4*(2), 160–166.

Schmidt, P., Batteiger, V., Roth, A., Weindorf, W., & Raksha, T. (2018). Power-to-liquids as renewable fuel option for aviation: A review. *Chemie Ingenieur Technik*, *90*(1-2), 127–140.

Schmidt, P., Weindorf, W., Roth, A., Batteiger, V., & Riegel, F. (2016). Power-to-liquids: Potentials and perspectives for the future supply of renewable aviation fuel.

Schmitt, A., & Brunner, B. (1992). Emissions from aviation and their development over time. *Pollutants from air traffic–results of atmospheric research*, *1997*, 97–04.

Schreiber, A., Peschel, A., Hentschel, B., & Zapp, P. (2020). Life cycle assessment of power-to-syngas: Comparing high temperature co-electrolysis and steam methane reforming. front. *Energy Res*, *8*, 533850.

Sforza, P. (2014). Chapter 3 - fuselage design. In P. Sforza (Ed.), *Commercial airplane design principles* (p. 47-79). Boston: Butterworth-Heinemann. Retrieved from `https://www.sciencedirect.com/science/article/pii/B9780124199538000036` doi: https://doi.org/10.1016/B978-0-12-419953-8.00003-6

Sherwin, E. D. (2021). Electrofuel synthesis from variable renewable electricity: An optimization-based techno-economic analysis. *Available at SSRN 3646570*.

Stratton, R. W., Wong, H. M., & Hileman, J. I. (2011). Quantifying variability in life cycle greenhouse gas inventories of alternative middle distillate transportation fuels. *Environmental science & technology*, *45*(10), 4637–4644.

Stratton, R. W., Wong, H. M., Hileman, J. I., et al. (2010). Life cycle greenhouse gas emissions from alternative jet fuels. *PARTNER project*, *28*, 133.

ToolBox, E. (2003). *U.s. standard atmosphere.* `https://www.engineeringtoolbox.com/standard-atmosphere-d_604.html`. ((Accessed on 05/07/2021))

UNEP. (2020). Emissions gap report 2020.

Utgikar, V., & Thiesen, T. (2006). Life cycle assessment of high temperature electrolysis for hydrogen production via nuclear energy. *International Journal of Hydrogen Energy*, *31*(7), 939–944.

van der Giesen, C., Kleijn, R., & Kramer, G. J. (2014). Energy and climate impacts of producing synthetic hydrocarbon fuels from co2. *Environmental science & technology*, *48*(12), 7111–7121.

Van Vuuren, D. P., Edmonds, J., Kainuma, M., Riahi, K., Thomson, A., Hibbard, K., ... others (2011). The representative concentration pathways: an overview. *Climatic change*, *109*(1-2), 5.

Wang, M., Lee, H., & Molburg, J. (2004). Allocation of energy use in petroleum refineries to petroleum products. *The International Journal of Life Cycle Assessment*, *9*(1), 34–44.

Wang, W.-C., & Tao, L. (2016). Bio-jet fuel conversion technologies. *Renewable and Sustainable Energy Reviews*, *53*, 801–822.

Wilkerson, J., Jacobson, M. Z., Malwitz, A., Balasubramanian, S., Wayson, R., Fleming, G., ... others (2010). Analysis of emission data from global commercial aviation: 2004 and 2006.

Worldoil. (2021). *Methane emissions fell in 2020 on lower oil and gas pro-*

duction. https://www.worldoil.com/news/2021/1/18/methane-emissions-fell-in-2020-on-lower-oil-and-gas-production. ((Accessed on 06/06/2021))

A | Excluded results

A.1 Total environmental impacts

Table A.1.1: Total well to wake environmental impacts per MJ jet fuel for fossil jet fuel, PtL jet fuel produced using alkaline electrolyser and wind power, and PtL jet fuel produced using high temperature co-electrolysis and wind power. The results are given in absolute values, and the PtL results are colored green if they are lower and red if they are higher than the fossil jet fuel, for the same impact category.

Impact Category	Unit	Fossil Jet Fuel	PtL alkaline electrolysis, wind power	PtL HT co-electrolysis, wind power
GWP	kg CO_2 eq	9,40E-02	2,22E-02	1,99E-02
FDP	kg oil eq	5,78E-02	6,76E-03	6,38E-03
WDP	m^3	8,37E-04	1,83E-03	1,68E-03
FETP	kg 1,4-DB eq	2,05E-04	6,36E-03	5,42E-03
METP	kg 1,4-DB eq	1,80E-04	5,56E-03	4,74E-03
TETP	kg 1,4-DB eq	1,71E-05	2,17E-06	1,99E-06
HTP	kg 1,4-DB eq	4,89E-03	1,86E-02	1,68E-02
ALOP	m^2year	3,89E-04	5,74E-04	5,66E-04
ULOP	m^2year	3,89E-04	8,80E-04	7,51E-04
MDP	kg Fe eq	1,30E-03	1,57E-02	1,30E-02
TAP	kg SO_2 eq	3,87E-04	2,00E-04	1,96E-04
PMFP	kg PM_{10} eq	1,24E-04	1,00E-04	9,31E-05
FEP	kg P eq	4,47E-06	1,08E-05	1,01E-05
IRP	kg U^{235} eq	1,27E-02	1,59E-03	1,54E-03
MEP	kg N eq	1,18E-05	1,35E-05	1,31E-05
LTP	m^2	8,95E-05	2,67E-06	2,50E-06
ODP	kg CFC-11 eq	2,76E-08	4,68E-08	4,74E-08
POFP	kg NMVOC	3,47E-04	2,34E-04	2,26E-04

A.2 LCA contribution analysis of fossil jet fuel

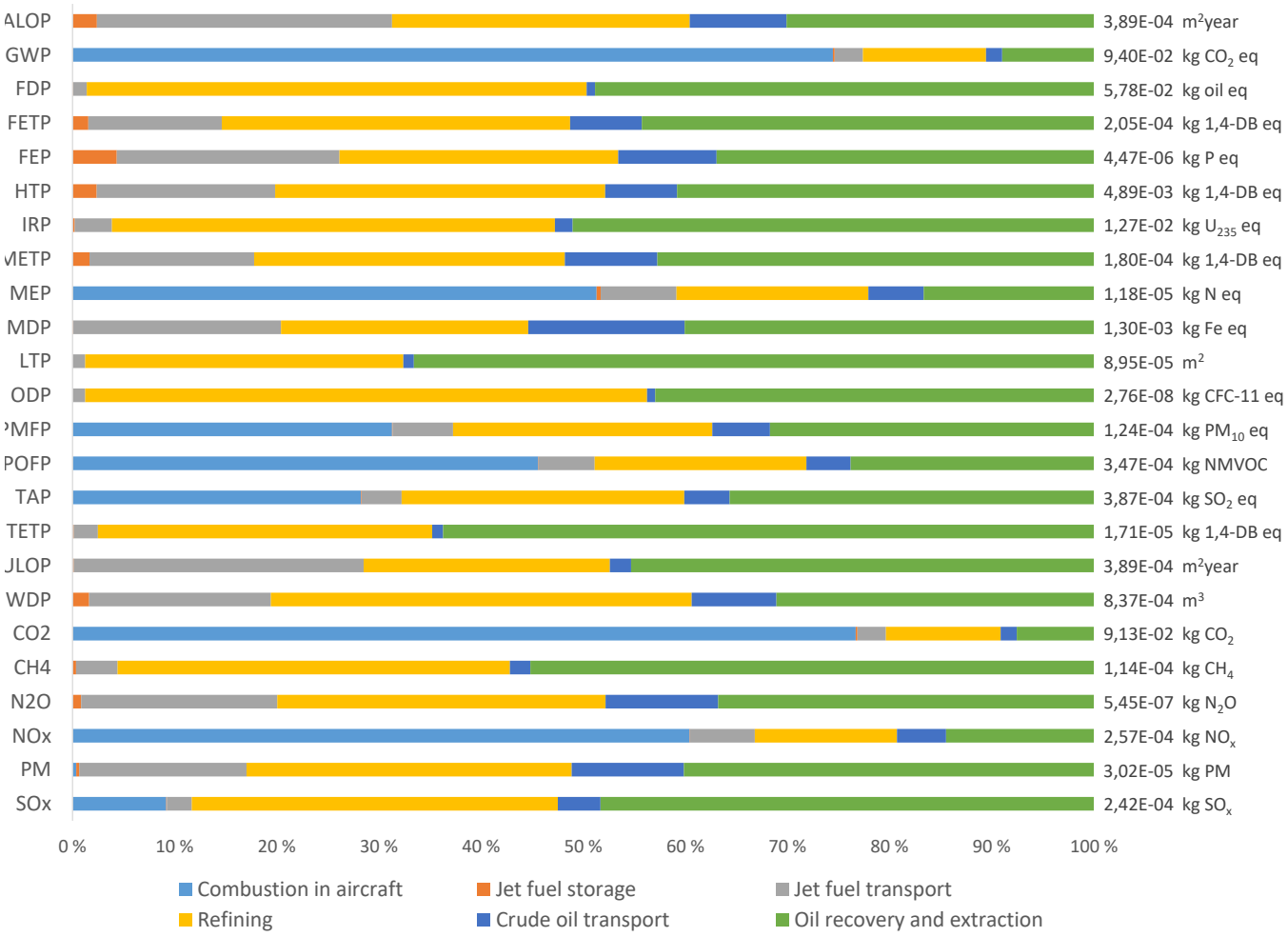

Figure A.2.1: Contribution analysis of all impact categories and stressors for fossil jet fuel. The absolute value per MJ jet fuel for each impact category and stressor is displayed to the right of the figure, while the bars show the percent wise distribution of the emissions on the different processes.

A.3 LCA contribution analysis of PtL alkaline jet fuel using wind power

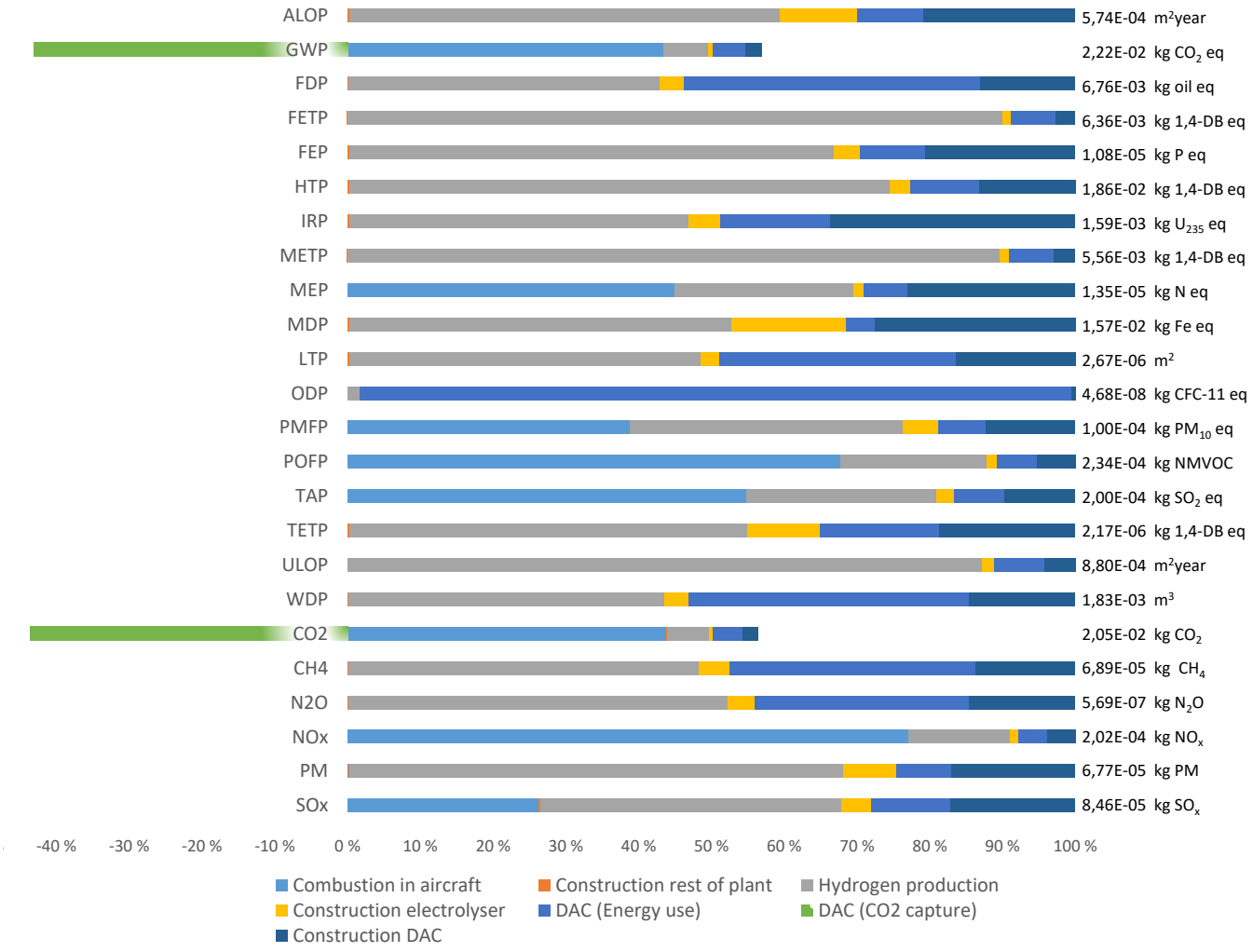

Figure A.3.1: Contribution analysis of impact categories and stressors, for PtL jet fuel produced using alkaline electrolyser and wind power. The absolute value per MJ jet fuel for each impact category and stressor is displayed to the right of the figure, while the bars show the percent wise distribution of the emissions on the different processes.

A.4 LCA contribution analysis of PtL HT jet fuel using wind power

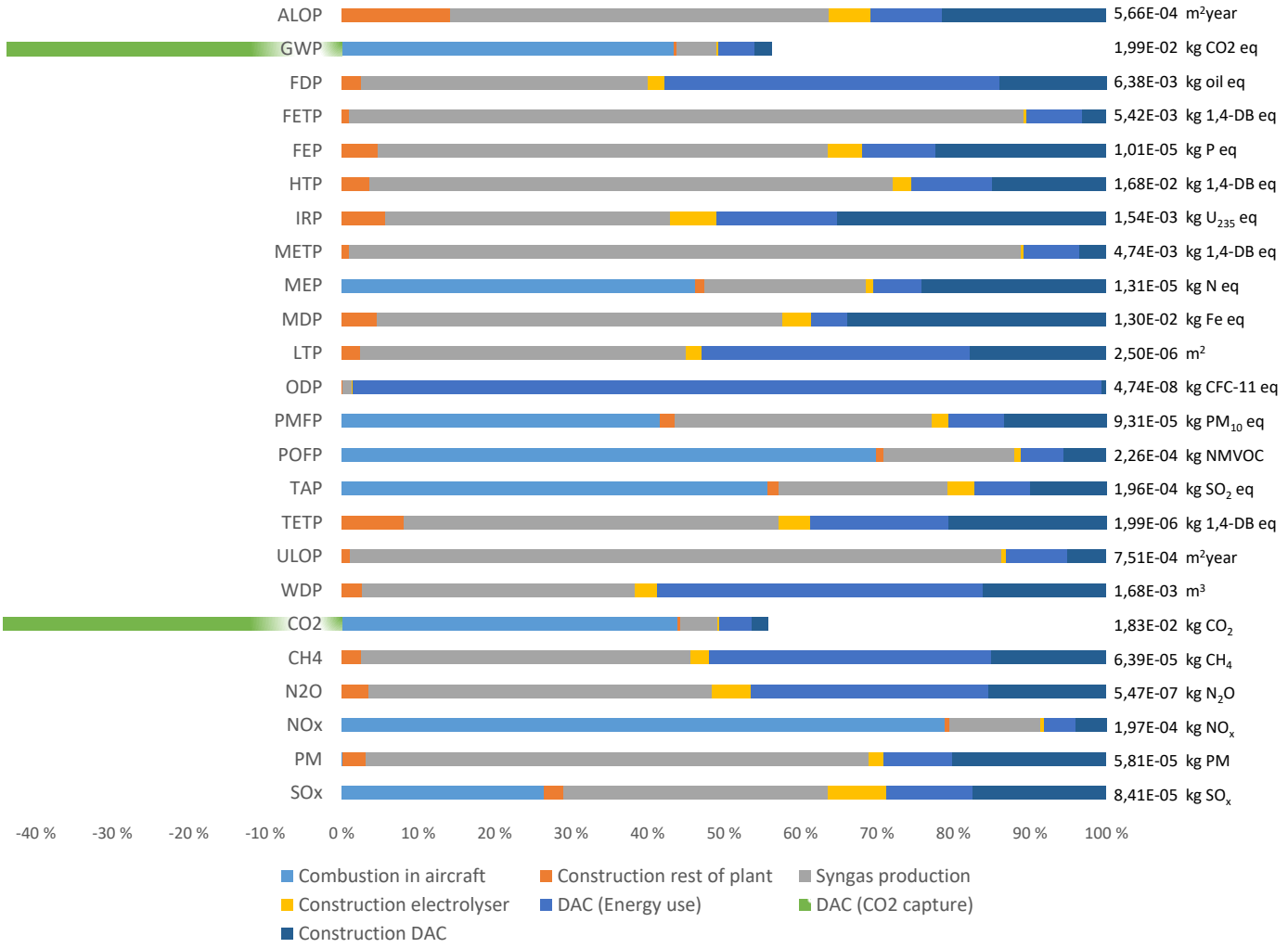

Figure A.4.1: Contribution analysis of impact categories and stressors for PtL jet fuel produced using HT co-electorlysis and wind power. The absolute value per MJ jet fuel for each impact category and stressor is displayed to the right of the figure, while the bars show the percent wise distribution of the emissions on the different processes.

A.5 Data spread of the aircraft clusters

Table A.5.1: Normalized standard deviations calculated for technical aircraft parameters, for each of the nine clusters. Clustering parameters are colored blue, while parameters used to calculate fuel consumption in cruise configuration is colored green. The engine type is also a clustering, but have no standard deviation. Cluster 1 are piston aircraft, cluster 3 are turboprop aircraft, while the rest are jet aircraft.

Parameter	C1 std/mean	C2 std/mean	C3 std/mean	C4 std/mean	C5A std/mean	C5B std/mean	C6 std/mean	C7 std/mean	C8 std/mean
mass_reference	9,35E-01	5,17E-01	1,02E+00	1,83E-01	5,54E-02	1,42E-01	1,46E-01	1,10E-01	2,01E-01
mass_maximum	1,00E+00	5,26E-01	1,08E+00	1,70E-01	6,26E-02	1,53E-01	1,29E-01	1,07E-01	1,68E-01
mass_max_payload	6,62E-01	8,77E-01	1,08E+00	3,82E-01	9,95E-02	1,92E-01	2,50E-01	2,28E-01	3,24E-01
cruise_mc_LO	2,63E-01	1,13E-01	2,02E-01	9,00E-02	1,88E-02	1,48E-02	5,26E-02	1,88E-02	5,04E-02
aero_surf	3,58E-01	3,62E-01	7,40E-01	1,80E-01	9,49E-02	2,11E-01	9,42E-02	9,32E-02	2,40E-01
config_cr_CD0	4,58E-01	2,95E-01	3,96E-01	3,31E-01	2,06E-01	2,05E-01	3,88E-01	1,34E-01	1,86E-01
config_cr_CD2	3,13E-01	3,02E-01	2,88E-01	1,95E-01	1,77E-01	2,95E-01	1,74E-01	2,36E-01	2,10E-01
fuel_cf_1	1,32E+00	5,82E-01	6,35E-01	4,06E-01	0,00E+00	2,77E-01	4,94E-01	2,41E-01	3,43E-01
fuel_cf_2	-	5,24E+00	3,68E+00	4,01E+00	5,68E-01	1,48E+00	4,85E-01	4,56E-01	1,28E+00
fuel_cf_cr	2,38E-01	1,22E-01	2,25E-01	3,41E-02	2,97E-02	3,32E-02	5,98E-02	4,92E-02	3,91E-02

A.6 Aircraft deliveries

The simulated deliveries of the original and updated model is presented below in figure A.6.1. From 2039 to 2040, the deliveries of regional aircraft and aircraft representations A1-A3 experience a spike. This sudden change is due to an assumption made in the model. Up until 2039, regional aircraft and aircraft representations A1-A3's size is increasing. The model is not able to keep track of the size of individual aircraft, which means that the entire fleet's size is increasing, not only the aircraft being introduced. This leads to a diminishing number of regional and A1-A3 aircraft being delivered towards 2039, despite increasing demand. These aircraft can only grow to a certain size before changing aircraft type. The size development is therefore stopped from 2040. Then the regional aircraft and the A1-A3 aircraft representations no longer take care of the increasing demand by increasing in size, resulting in a spike in deliveries in 2040.

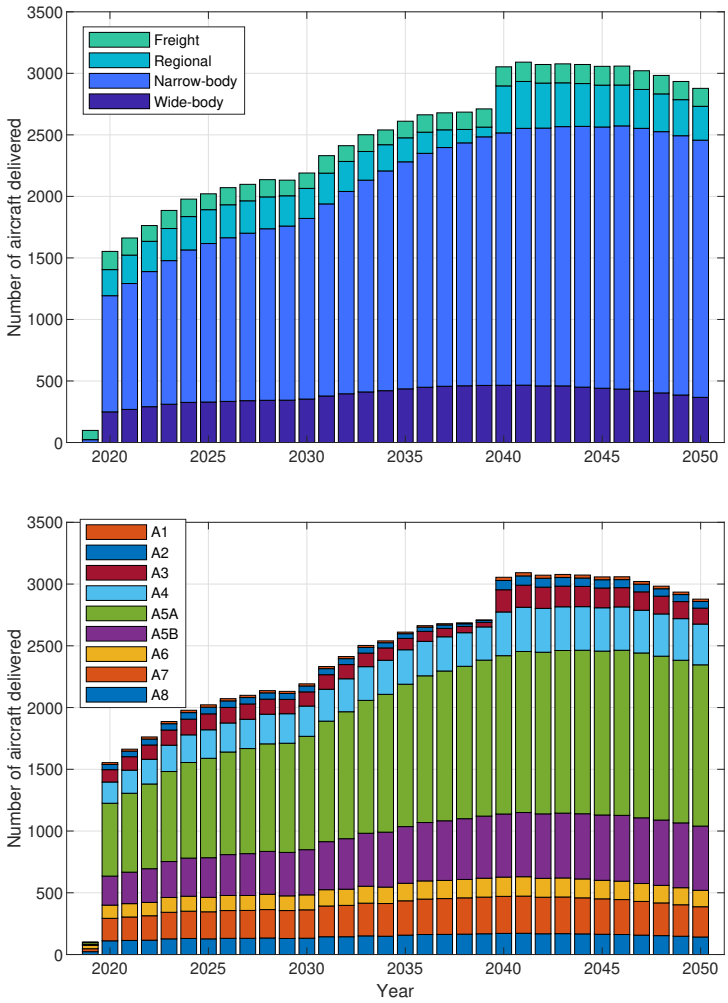

Figure A.6.1: Aircraft deliveries to the aircraft fleet for the original and updated model from 2019-2050.

A.7 Aircraft retirements

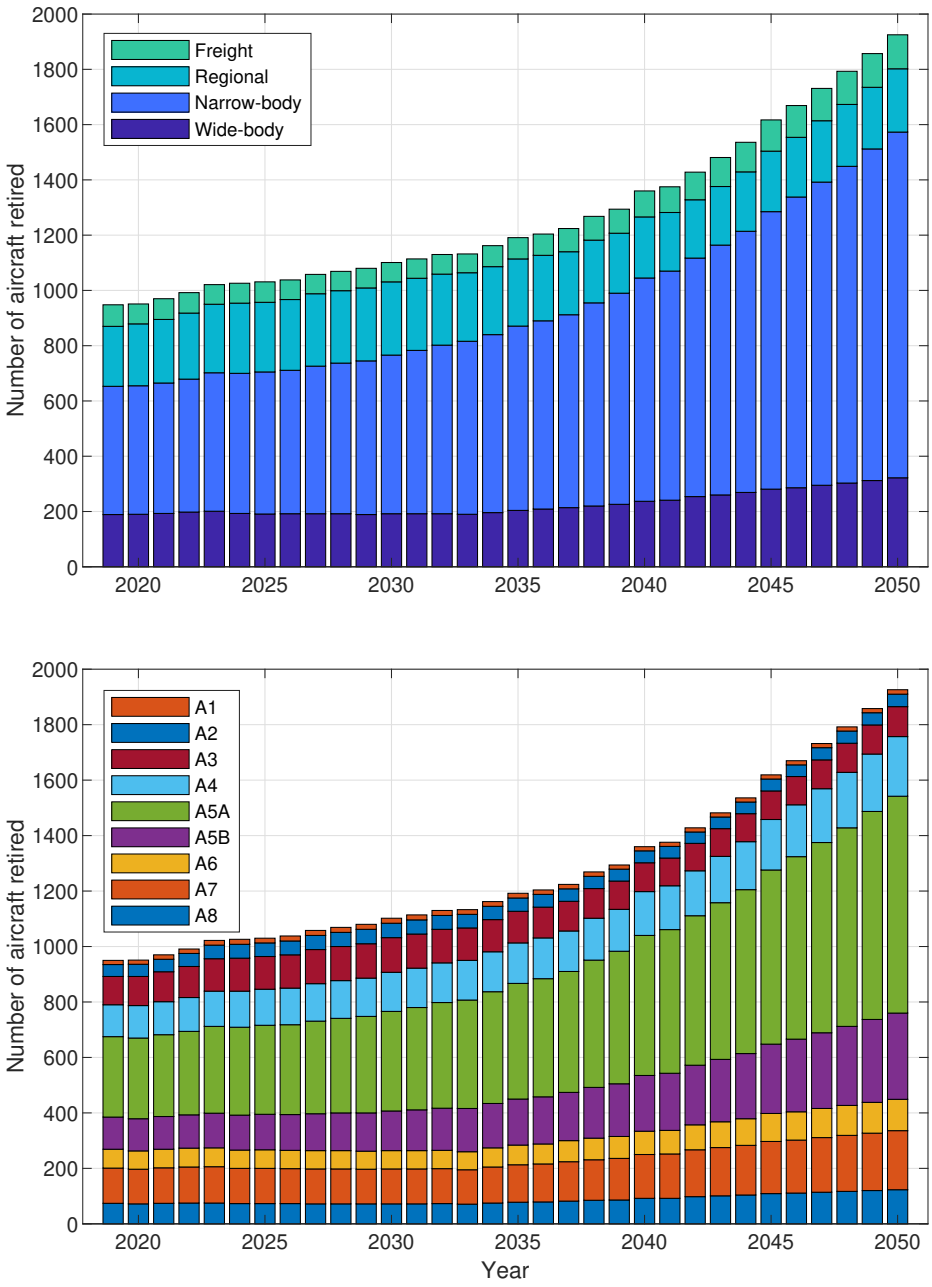

Figure A.7.1: Aircraft retirements from the aircraft fleet for the original and updated model from 2019-2050.

A.8 Cumulative emissions of the aircraft fleet

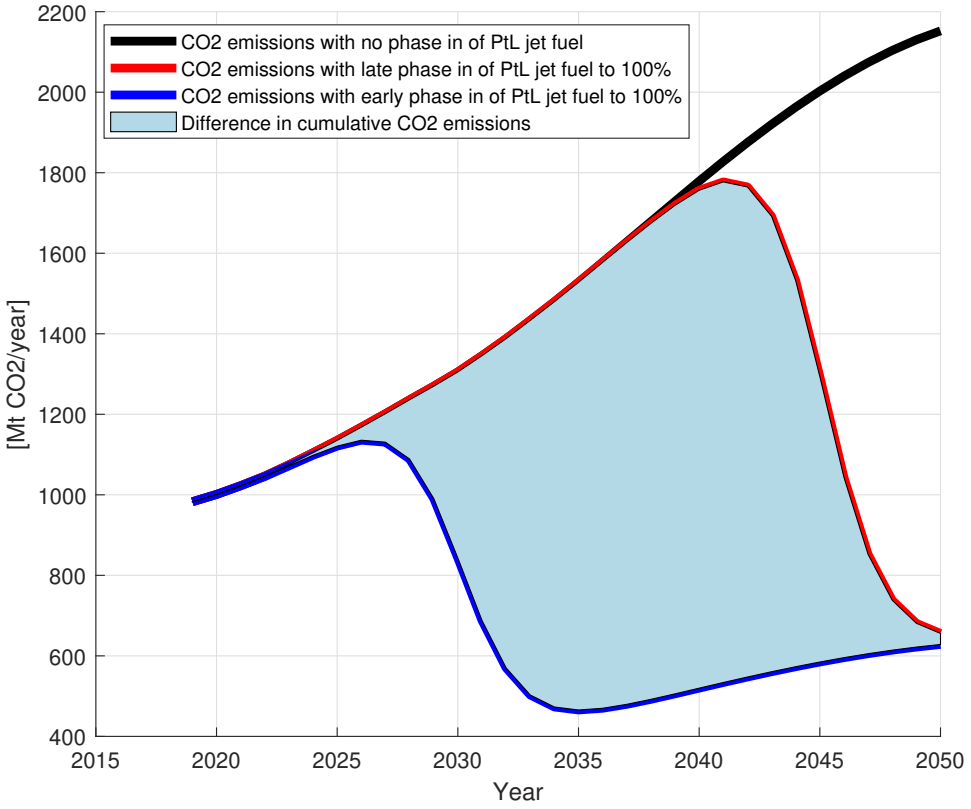

Figure A.8.1: Exploratory figure showing two different phase-in scenarios for PtL jet fuel to 100%. The blue line represents an early phase-in, centered around the year 2030. The red line represents a late phase-in, centered around the year 2045. The black line represents no phase-in of PtL jet fuel. The colored fields represent the difference of cumulative CO2 emissions between the early and late phase-in of PtL jet fuel of 17 542 Mt CO2.

A.9 Fleet fuel efficiency

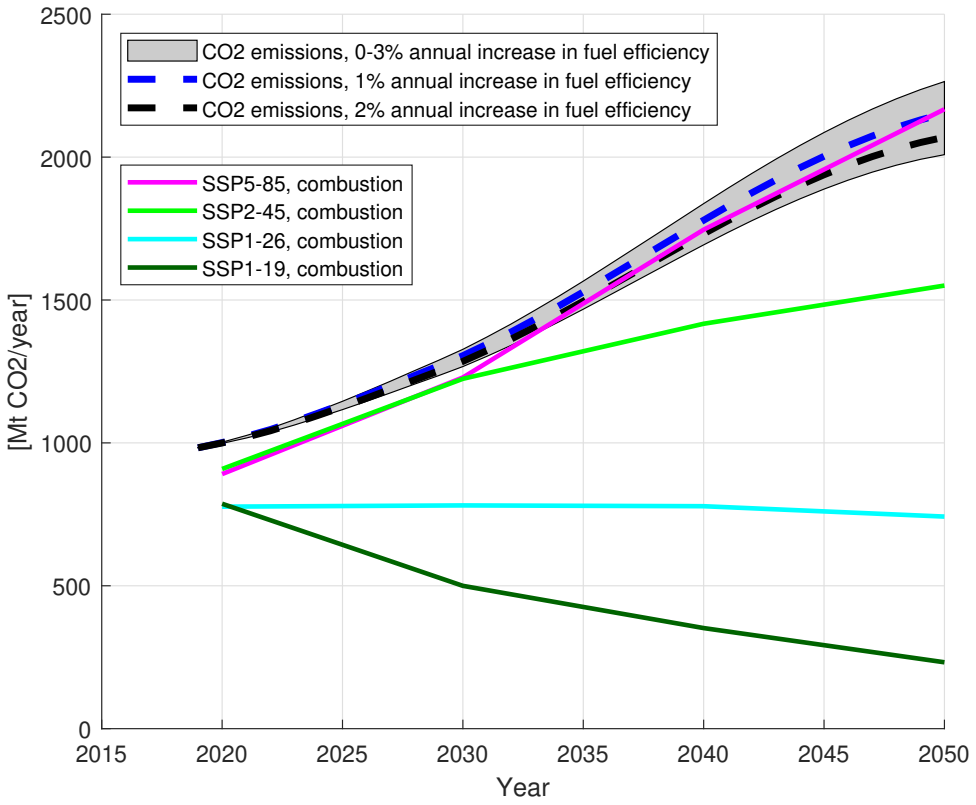

Figure A.9.1: Simulation results of the total CO_2 combustion emissions [Mt CO_2/year] for different fuel efficiency developments in the aircraft fleet, compared to four SSP-RCP scenarios, from 2019-2050. The gray area display the spread in CO_2 emissions from 0-3% annual improvement in fleet fuel efficiency. The blue and black lines represent the CO_2 emission with 1% and 2% annual improvement of the fleet fuel efficiency, respectively.

B | The original aircraft stock cohort model

This master thesis updates the aircraft stock cohort model developed in the project work. Appendix B is included to provide information and clarity about the original model. In the following sections, a brief description of the original aircraft stock cohort model is presented.

B.1 Framework of the model

The framework of the aircraft stock cohort model is presented in figure B.1.1 below. The model divides the aircraft fleet into four aircraft types and 45 age segments. For every iteration the aircraft fleet is updated. Every aircraft ages by one year and aircraft are retired from the fleet based on a retirement rate. New aircraft are delivered to the fleet based on the difference between the number of aircraft in the current fleet and the number of aircraft needed to cover the air travel demand. Therefore, the air travel demand acts as a driving force in the simulations.

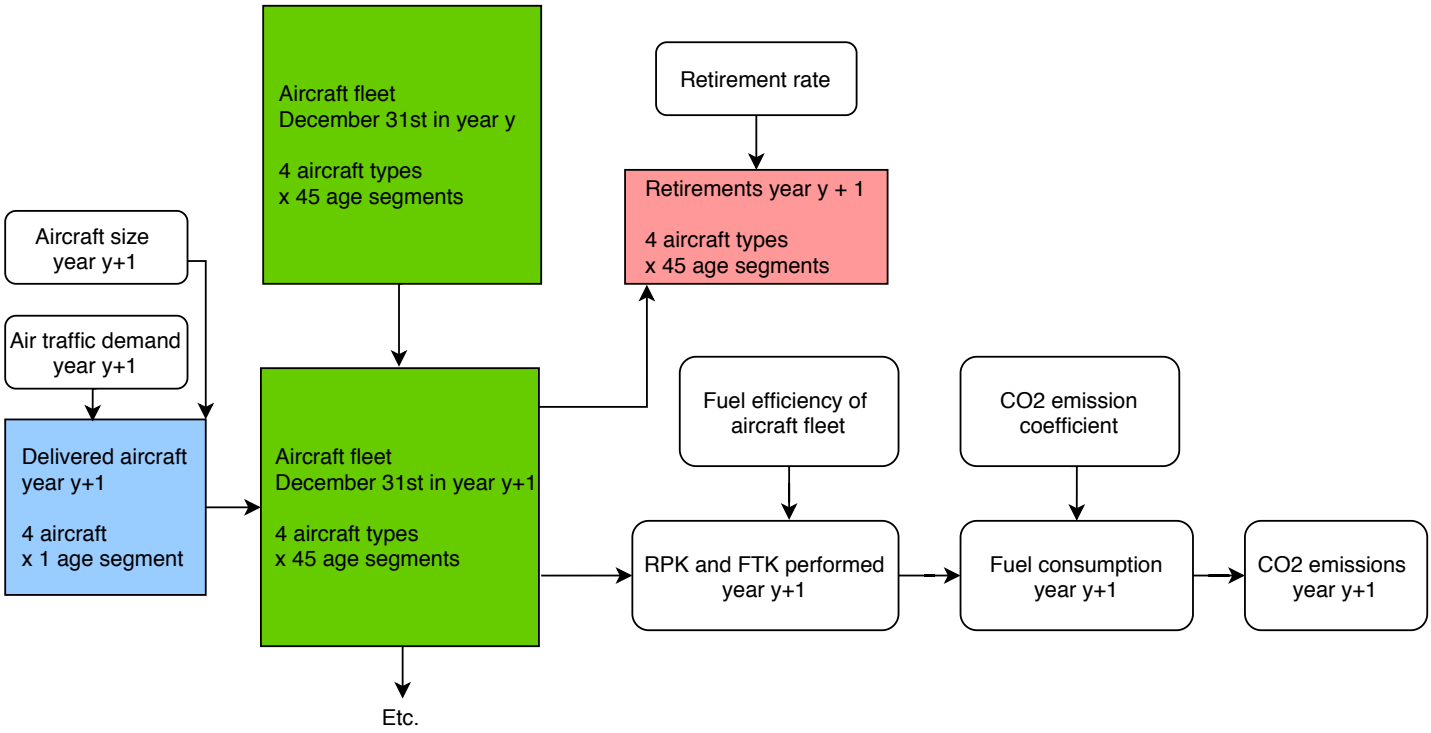

Figure B.1.1: Flowchart of the aircraft stock cohort model from the project work showing the first iteration of the simulation. The green boxes are the initialized and first iteration of the aircraft fleet, the blue box is the delivered aircraft while the red box is the retired aircraft (Enes, 2020).

B.2 Air travel demand

The air travel demand per route is distributed on the different aircraft types based on a set of assumptions: All intercontinental flights are covered by wide-body aircraft, the remaining wide-body capacity is distributed on the routes based on the number of wide-body aircraft on the continents, regional aircraft only cover intracontinental flights, narrow-body aircraft cover the remaining demand. The resulting table B.2.1 presented below splits the air travel demand by route into demand per aircraft. This distribution is essential when calculating the number of aircraft needed of each aircraft type to cover the air travel demand.

Table B.2.1: Transformation matrix with the shares of total air traffic covered by regional, narrow-body and wide-body aircraft on the 21 ICAO-routes. Every route is covered by one or more aircraft types, such that each row represent 100% (Enes, 2020).

Route	% covered by regional	% covered by narrow-body	% covered by wide-body
Intra-Asia/Pacific	2 %	93 %	5 %
Intra-North America	9 %	86 %	5 %
Intra-Europe	6 %	89 %	6 %
Europe <->North America	0 %	0 %	100 %
Asia/Pacific <->Europe	0 %	0 %	100 %
Asia/Pacific <->North America	0 %	0 %	100 %
Asia/Pacific <->Middle East	0 %	0 %	100 %
Intra-Latin America/Caribbean	9 %	88 %	3 %
Europe <->Middle East	0 %	0 %	100 %
Latin America/Caribbean <->North America	0 %	0 %	100 %
Europe <->Latin America/Caribbean	0 %	0 %	100 %
Africa <->Europe	0 %	0 %	100 %
Intra-Middle East	6 %	38 %	56 %
Middle East <->North America	0 %	0 %	100 %
Intra-Africa	32 %	54 %	14 %
Africa <->Middle East	0 %	0 %	100 %
Africa <->Asia/Pacific	0 %	0 %	100 %
Africa <->North America	0 %	0 %	100 %
Asia/Pacific <->Latin America/Caribbean	0 %	0 %	100 %
Latin America/Caribbean <->Middle East	0 %	0 %	100 %
Africa <->Latin America/Caribbean	0 %	0 %	100 %

B.3 Data collection

An overview of the data collected and implemented in the original aircraft stock cohort model is presented in table B.3.1 below.

Table B.3.1: Overview of collected input data used in the original aircraft stock cohort model. Each row presents the type of data collected, the data unit, the available years of the data, the years where data is constructed, the method of constructing the data, and finally the sources of the data (Enes, 2020).

Data collected	**Unit**	**Available years**	**Constructed years**	**Method**	**Data source**
Global air traffic	[Million RPK]	1929-2018	-	-	(A4A, 2018a), (ICAO, 2013, 2015)
Air traffic by route	[Million RPK]	1985, 1990, 1995, 2000-2019	1986-1989, 1991-1994, 1996-1999	Interpolation	(Boeing, 2005, 2009, 2020c)
Global air freight	[Million FTK]	1995-2019	1990-1994	Extrapolation	(ICAO, 2019a)
Number of regional, narrow-body and wide-body aircraft	[Aircraft]	1992, 2004, 2008-2009, 2012, 2014-2015, 2017	-	-	(Boeing, 2005, 2009, 2013, 2014, 2016, 2018), (OW, 2018, 2019)
Number of freighter aircraft	[Aircraft]	2004, 2014-2015, 2017	-	-	(Boeing, 2005, 2014, 2016, 2018)
Projected air traffic by route, Boeing	[Billion RPK]	2019, 2029, 2039	2020-2028, 2030-2038, 2040-2050	Interpolation Extrapolation	(Boeing, 2020c)
Projected global air traffic, Airbus	[Billion RPK]	2019-2038	2039-2050	Extrapolation	(Airbus, 2019b)
Projected global air traffic, IATA	[Billion RPK]	2019-2050	-	-	(IATA, 2019)
Projected global air traffic, ICAO	[Billion RPK]	2019-2045	2046-2050	Extrapolation	(ICAO, 2018)
Projected global air freight	[Billion FTK]	2019-2042	2043-2050	Extrapolation	(ICAO, 2017)
Projected aircraft fleet	[Aircraft]	2039	-	-	(Boeing, 2020c)
Projected aircraft emissions, SSP-RCP scenarios	[Mt CO2/year]	2020, 2030, 2040, 2050	2021-2029, 2031-2039, 2041-2049	Interpolation	(Riahi et al., 2017), (Rogelj et al., 2018), (Gidden et al., 2019)
Fuel burn new commercial aircraft	[g fuel/RPK]	2014	1975-2013, 2015-2050	(Enes, 2020)	(Kharina & Rutherford, 2015)
Average fuel burn freighter aircraft	[g fuel/FTK]	2019	1990-2018, 2020-2050	(Enes, 2020)	(Graver, Zhang, & Rutherford, 2019b)

C | Life cycle inventory data

C.1 Life cycle inventory data for the PtL plant using alkaline electrolysis

C.1.1 Construction data for the alkaline electrolyzer

Economic inflows	Value	Unit
reinforcing steel, at plant[RER]	4,00E+03	kg
disposal, building, fibre board, to final disposal[CH]	51	kg
disposal, building, bulk iron (excluding reinforcement), to sorting plant[CH]	8,00E+03	kg
chromium steel 18/8, at plant[RER]	8,00E+03	kg
transport, freight, rail[RER]	2,55E+03	tkm
nitrogen, liquid, at plant[RER]	85	kg
potassium hydroxide, at regional storage[RER]	30	kg
sodium silicate, spray powder 80%, at plant[RER]	200	kg
corrugated board, recycling fibre, double wall, at plant[RER]	51	kg
disposal, building, reinforcement steel, to sorting plant[CH]	4,00E+03	kg
transport, lorry 16-32t, EURO3[RER]	1,23E+03	tkm

Economic outflows	Value	Unit
Electrolyser for hydrogen production	1	unit

Environmental resources	Value	Unit
Occupation, industrial area, built up[resource_land]	29,8	m2a

Environmental emissions	Value	Unit
Hydrogen[air_unspecified]	5,36	kg

Figure C.1.1: Construction data for the alkaline electrolyzer taken from the supplementary information from (van der Giesen et al., 2014)

C.1.2 Construction data for the hydrogen compressor

Economic inflows	Value	Unit
steel, low-alloyed, at plant[RER]	3,00E+03	kg
disposal, building, concrete, not reinforced, to sorting plant[CH]	2,60E+04	kg
aluminium, production mix, at plant[RER]	500	kg
concrete, normal, at plant[CH]	12	m3
disposal, building, bulk iron (excluding reinforcement), to sorting plant[CH]	8,00E+03	kg
chromium steel 18/8, at plant[RER]	5,00E+03	kg
lubricating oil, at plant[RER]	150	kg
transport, freight, rail[RER]	1,79E+03	tkm
disposal, aluminium, 0% water, to municipal incineration[CH]	500	kg
transport, lorry 16-32t, EURO3[RER]	2,16E+03	tkm
Economic outflows		
Hydrogen compressor	1	unit
Environmental resources		
Occupation, industrial area, built up[resource_land]	16,2	m2a
Environmental emissions		
-		

Figure C.1.2: Construction data for the hydrogen compressor taken from the supplementary information from (van der Giesen et al., 2014).

C.1.3 Construction data for the fixed bed reactor

Economic inflows	Value	Unit
steel, low-alloyed, at plant[RER]	4,76E+03	kg
disposal, building, bulk iron (excluding reinforcement), to sorting plant[CH]	9,52E+03	kg
chromium steel 18/8, at plant[RER]	4,76E+03	kg
zeolite, powder, at plant[RER]	2,67E+04	kg
RWGS catalyst	6,60E+03	kg
Economic outflows		
Fixed bed reactor for RWGS	1	unit
Environmental resources		
Occupation, industrial area[resource_land]	3,14	m2a
Environmental emissions		
-		

Figure C.1.3: Construction data for the fixed bed reactor taken from the supplementary information from (van der Giesen et al., 2014).

C.2 Life cycle inventory data for the PtL plant using high-temperature co- electrolysis

C.2.1 Construction data for the electrolyzer cell

Ecoinvent 3.5 process	Unit	Value
Input		
Cerium oxide[1]	g	0.201
Lanthanum oxide[1]	g	1.98
Gadolinium oxide[1]	g	0.053
Yttrium oxide[1]	g	2.42
Strontium carbonate[2]	g	0.324
Iron(III) oxide-hydroxide FeO(OH)[2]	g	0.389
Nickel mix, ts[3]	g	17.9
Cobalt hydroxide $Co(OH)_2$[2]	g	0.394
GLO: market for zirconium oxide	g	14.9
GLO: manganese dioxide production	g	0.351
RER: copper oxide production	g	0.143
GLO: transport, freight, sea, transoceanic ship	tkm	0.401
RER: transport, freight, lorry 16-32 metric ton, EURO5	tkm	6.9E-03
DE: transport, freight train	tkm	0.014
DE: market for electricity, low voltage	kWh	0.12
CH: treatment of inert waste, inert material landfill	g	38.6
Nitric acid (98%), ts[3]	g	8.73
RER: methyl ethyl ketone production	g	7.62
RER: carboxymethyl cellulose production, powder	g	3.01
RER: market for ethanol, without water, in 99.7% solution state, from ethylene	g	7.62
RER: benzyl alcohol production	g	3.01
Output		
cell	piece	1
Nitrogen oxides [Inorganic emissions to air]	g	0.32
NMVOC (unspecified) [Group NMVOC to air]	g	6.38

Figure C.2.1: Construction data for the electrolyzer cell taken from the supplementary information from (Schreiber et al., 2020)

C.2.2 Construction data for the electrolyzer stack

Ecoinvent 3.5 process	Unit	Value
Input		
glass-cermet[1]	kg	19.9
RER: cast iron production	kg	414
RER: chromium production	kg	117
GLO: market for titanium, primary	kg	0.374
RER: manganese production	kg	2.84
Nickel mix, ts[2]	kg	19.8
Lanthanum[3]	kg	0.483
GLO: cobalt production	kg	1.5
RER: sheet rolling, chromium steel	kg	534
GLO: transport, freight, sea, transoceanic ship	tkm	9.89
RER: transport, freight, lorry 16-32 metric ton, EURO5	tkm	55.6
DE: transport, freight train	tkm	111
DE: market for electricity, low voltage	kWh	3611.5
Europe without Switzerland: heat production, natural gas, at industrial furnace low-NOx >100kW	kWh	606
CH: building construction, hall, steel construction	m^2	0.029
RER: building construction, multi-storey	m^3	0.175
Industrial area (regionalized, DE) [Occupation]	m^2*y	5.26
From unspecified (regionalized, DE) [Transformation]	m^2	0.105
To industrial area (regionalized, DE) [Transformation]	m^2	0.105
Output		
HT-co-electrolysis stack 150 kW	piece	1

Figure C.2.2: Construction data for the electrolyzer stack taken from the supplementary information from (Schreiber et al., 2020)

C.2.3 Construction data for the rest of plant

Ecoinvent 3.5 process	Unit	Value
Input		
RER: steel production, converter, chromium steel 18/8	kg	1875
RER: sheet rolling, chromium steel	kg	1875
Europe without Switzerland: market for tap water	kg	4086
CH: treatment of wastewater, unpolluted, from residence, capacity 1.1E10l/year	m^3	4.09
RER: transport, freight, lorry 16-32 metric ton, EURO5	tkm	188
DE: transport, freight train	tkm	375
RER: transport, passenger car, large size, diesel, EURO 5	km	3600
DE: market for electricity, low voltage	kWh	1440
DE: market for electricity, medium voltage	kWh	7242
Europe without Switzerland: heat production, natural gas, at industrial furnace low-NOx >100kW	kWh	3535
CH: heat production, light fuel oil, at boiler 100kW condensing, non-modulating	kWh	3000
CH: building construction, hall, steel construction	m^2	0.672
RER: building construction, multi-storey	m^3	4.08
RER: construction work, heat and power co-generation unit, 160kW electrical	piece	4.2
RER: inverter production, 500kW	piece	0.3
From unspecified (regionalized, DE) [Transformation]	m^2	2.42
Industrial area (regionalized, DE) [Occupation]	m^2*y	121
To industrial area (regionalized, DE) [Transformation]	m^2	2.42
Output		
Balance-of-plant of HT-co-electrolysis stack 150 kW	piece	1

Figure C.2.3: Construction data for the rest of plant taken from the supplementary information from (Schreiber et al., 2020)

C.3 Life cycle inventory data used in both PtL plants

C.3.1 Construction data for the DAC unit

Material, Ecoinvent 3.5 process	Unit	Input/DAC unit
CH: market for concrete, normal	t	52
RER: steel production, chromium steel 18/8, hot rolled	t	36.3 (3.63[1])
IAI area EU-27 & EFTA: aluminum production, primary, ingot	t	26.2 (2.096[2])
GLO: market for steel, low-alloyed	t	30.3 (3.03[1])
RER: copper production, primary	t	1.7
RER: wire drawing, copper	t	1.7
CH: market for gravel, crushed	t	93.1
CH: gravel and sand quarry operation	t	89.6
CH: stone wool production	t	8.7
RER: ethylene glycol production	t	15
EU-28: silicone sealing compound (EN15804 A1-A3)	t	1.1
CH: market for inert waste, for final disposal	t	243.4[3]
RER: transport, freight, lorry 16-32 metric ton, EURO5	tkm	244,895
RER: transport, freight train	tkm	37,412

Figure C.3.1: Construction data for the DAC unit taken from the supplementary information from (Schreiber et al., 2020)

C.3.2 Construction data for the gas-to-liquid plant

Economic inflows	Value	Unit
concrete, sole plate and foundation, at plant[CH]	3,45E+05	m3
steel, low-alloyed, at plant[RER]	7,20E+06	kg
reinforcing steel, at plant[RER]	7,20E+06	kg
disposal, building, reinforced concrete, to final disposal[CH]	8,28E+08	kg
disposal, building, bulk iron (excluding reinforcement), to sorting plant[CH]	1,44E+07	kg
Economic outflows		
GTL plant	1	unit
Environmental resources		
Occupation, industrial area[resource_land]	1,12E+06	m2a
Environmental emissions		
-		

Figure C.3.2: Construction data for the gas-to-liquid plant taken from the supplementary information from (van der Giesen et al., 2014).

Jon Enes

Mitigation of the aviation sector

NTNU
Norwegian University of
Science and Technology